UNIVERSITÀ DEGLI STUDI DI CATANIA

Dottorato di Ricerca in Biotecnologie

XXVI Ciclo

Andrea Magrì

VDAC and SOD1: two major players in mitochondrial metabolism and in ALS

TESI DI DOTTORATO

Relatore: Chiar.mo Prof. Vito De Pinto

Coordinatore: Chiar.mo Prof. Vito De Pinto

A.A. 2011-2014

ABSTRACT

The Thesis work presented here has been devoted to two proteins, the *Voltage-Dependent Anion Channel* (*VDAC*) and the *Superoxide Dismutase I* (*SOD1*) and has been especially focused on the relationships between them in physiological or pathological conditions of the cell.

VDAC is a pore-forming protein located in the outer mitochondrial membrane, where it is suspected to play a key role in metabolism regulation, as the interface between mitochondria and cytosol, and in apoptosis regulation. In the small family of VDAC proteins, composed of three isoforms in chordates, VDAC3 is the least known. Conversely from isoforms 1 and 2, its ability to form pores has been questioned. In this thesis, we present the first complete electrophysiological characterization of VDAC3, showing that this protein is able to forms smaller pores compared to VDAC1, under physiological condition of pH. Another point examined here has been the gating of VDAC1. This protein, in vitro, shows the important feature of gating the pore in dependence of high voltage applied. It is believed that the N-terminal domain has a crucial role in voltage-dependent gating and in the stabilization of the protein through its interaction with the pore-wall.

By producing several mutants of VDAC1, in this work we have shown that the Voltage-dependence may be modulated in an asymmetrical way by modifying sequences or deleting β-strands required for the interaction with N-terminal domain.

The *Superoxide Dismutase I* (*SOD1*) is the most important antioxidant enzyme of all eukaryotic cells, since it inactivates the superoxide anion. Many recent evidences suggest that SOD1 is important for mitochondrial function, both in physiological and pathological conditions. SOD1 protects, among others, VDAC from oxidative stress, and may affect mitochondrial proteins expression levels. In addition, in the neurodegenerative disease *Amyotrophic Lateral Sclerosis* (*ALS*), SOD1 mutants were reported to directly bind the cytosolic surface of mitochondria, using VDAC1 as docking site. To understand the relationships between VDAC and SOD1, in this work, we studied the influence of hSOD1 on mitochondria when it was overexpressed in a yeast strain devoid of yeast

endogenous VDAC. Our results sturprisingly indicate that SOD1 may have a metabolic role and can support the mitochondrial recovery in the strain Δpor1, heavily slowed down by the lack of porin1. Our results support the recent claim that SOD1 may act on the expression of other mitochondrial proteins. In addition, the characterization of the interaction between VDAC1 and two of the most diffused ALS-linked SOD1 mutants was also obtained and might be considered the molecular basis in understanding the mitochondrial involvement in ALS.

SUMMARY

1. INTRODUCTION

1.1 Yeast, a perfect model organism for metabolic studies

1.1.1 A story of success

The unicellular yeast *Saccharomyces cerevisiae* is one of the most known, studied and used model organisms. First traces of its use date back to ancient Egypt, even though, only in the XIX century Louis Pasteur fully realized the enormous potential of this microorganism for the development of biotechnology. Today, yeast is widely used for research and plays a key role for food and pharmaceutical industry, where it used for beer brewing, bakery, and production of recombinant molecules.

The extraordinary success of this organism as research model organism depends on several aspects.

First, yeast is extremely easy to manipulate, requires simple and inexpensive culture media, has a short generation time and is not pathogenic. These properties allow for the swift production and maintenance of multiple specimen lines at low cost.

Second, *S. cerevisiae* genome was completely sequenced in 1996. The genome of 12068 Kb is organized in 16 chromosomes, and includes approximately 6200 ORFs (open reading frame) of which 5800 ORFs correspond to protein coding genes [1]. The complete genome knowledge has allowed to genetically modifying the yeast DNA, producing many deletion mutants, which played a key role in understanding the function of many proteins.

Third, *S. cerevisiae* is evolutionarily close to higher eukaryotes. It has been estimated that around 30% of yeast genes have homologous genes in humans; moreover, yeast shows absolutely conserved molecular mechanisms, such as DNA replication, RNA synthesis and processing, protein synthesis and post-traslational modifications, the main metabolic pathways, cellular respiration, signal transduction, cell cycle regulation, apoptosis [2]. Thus, higher eukaryotes genes are often successfully expressed in *S. cerevisiae* and, in many case, the heterologous protein is able to complement the absence of the endogenous one. The heterologous expression in yeast allows to study protein properties and

behavior, the effects of mutations and protein-protein interactions in a relatively simple system.

1.1.2 Biology of *S. cerevisiae*

S. cerevisiae is a unicellular yeast belonging to the class of *Ascomycetes*. Cells show an ellipsoidal shape, with a diameter between 5 and 10 micrometers, and are characterized by a resistant outer wall essential for yeast survival (Fig. 1A). Cell wall is composed prevalently by polysaccharides, β(1→3)-d-glucan and β(1→6)-d-glucan, that appear to have a structural function, and mannoproteins that act as "filler" and are important for the permeability of the wall [3]. As an eukaryote, *S. cerevisiae* shares the complex internal cell structure of plants and animals cells, with a well-defined nucleus, containing a genome that is devoid of the high percentage of non-coding DNA (typical of higher eukaryotes), and all organelles (Fig. 1B).

S. cerevisiae generally reproduces by *budding*, doubling their population around every 100 minutes, although growth rates vary depending from several conditions. Yeast growth is synchronized with bud growth, which reaches the size of the mature cell by the time it separates from the parent cell; both mother and daughter cells can initiate bud formation before cell separation has occurred.

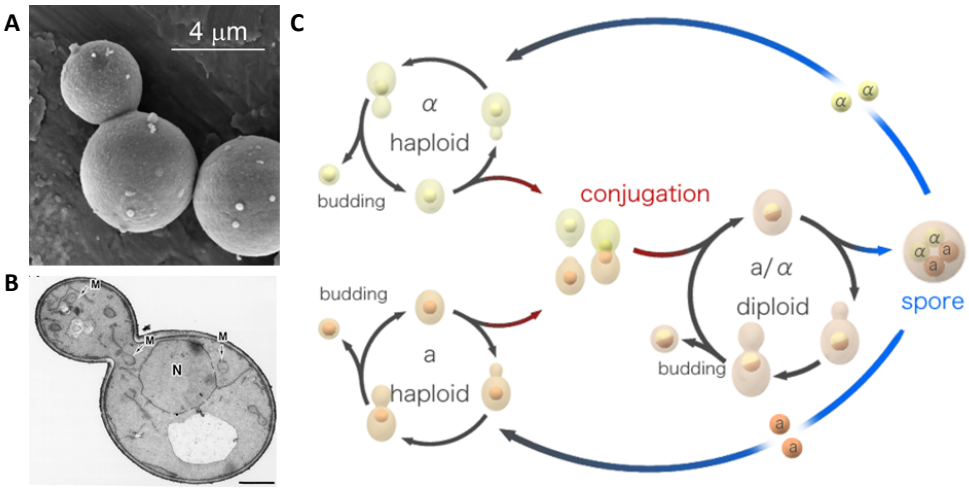

Fig 1 ***Yeast morphology and life cycle.*** **A)** Yeast *S. cerevisiae* morphology showed by SEM microscopy. **B)** A thin-section of budding yeast cell by electron microscopy; N indicates nucleus, M mitochondria. Picture taken from [4]. **C)** Schematic representation of life cell cycle of yeast; it is showed the alternation between diploid and haploid population.

S. cerevisiae is a *haplodiplont* organism, which may alternates haploid or diploid generations (Fig. 1C). The haploid stage represents the asexual form of yeast and undergoes a simple life cycle of mitosis and growth; however, under stress conditions, haploid cells generally die. Conversely, the diploid stage represents the sexual and the preferential form of yeast and, similarly to the haploid, undergoes a simple life cycle of mitosis, growing with a faster rate.

Under stress conditions, diploid cells are more resistant and are subjected to *sporulation* by meiosis, a process that promotes the production of four haploid spores characterized by two different mating type, called *a* and *α* (alpha) [5]. Thus, the haploid cells of opposite mating type can mate to form diploid cells that can sporulate, to form another generation of haploid cells, or continue to exist as diploid cells. As in many other eukaryotes, aim of mating is promoting the genetic recombination, through the production of novel combinations of chromosomes and combine plasmids and proteins.

Yeast metabolism was well characterized. Yeast is able to grow in presence of many carbon sources, but independently from them, yeast normally grows in three main phases. When yeast cells are inoculated in a fresh growth medium, cells enter an adaptation phase, called *lag phase*, in which they are biochemically active but not dividing and number of cells remains relatively constant. Length of lag phase strongly depends from carbon source, but it also influenced by several factors, such as temperature, oxygen and pH. During this phase, cells activate the most appropriate metabolic pathways, according to nutrients availability in growth medium. Once metabolism is completely active, cells start DNA replication and cell division: this is the second phase of growth, called *exponential phase*, in which the cells grow most rapidly. The third phase of growth is the *stationary phase*: metabolism slows and the cells stop rapid cell division. The factors that cause cells to enter stationary phase are related to change in the environment, such as lower availability of nutrients, normally caused by high cell density.

1.1.3 Yeast fermentative metabolism

S. cerevisiae is characterized by fermentative or respiratory metabolism, depending from environmental conditions. Both carbon sources in the growth

media and oxygen availability have a strong impact on metabolism physiology. Yeast can use a broad set of carbon sources such as alcohols, amino acids and organic acids, which can support their growth; however, yeasts preferentially metabolizes sugars, and glucose certainly represents the favorite carbon source also for *S. cerevisiae* [6].

Glucose utilization starts with the uptake of the sugar into the yeast cells, thanks to the presence of specific carriers located on the plasma membrane. *S. cerevisiae* has a large gene family codifying for hexose transporters, that consists of more than 20 members, including 18 genes encoding for transporters (HXT family, GAL2) and 2 genes encoding for sugar sensors (SNF3, RGT2) [7]. Once in the cytosol, glucose metabolism occurs prevalently through glycolysis and pentose phosphate pathway, although this last pathway is predominantly used for NADPH production [8-9]. The concentration of sugars in the growth medium strongly influences the enzyme levels of several metabolic pathways. Glucose acts on an extensive transcriptional regulation of a large number of genes, leading to the adaptation to fermentative metabolism such as genes required for the glycolytic pathway.

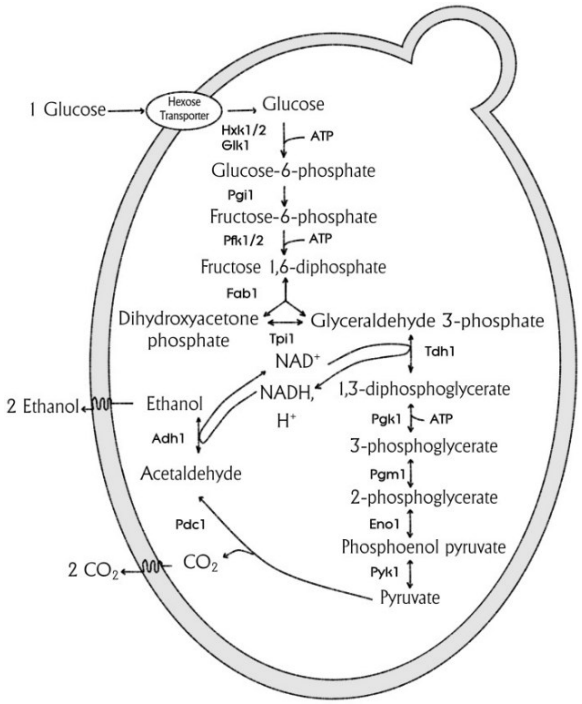

Fig 2 ***Yeast fermentative metabolism.*** Schematic representation of glucose metabolism that occurs prevalently by glycolysis and alcoholic fermentation. Glucose undergoes through glycolysis, producing 2 ATP and 2 NADH molecules; the final product of glycolysis, pyruvate, undergoes decarboxylation up to ethanol, that is normal secreted outside the cell. Picture taken from [6].

At the same time, glucose acts as repressor of genes encoding for proteins involved in the gluconeogenic and respiratory pathways, a process known as *catabolite repression* [10].

Through glycolysis, glucose is metabolized to pyruvate, whereby production of energy, in form of two molecules of ATP per each molecule of glucose, is coupled to the generation of reducing intermediates as NADH [11]. Pyruvate can follow different metabolic fates, which strongly depends on the environmental conditions.

In anaerobic conditions, pyruvate metabolism occurs through the *alcoholic fermentation*, in which it is decarboxylated to give acetaldehyde and CO_2; then, acetaldehyde is converted in ethanol that is normally secreted outside the cell together with CO_2, and this process promotes the re-oxidation of NADH to NAD^+, making it available again for glycolysis. The alcoholic fermentation is the basis of some industrial processes, such as bakery: CO_2 is responsible for the formation of bubbles in the bread while ethanol evaporates during cooking. Absence of oxygen does not represent a strict rule for alcoholic fermentation: indeed, even in the presence of high levels of oxygen, yeasts normally choose to use fermentation instead of respiration, when glucose is fully accessible. This phenomenon, known as *Crabtree effect*, consists in the inhibition of gene expression involved in aerobic metabolism when glucose is available, which may occur both in the presence or absence of oxygen [12]. In fact, although fermentation is not by itself a highly energetically efficient process, the high concentration of glucose strongly promotes the acceleration of glycolysis, producing appreciable amounts of ATP and allows the yeast to grow in a rapid and exponential way.

As the level of glucose drops, the diauxic shift occurs, that promote the yeast adaptation from fermentative to respiratory metabolism. The repression of respiration mediated by glucose is left and synthesis of proteins involved in the mitochondrial respiration machinery occurs. In this stage, ethanol becomes the primary mode of ATP generation by respiratory metabolism and the overall growth rate becomes much slower: this is the main feature of the stationary phase [13].

1.1.4 Mitochondria and the respiratory metabolism

Respiratory metabolism starts with the presence of the acetyl–cofactor A (acetyl-CoA), considered the first intermediate of *Tricarboxylic Acid* (*TCA*) *Cycle.* Acetyl-CoA can be obtained from metabolism of both fermentable and non-fermentable carbon sources, through pyruvate formation, which undergoes, through oxidative decarboxylation, catalysis by the pyruvate dehydrogenase enzymatic complex. Other source of acetyl-CoA is the oxidation of fatty acids, as well as the final product of fermentation, ethanol: under certain conditions, it is re-converted in acetaldehyde up to the formation of acetyl-CoA.

In TCA cycle, acetil-CoA molecules are totally oxidized to CO_2, furnishing a set of intermediates commonly used by other metabolic reactions [14]. Electrons, obtained from decarboxylation, are able to reduce NAD^+ and FAD molecules to NADH and $FADH_2$ respectively, that are high-energy intermediates; then, NADH and $FADH_2$ produced will be re-oxidated during *oxidative phosphorylation*, a process that convert potential energy in ATP molecules [15].

TCA cycle, as well as oxidative phosphorylation, occurs in a separate cellular compartment, the *mitochondria*. They are membrane bound organelles that represent the "power plants" of most eukaryotic cells. Their primary role, indeed, consist in the conversion of most part of the energy to ATP, even if they are involved in a set of interconnected metabolic functions, such as storage of calcium ions and modulation of cell cycle and apoptosis [16-17].

Mitochondria show a diameter between 0.2 and 1 µm with a peculiar structure that strongly reflects the function: they are characterized by two separate and functionally distinct membranes, the *outer* and the *inner mitochondrial membranes*, that encapsulate respectively the *intermembrane space* and the *matrix*. In addition, mitochondria are the only cellular organelles in animals that have their own DNA, which codifies for few mitochondrial proteins, while most of the proteins are encoded by nuclear genes and then imported into mitochondria.

Matrix is the site of mitochondrial DNA, of enzymes involved in DNA replication and in the TCA cycle: it is in the matrix that the oxidative degradation of metabolites occurs.

The inner mitochondrial membrane (IMM) contains the matrix and represents the principal site of ATP generation. Its composition is different from the others cellular membranes, since the lipid content resembles that of the prokaryotic membranes. In addition, IMM shows high level of impermeability to ions and small molecules, a critical property for maintaining the proton gradient that drives oxidative phosphorylation. IMM surface area is substantially increased by its folding into *cristae* that contain an unusually high percentage of proteins, including ATP synthase and a variety of cytochromes used in oxidative phosphorylation, as well as proteins involved in metabolites transport. Indeed, the high-energy electrons from NADH and $FADH_2$ are transferred to molecular oxygen through a series of carriers, located in the inner membrane of mitochondria and ranked according to a decreasing redox potential. The electron transfer reactions generates energy that is converted to potential energy stored in a proton gradient across the membrane, which is then used to drive ATP synthesis through ATP synthase.

Despite the electron transfer along the transport chain takes place in a controlled and selective way, it can generate as intermediates oxygen species partially reduced, called *Reactive Oxygen Species* (*ROS*), which can be harmful to the mitochondria and to the entire cell because of their reactivity. However, cells have developed enzymatic defense mechanisms against ROS aimed to destroy oxygen radicals.

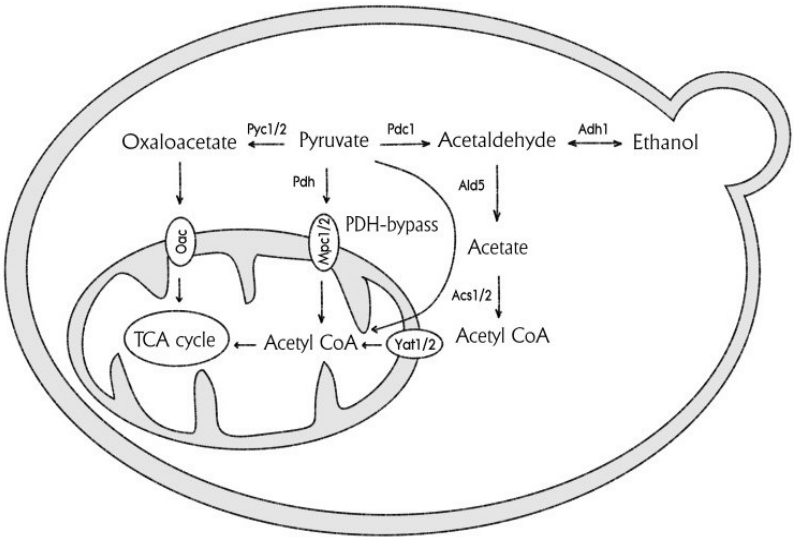

Fig 3 ***Yeast respirative metabolism.*** Schematic representation of pyruvate metabolism by TCA cycle. Pyruvate is transformed in acetil-CoA, that represent also the final product of fatty acids oxidation. Acetil-CoA is totally decarboxilated to CO_2 producing high-energy equivalents, which represent a source of potential energy for ATP production. Picture taken from [6].

In contrast to the IMM, the outer mitochondrial membrane (OMM) is highly permeable to small molecules, making the ion composition of the intermembrane space (IMS) similar to the cytosol. Thus IMM is considered the functional barrier against the free passage of small molecules between the cytosol and the matrix. It is able to maintain the proton gradient between the two sides of the membrane. Consequently, OMM plays a key role in the metabolic exchanges between cytosol and mitochondria; it owes its high permeability to its high content of pore-forming proteins, called *porins*, which form channels that allow the diffusion of ions and small molecules up to around 6000 Da, and specific transport proteins for larger molecules, which can cross OMM by active transport.

1.2 The VDAC family protein

1.2.1 Organization of the Outer Mitochondrial Membrane

The Outer Mitochondrial Membrane (OMM) represents the interface between cytosol and mitochondria. It shows a peculiar protein composition. OMM contains proteins involved in mitochondrial mobility (through its interaction with microtubules), apoptotic factors, enzymes, and others, involved in active and passive transport of proteins, ions and metabolites across OMM [18-19].

Most of these mitochondrial proteins are synthetized in cytosol, and are targeted to mitochondria by a pre-sequence of 20-35 amino acids, located at the N-terminal domain, which will be removed by proteolytic cleavage once the protein is imported into the organelle. Thus, OMM contains several proteins involved in traslocation of proteins: the *Translocator of Outer Membrane*, *TOM complex*, binds the pre-sequence of the polypeptide and promotes its insertion into OMM or the passage into the IMS, and the *Translocator of Inner Membrane*, *TIM complex*, able to allow the sorting of the protein to the mitochondrial matrix and to the other subcompartments [20].

One of the most abundant protein families of OMM is represented by the mitochondrial porins. They are integral membrane proteins that form a pore through which small molecules can selectively cross the OMM; porins are also suspected to modulate the metabolite flux by a not yet elucidated mechanism of

gating of the channel. Porins were initially discovered in 1974 in the outer membrane of the Gram-negative bacteria *Escherichia coli*; two years later, the existence of porins was proved also in eukaryotes: they were found in mitochondria of *Paramecium tetraaurelia* [21]. Afterward, porins with very similar features were identified in mitochondria from fungi, plants, metazoans and invertebrates.

The bacterial porin *Omp F* represents a typical example of porin: it has inspired also the structural investigations of the eukaryotic porins. Omp F is a non-specific pore with a weak cation selectivity that allows the passive diffusion of small and polar molecules of around 600-700 Da, such as water, ions, glucose as well as waste products [22].

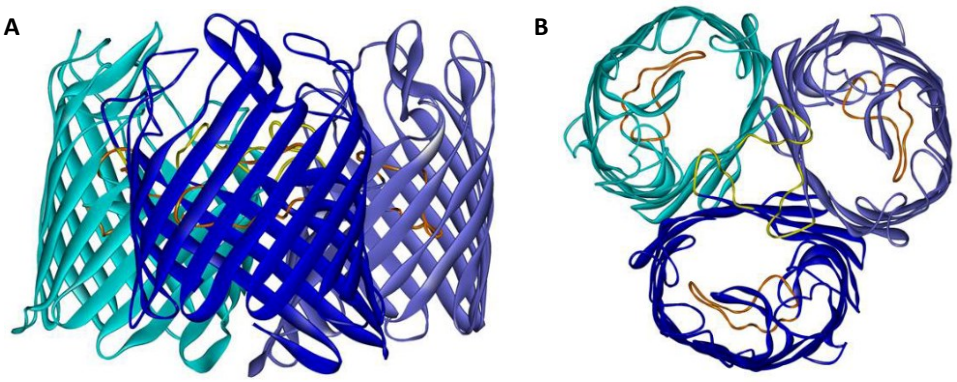

Fig 4 ***Tridimensional structure of Omp F.*** The bacterial porin Omp F forms trimeric structure on the surface of outer membrane of Gram-negative. **A)** The side view of the trimer complex of Omp F. **B)** The view from above of the complex. In yellow are indicated the loops inserted in the lumen of each sibunit, that are involved in gating process.

Omp F forms a trimeric complex in the bacterial outer membrane (Fig. 4). Each Omp F subunit spans the membrane with 16 β-strands that form a β-barrel structure. It is characterized by hydrophilic amino acid residues, protruding towards the aqueous inside of the pore, alternating with hydrophobic residues, in contact with the lipid bilayer of the membrane. Furthermore, the connections between the β-strands are very short ("turns") from the periplasmic side of the membrane and long loops on the external side of the membrane. In particular a major loop about 40 amino acids long (L3) is folded inside the pore's lumen and modulates its diffusion properties [23].

Omp F was characterized using electrophysiological methods, such as reconstitution in planar lipid bilayer, and incorporation in proteoliposomes loaded with sugars of permeable size. These experiments have demonstrated the voltage-dependence of Omp F, which consists in the modulation of opening/closing activity of the channel, a phenomenon happening only when the applied voltage is high [24].

Comparison of the sequences of prokaryotic porins with eukaryotic counterparts (VDAC; see below) shows only about 13% of sequence homology; despite this, the two proteins have similar secondary structure.

1.2.2 The Voltage-Dependent Anion Channel. General features.

Voltage-Dependent Anion Channel or *VDAC* indicates a family of pore-forming proteins of similar size of 28–32 kDa and around 280 amino acids, characterized by pores slightly selective for anions, with a conductance of around 4 nS. Their name indicates that the conductance may vary as well as the selectivity in dependence of the voltage applied when proteins are reconstituted on planar lipid bilayer [25]. Mammals, as well as most chordates, express three clades corresponding to three VDAC isoforms, called VDAC1, VDAC2 and VDAC3. From such evolutionary analysis, it is generally accepted that VDAC3 is the oldest protein, while VDAC1 is considered the most recent [26]. The organization of the three VDAC genes is very similar: genes are made of the same number of coding exons, sharing exactly the same size, with the VDAC2 gene containing an additional first exon encoding for the short pre-sequence of 11 amino acids, a peculiar feature of this isoform [27].

VDAC isoforms 1 and 2 are expressed more or less ubiquitously in all eukaryotes, while VDAC3 is more abundant in celebral cortex, liver, hearth, testis and spermatozoa [28]. In addition, analysis of the expression levels of human VDAC isoforms in HeLa cells, determined by Real-Time PCR, have shown that VDAC1 is the most abundant isoform, 10 times more abundant compared to VDAC2 and hundred times more abundant compared to VDAC3. Moreover, the over-expression of each single VDAC isoform affects the mRNA levels of the other two isoforms, suggesting that the ratios between VDAC isoforms are subject to a reciprocal control that avoids an imbalance among these proteins [29].

The multi-alignment of the three human VDAC protein sequence shows a high level of sequence conservation. Moreover, comparison between human and yeast VDAC1 homologous, POR1, suggests a sequence conservation of porins through evolution. Since the sequences are highly conserved, the structures of the three human VDAC isoforms results very similar and characterized by the typical β-barrel conformation. Despite this, the three human isoforms display different functional properties.

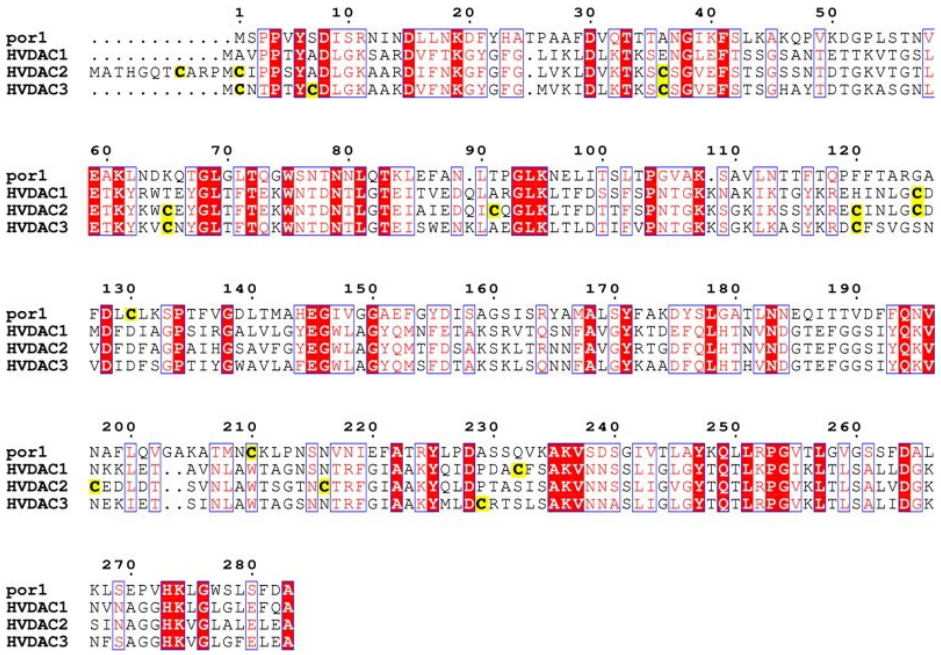

Fig 5 ***Comparison between yeast and human VDAC proteins sequences.*** The yeast porin POR1 was aligned with the three human VDAC isoforms. Sequences show high levels of identity, which can be calculated to be around 70%. In yellow are underlined the cystein residues, considered particularly important for VDAC3 peculiar features. Picture taken from [27].

Several experiments have demonstrated that recombinant VDAC1 and 2 are able to form pores in planar lipid bilayers (PLB), while VDAC3 shows a reduced ability to insert into the membrane [30]. However, in a very recent work it was demonstrated that VDAC3, in certain conditions, forms very small pores compared to the others isoforms, with a lower conductance [31]. These different features showed by VDAC3 may be partially explained by the presence of a higher content in cysteine residues, which can modulate its insertion on PLB under certain conditions. Moreover, these features have suggested an unknown and peculiar role for this isoform.

1.2.3 The structure of human VDAC1

VDAC1 is the most studied isoform of the three mammal VDAC proteins. In the past years, several studies based on structure prediction have suggested the presence of a transmembrane β-barrel domain associated to α-helix domain with amphipathic feature, corresponding to the N-terminal sequence of the protein [32]. This structural organization, common to others transmembrane proteins with different function, such as the subunit of TOM complex, *TOM40*, was confirmed in 2008 by the analysis of data obtained combining NMR and X-ray crystallography and independently by three groups [33-35].

The pore resembles an elliptical shape of approximately 3.1 x 3.5 nm in the horizontal dimensions and approximately 4 nm in the vertical directions; the diameter of the pore's lumen is reduced to approximately 1.5 x 1 nm (Fig. 6). Surprisingly, at variance with bacterial porins formed by an even number of β-strands (usually 16 strands), VDAC1 β-barrel is organized with 19 antiparallel β-strands, approximately 10 amino acids long. The odd number of strands requires one parallel interaction between the adjacent β-strands 1 and 19.

The N-terminal region has been much studied. CD and NMR studies have shown that a synthetic peptide corresponding to VDAC1 residues 2–20 exists as an unstructured peptide in aqueous solvent, while it forms α-helix structure from residues 5–16 in SDS [36]. The amphipathic α-helix is not part of the transmembrane domain: in particular, the portion including residues between Tyr7 and Val17 is located halfway into the pore's lumen, approximately in a central position corresponding to the hydrophobic layer of the membrane [33]. The N-terminus interacts with several β-strands, less stable than other regions of the β-barrel, probably due to the possibility of VDAC1 N-terminus to assume different conformations. As a cause or an effect of these conformational changes, the hydrogen bonds between the α-helix and the β-barrel are temporarily destroyed and rebuilt. Moreover, the fact that the α-helix is not a hydrophobic domain suggests that it could not be inserted permanently in the lumen, but can resides transiently on one side of the phospholipid bilayer [37]. The features of N-terminal domain will be discussed later.

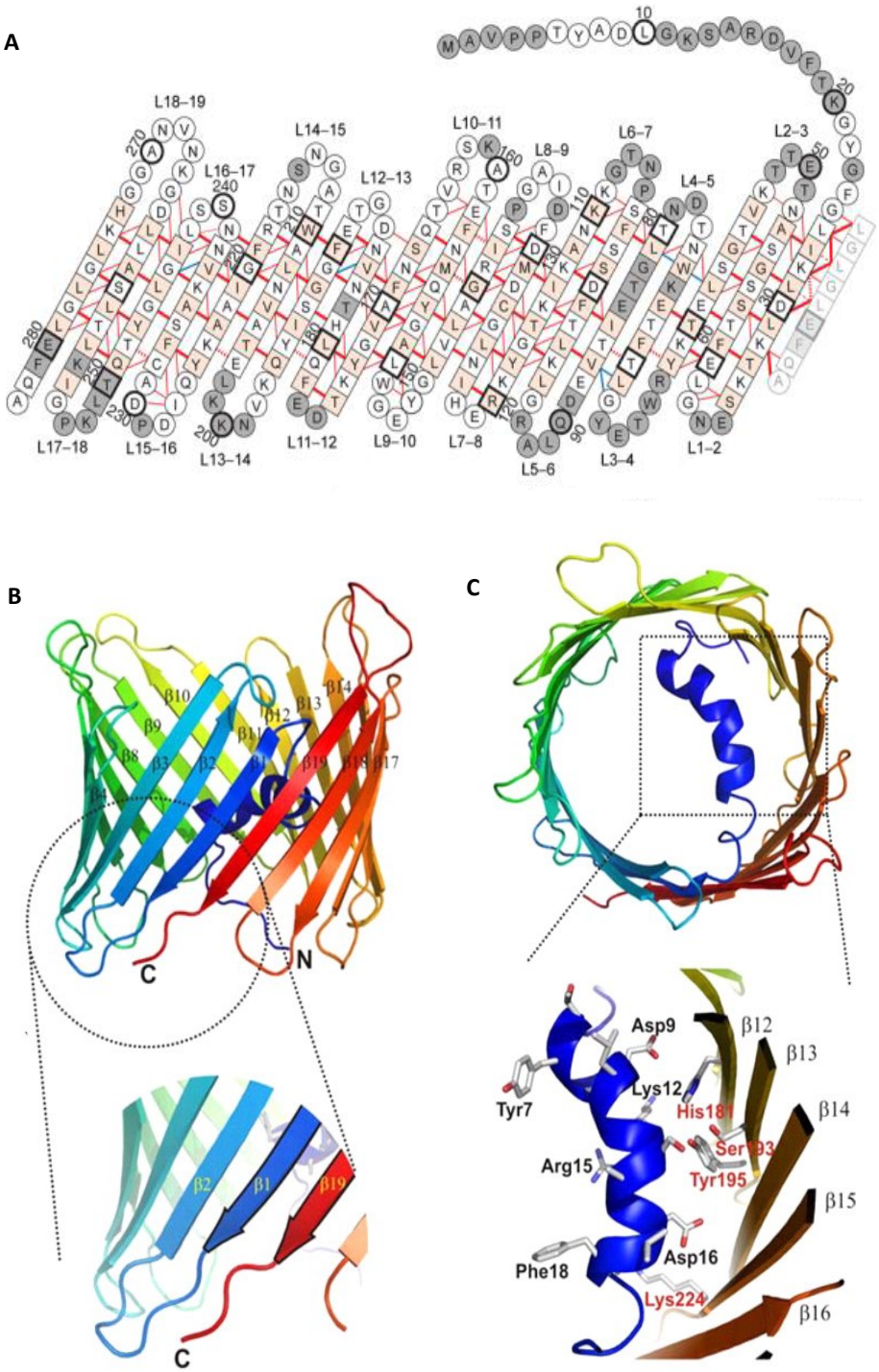

Fig 6 ***Architecture of human VDAC1.*** **A)** Schematic representation of the secondary structure of VDAC1, in which the amino acids in squares denote β-strands structure while all others amino acids are represented in circle. Red lines indicate the interaction between amino acids of the two interacting β-strands. Picture taken from [34] **B)** Tridimensional structure of VDAC1 from side view; in the enlargement it is showed the C-terminal domain of the protein. **C)** Structure of VDAC1 view from above; it shows the α-helix N-terminal domain located into the pore's lumen. The enlargement shows the interaction between the helix and specific residues of the β-barrel. Pictures taken from [33].

Due to its conformation, VDAC1 needs a specific transport system to the OMM. Mitochondria have developed several different system for the import of nuclear-encoded proteins. The fate of VDAC is inextricably related to the presence of the *Sorting and Assembly Machinery complex*, *SAM complex*, which promotes the incorporation of β-barrel proteins into the OMM. SAM complex consists of a membrane-embedded component, the subunit *SAM50* that has been shown to have a conserved role in VDAC biogenesis from yeast to mammalian. SAM complex is also important for the incorporation of TOM40, the main component of TOM complex, that, in turn, facilitates the recognition of most pre-proteins with a mitochondrial targeting sequence, their transfer through the membrane and the insertion of resident outer membrane proteins. Interestingly, as VDACs, also TOM40 and SAM50 are predicted to have a β-barrel topology [38].

1.2.4 Electrophysiological features of VDAC1

Functional properties of VDAC proteins have been examined using typical methods used for transmembrane proteins with a transfer function, which consist in their reconstitution in artificial phospholipid bilayers, such as vesicles or PLB. Despite the phylogenetic distance among eukaryotes as well as the divergence between protein sequences, analysis of reconstituted VDAC has shown a highly conserved pore formation activity and electrophysiological properties [39].

VDAC channels show a conductance or 4-4.5 nS in 1M KCl, which corresponds to the maximum theoretical value of a channel with VDAC dimension [40-41]. In addition, VDAC shows a weak anion selectivity and this feature can be perfectly explained by the presence of positively charged residues on the pore's lumen [35].

The main VDAC feature is its dependency from voltage.

At low voltages, from 0 up to around ± 10-20 mV, VDAC is stable in the open state, while at high voltages, either positive or negative, and starting from ± 30-40 mV, VDAC switch in a set of multiple partially closed sub-states with different ionic selectivities and permeabilities [42], as showed in Fig. 7.

A direct involvement of N-terminal domain in voltage-gating properties of VDAC1 was proposed.

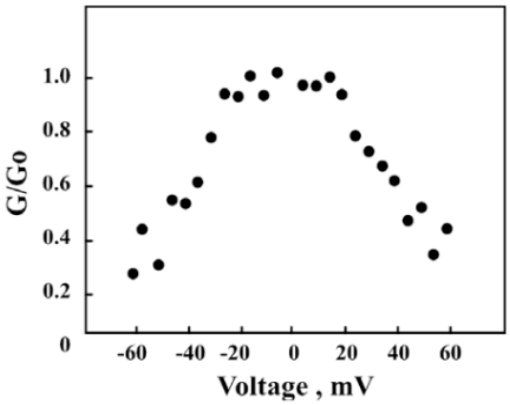

Fig 7 ***VDAC1 voltage-dependence.*** The average VDAC1 conductance analyzed at PLB is showed as function of the applied voltage; this voltage-dependence diagram for VDAC1 is a common and well known feature.

Indeed, the removal of N-terminal domain from VDAC1 results in the loss of voltage dependency: reconstituted VDAC1 in PLB maintains the open state at applied potentials higher than ± 40 mV [43]. The N-terminal domain is considered the most flexibly moiety of the entire protein; it was hypothesized that this domain can interact with different portion of the β-barrel lumen, modulating the opening and closing of the channel [44]. This hypothesis is supported by the presence of several hydrophobic residues on the β-barrel and on N-terminal domain, that can transient interact through hydrophobic interaction (see VDAC1 crystal structure in [34]).

1.2.5 The role of VDAC1 in the cell

VDAC proteins play a primary role in cell metabolism since they are considered responsible of the metabolic flux across OMM, which is crucial for the mitochondrial function and cell viability (Fig. 8). Metabolites, such as pyruvate and succinate, small molecules such as ATP/ADP, ions such as phosphate, magnesium and calcium, they all use VDAC pores to cross OMM [45-46]. In addition, VDAC interacts with several enzymes involved in glycolysis, such as *hexokinase*, *glucokinase* and *glycerol kinase*: this location guarantees to the enzymes a preferential access to mitochondrial ATP.

In general, VDAC behaves as an interface between cytosol and mitochondria, interacting with many cytosolic and mitochondrial proteins; these interactions, at times, can modulate VDAC activity and affect several physiological and pathological cellular mechanisms.

Hexokinase (HK) isoforms I and II catalyze the first step of glycolysis, using VDAC as mitochondrial docking site, and this interaction was proposed as a central point in promoting growth and survival of cancer cells [47]. Indeed, cancer cells show high propensity to utilize glucose via glycolysis at a much higher rate than normal cells, a phenomenon known as *Warburg effect*. It was found that HKI and II were overexpressed in many types of cancer, including colon, prostate, lymphoma, glioma, gastric adenomas, carcinomas and breast cancers; thus, the interaction between HK and VDAC proteins increases ATP availability and promotes the high rate of tumor growth [48-49].

In addition, the HK-VDAC1 binding protects cancer cells from mitochondria-mediated cell death. It has been demonstrated that VDAC regulates apoptosis through interaction with *Bcl-2* proteins, a family of regulators proteins of apoptosis in mammals, which includes both pro- and anti-apoptotic members. Under certain stimuli, the pro-apoptotic proteins *Bak* and *Bax* translocate to mitochondria and interact specifically with VDAC1, where they promote a death signal leading to OMM permeabilization, Cytochrome C (Cyt C) release and caspase activation [50-51]. In cancer cells, HK interaction with VDAC1 protects cells from apoptosis, blocking the interaction of Bax with VDAC1 [48].

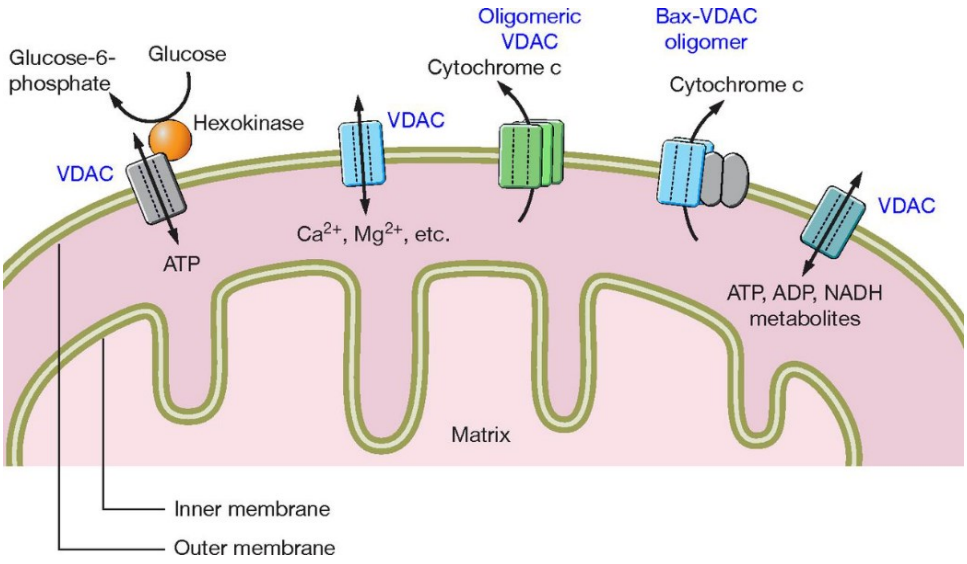

Fig 8 ***VDAC functions in OMM.*** VDAC represents one of the most important metabolic protein, since its involvement in ATP, metabolites, ions transport across OMM, and its interaction with several enzymes, such as Hexokinases, involved in glycolysis. However, VDAC plays a key role also in apoptosis regulation. VDAC can interact with the pro-apoptotic protein Bax, and it is supposed to be directly involved in Cytochrome c releases, the most known hallmark of mitochondria-mediated apoptosis. Picture taken from [45].

Independently from HK interaction, VDAC1 regulates apoptosis in response to several stimuli, such as increased levels of cytoplasmic calcium or ROS: in these conditions VDAC promotes OMM permeabilization that culminates with release of many apoptotic factors, such as Cyt C and AIF. These factors are responsible of caspase activation, destroying the cells from within. It has been proposed a direct VDAC involvement in OMM permeabilization and Cyt C releases: VDAC may form oligomers or hetero-oligomers with pro-apototic proteins Bax, that may result in larger pores through which Cyt C is released [52].

1.2.6 VDAC proteins in *S. cerevisiae*

The most known mitochondrial porin of *S. cerevisiae* is encoded by the single copy genes *por1* and is called *POR1* or *YVDAC1*, which represents one of the most expressed cellular protein, with more of 67000 unit per cell. As in high eukaryotes, POR1 provides the metabolic exchanges and it is involved maintenance of mitochondrial osmotic stability and mitochondrial membrane permeability.

Por1 gene is the fifty-fifth ORF of chromosome XIV and is constituted by a single exon of 852 bp that encodes for a protein of 283 amino acids. The protein shows a sequence homology of about 40% with the three isoforms of human VDAC and ability to form channel in PLB [53].

POR1 represents a fundamental protein for yeast viability under certain conditions. Yeast cells devoid of endogenous POR1 (*Δpor1*) show a partial growth defect on a non-fermentable carbon source, such as glycerol at 30°C, that is aggravated at elevated temperature, such as 37°C [54]. However, the ability of the *Δpor1* mutant of M22-2 yeast strain to grow at lower temperature means that some other protein must be able to partially substitute for that function. The analysis of yeast genome resulted in the discovery of a *por1* gene paralog, called *por2*. The encoded protein *POR2* or *YVDAC2* is definitely less characterized. It shares with POR1 around 49% of sequence homology (Fig. 9A) and, if overexpressed, is able to complement *Δpor1* growth defect on glycerol. While deletion of *por2* gene had no detectable phenotype, double mutant lacking both porins genes (*Δpor1Δpor2*) is viable but shows a more severe growth defect (Fig. 9B).

A

```
YVDAC1- MSPPVYSDISRNINDLLNKDFYHATPAAFDVQTTTANGIKFSLKAKQPVKDGPL  54
   Con-       ++DISR++N L N+DF+H  P + ++ TTT NG+ F+LKAKQ V +GP+
YVDAC2- MALRFFNDISRDVNGLFNRDFFHTNPLSLNISTTTENGVNFTLKAKQGVTEGPI  54

YVDAC1- STNVEAKLNDKQTGLGLTQGWSNTNNLQTKLEFANLTPGLKNELITSLTPGVAK 108
   Con-  T+VE +  D++ G+ L+Q WSN N L T++EF+ + PG K ++   LTP   K
YVDAC2- QTSVEGRFYDRKEGVSLSQSWSNQNRLNTRIEFSKIAPGWKGDVNAFLTPQSIK 108

YVDAC1- SAVLNTTFTEPFFTARGAFDLCLKSPTFVGDLTMAHEGIVGGAEFGYDISAGSI 162
   Con- +A  N ++ +  F AR + D+ L+   FVG +T+ H G VGG +  YD +AG
YVDAC2- NAKFNLSYAQKSFAARTSIDI-LQPKDFVGSVTLGHRGFVGGTDIAYDTAAGLC 161

YVDAC1- SRYAMALSYFAKDYSLGATLNNEQITTVDFFQNVNAFLQVGAKATMNCKLPNSN 216
   Con- +RYAM++ Y A++YS   + NN Q  T  FFQNVN +LQVG KAT+  K  +SN
YVDAC2- ARYAMSIGYLAREYSFILSTNNRQCATASFFQNVNRYLQVGTKATLQSKT-SSN 214

YVDAC1- VNIEFATRYLPDASSQVKAKVSDSGIVTLAYKQLLRPGVTLGVGSSFDALKLSE 270
   Con- +NIEF TRY+PD+ SQVKAK++DSG+ TL+YK+ L   ++LGVG SF+AL+L+E
YVDAC2- MNIEFVTRYVPDSISQVKAKIADSGLTTLSYKRNLNKDISLGVGMSFNALQLTE 268

YVDAC1- PVHKLGWSLSFDA                                        283
   Con- PVHK GWSLSF
YVDAC2- PVHKFGWSLSFSP                                        281
```

B

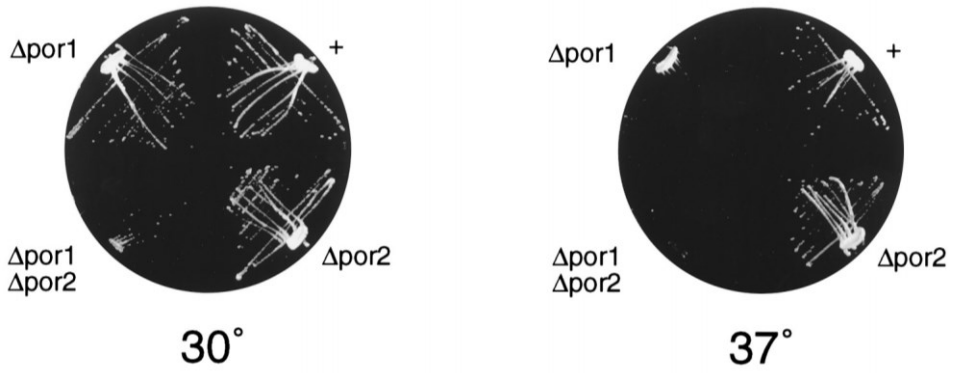

Fig 9 ***Properties of yeast VDAC proteins sequences.*** **A)** Alignment between the two yeast VDAC isoforms; sequence identities are indicated by the single-letter amino acid code in the line labeled Con. Dashes in the POR2 sequence indicate gaps introduced to optimize alignment. **B)** Growth of Δpor1, Δpor2 and double mutant yeasts compared to wild-type yeast (+). Strains were streaked on glycerol based medium and incubated at the indicated temperatures. Picture taken from [55].

However, POR2 was not able to form channels in reconstitution experiments [55]. Indeed, mitochondrial membranes from wild-type cells and from single and double mutant overexpressing POR2, do not confer any permeability when incorporated to liposomes. These results strongly suggest that POR2 is normally not able to form channels.

The *Δpor1* yeast strain has become a very convenient model system to study heterologous VDAC proteins from other sources. For example, it has been showed that mouse or human VDAC isoforms can partially or totally complement the absence of endogenous VDAC in yeast. While VDAC1 and 2 can fully recover the yeast growth defect, VDAC3 can partially recover the growth defect, underlining once again a difference in VDAC3 function [56-57].

1.2.7 VDAC N-terminal domain

The VDAC1 N-terminal domain has been the subject of considerable interest. This domain is not only involved in voltage gating, as previously described, but it plays a key role in interaction with other molecules such as HK [58] and in apoptosis regulation: N-terminal deletion, indeed, decreases the pro-apoptotic effect of VDAC1 over-expression [43]. In addition, N-terminus is considered responsible of the gating of the pore, due to conformational changes or movements mediated by this moiety [60]. Particularly, have been identified several hydrophobic residues on both β-barrel and N-terminus, that can transiently interact. NMR analysis have revealed that the contact between two part of the protein is based on the interaction between the methyl groups of Leucine 10, located on the N-terminal α-helix, and the Valine 143 and Leucine 150, located on the opposite side of the β-barrel. This data is supported by the fact that Val 143 and Leu 150 are the only residues with a hydrophobic side chains in the barrel wall pointing to the lumen. [34, 60]. A model of interaction is reported in Fig. 10.

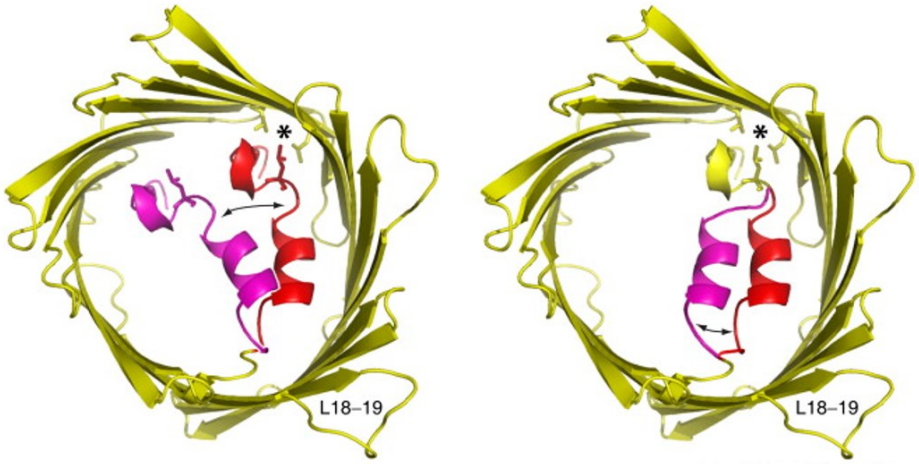

Fig 10 ***N-terminus involvement in voltage gating.*** A gating models for VDAC1. Shown in yellow and red is the 2.3 Å crystal structure of VDAC-1 (PDB: 3EMN). The side chains of residues Leu 10, Val 143 and Leu 150 are shown in stick representation and their hydrophobic contact point is marked with an asterisk. In each model, a certain amino acid segment, which is marked red, undergoes a conformational exchange to a fictive, magenta conformation, indicated by black arrows. Picture taken from [60].

Most part of the differences between human VDAC isoforms are present in the N-terminal domain. Compared to VDAC1, isoform 2 shows an N-terminal domain longer of 12 amino acids, even if this difference does not modify the voltage-dependency and the ability to complement the absence of endogenous porin in

Δpor1 strain. The N-terminal region of VDAC3 differs form VDAC1 for presence of two cysteine residues in position 2 and 8. Cysteine content, that represents a peculiarity of isoform 3, seems to be the basis of the different behavior of this isoform. To fully understand the peculiar role of VDAC3 N-terminal domain, a set of chimerical protein were created by the swapping of the first 20 amino acids of VDAC3 with the corresponding regions of VDAC1 (*N1-VDAC3* chimera) and VDAC2 (*N2-VDAC3*), and then expressed in yeast *S. cerevisiae Δpor1* strain. It has been found that expression of these chimerical proteins in yeast cells confers an increased life span compared to VDAC3 and confers resistance to the yeast against incubation with reactive oxygen species [61].

1.3 The Superoxide Dismutase I

1.3.1 Appearance of antioxidant enzymes

The appearance of molecular oxygen on Earth can be considered the factor most responsible of the environmental changes started around 3.5 billions of years ago. Produced by the first photosynthetic cyanobacteria, oxygen has started to accumulate in the atmosphere and, for the first time, to interact with oxidizable elements such as iron, modifying the atmosphere composition through the conversion of methane in carbon dioxide [62]. This process provided new opportunities for the living organisms, energetically limited at that time, promoting the biological diversification: the oxygen availability has increased significantly the energy sources and imprinted an important thrust for metabolism evolution.

Life, as we know it today, requires oxygen for its existence and has developed cellular systems able to use oxygen efficiently, such as mitochondria; nevertheless, oxygen is considered a highly reactive molecule. The molecular oxygen (O_2) is a bi-radical containing two unpaired electrons in the outer shell; this molecule can only react with one electron at a time, producing a set of relatively stable intermediates known as ROS, Reactive Oxygen Species [63]. The product of one-electron reduction of O_2 is the *superoxide anion* ($O_2^{-}\bullet$). Quite toxic for the cell, superoxide anion represents the precursor of most ROS: its spontaneous or enzymatic

dismutation produces *hydrogen peroxide* (H_2O_2), which may be fully reduced to water or partially reduced to *hydroxyl radical* (OH•) [64].

The primary source of superoxide anion *in vivo* is represented by mitochondrion: most steps in the mitochondrial electron transport chain involve single-electron reactions, further favoring the superoxide anion production [65].

Although small fluctuations in the steady-state concentration of ROS plays a key role in intracellular signaling, accumulation of ROS in the cell actually promotes damage in mitochondria and cellular organelles. In general, harmful effects of ROS are represented by damages of mitochondrial and nuclear DNA [66], lipid peroxidation [67], oxidations of amino acids in proteins, oxidation of co-factors in specific enzyme [68].

Many molecules, introduced by the diet, show an antioxidant activity: e.g., ascorbic acid (vitamin C), with its reducing activity, may be oxidized by ROS with the loss of two electrons (one by one, forming a radical intermediate) to form a stable molecule of dehydroascorbic acid. Other molecules, such as vitamin E, glutathione, polyphenol, uric acid, use a similar mechanism. However, cells have evolved well-defined strategies to defend themselves against ROS damage. Specific enzymes, such as *Superoxide Dismutases* (*SOD*), *Catalases*, *Peroxiredoxins* and *Glutathione peroxidases*, destroy ROS using a more complex mechanisms; indeed, all these enzymes contain one or more metal co-factors directly involved in the catalysis. Differently from antioxidant molecules, enzymes act in specific manner: e.g., SOD catalyzes dismutation of superoxide anion producing hydrogen peroxide that, in turn, represents the substrate for catalases and peroxidases.

Despite the presence of this massive antioxidant arsenal in the living organisms, ROS can be responsible of several inflammatory states and pathologies. It has been demonstrated by many studies that excessive amounts of ROS can lead to cell injury and death, contributing to development of diseases as myocardial infarction, diabetes and cancer; particularly, ROS can react with genomic DNA, resulting in mutations that potentially affect cell cycle [69]. ROS accumulation is also associated to several neurodegenerative diseases, such as Parkinson’s and Alzheimer's disease and several forms of schizophrenia [70]. In addition, several

evidences correlated ROS accumulation with aging, proposing that free radicals underlie the aging process itself.

1.3.2 The Superoxide Dismutase family

The *Superoxide Dismutase* (*SOD*) enzymes are a big family belonging to the *oxidoreductase* class. Initially classified as a metalloprotein with unknown function, SOD activity was discovered in 1969 by Fridovich and McCord. SOD enzymes catalyze the dismutation of superoxide anion into molecular oxygen and hydrogen peroxide, due to the presence of a metal co-factor in the active site [71]. It has been estimated that under physiological conditions, the rate of the enzymatic reaction is around 10^4 times faster than that of the spontaneous disproportionation of superoxide anion in solution. Reaction of dismutation mediated by SOD is composed by two sequential steps, and is described below:

$$M^{(n+1)+}\text{-SOD} + O_2^- \rightarrow M^{n+}\text{-SOD} + O_2$$

$$M^{n+}\text{-SOD} + O_2^- + 2H^+ \rightarrow M^{(n+1)+}\text{-SOD} + H_2O_2$$

in which *M* represents the metal co-factor and *n* is the oxidation state of metal cation, that oscillates between *n* and *n*+1.

Based on the metal co-factor, SOD proteins are divided into three major groups, as showed in Fig. 11. They are:

- *Cu/Zn-SOD*, containing both copper and zinc ions, shows dimeric or tetrameric structure and it is localized mainly in cytosol of all eukaryotes;

- *Fe-SOD* and *Mn-SOD*, containing alternatively iron or manganese ions, show tetrameric structure and were found prevalently in prokaryotes and protists, but also in plant chloroplast (Fe-SOD) and mitochondria (Mn-SOD);

- *Ni-SOD*, containing nickel, shows hexameric structure and it was found exclusively in prokaryotic cells [72].

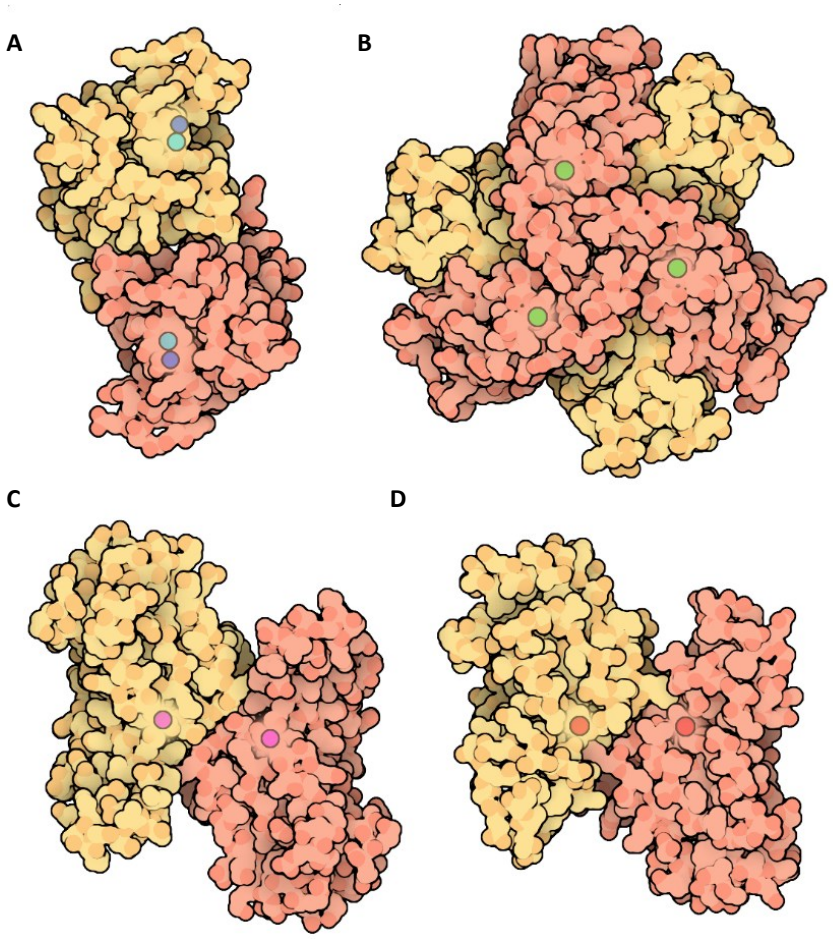

Fig 11 ***Structures of SOD proteins***. Tridimensional structures of SOD proteins. **A)** The dimeric form of Cu,Zn-SOD. **B)** The Ni-SOD structure. **C)** The Fe-SOD structure. **D)** The Ni-SOD. Picture taken from Protein Data Bank.

Humans, such as most mammals and chordates, contain three different SOD isoforms encoded by three different genes, whose structures have been extensively characterized [73]. The *sod1* gene is located on chromosome 22 (21q22.1) and encodes for a dimeric Cu/Zn-SOD, located mainly in the cytosol. The protein SOD1 represents the most abundant isoform and performs around 95% of dismutase activity. SOD1 will be described subsequently.

Sod2 gene is located on chromosome 6 (6q25.3) and encodes for a Mn-SOD called SOD2. Both genomic organization and encoding sequence of s*od2* show high level of interspecies conservation but no homology with s*od1*, suggesting an independent origin for these two proteins. SOD2 protein is a tetramer formed by four identical subunit; each subunit shows a molecular weight of 23 kDa and contains one Mn^{2+} ion in the active site. Although the expression profiles of SOD1

and 2 are really similar in humans, SOD2 is located exclusively in the mitochondrial matrix, where it is supposed to have a primary role in detoxification from ROS produced in mitochondria. The importance of SOD2 function in mammals was confirmed by disruption of the gene, which turns out to be lethal for mice due to neurodegeneration and damage to the heart [74]; moreover, mutations in *sod2* gene have been associated with several pathologies, as idiopathic cardiomyopathy, cancer and motor neuron disease.

The *sod3* gene is on chromosome 4 (4p15.3-p15.1) and encodes for a Cu/Zn-SOD called SOD3. *Sod3* shares around 50% of similarity with *sod1* at the exon level, but no similarity with *sod2*. SOD3 is the most recently discovered and least characterized member of SOD family. SOD3 is a tetramer formed by four identical subunit of around 33 kDa, with one Cu^{2+} and one Zn^{2+} ions per subunit; the enzyme is also known as Extracellular-SOD (Ec-SOD) because it is exclusively present in extracellular fluids, such as human plasma, lymph, ascites and cerebrospinal fluids [75]. Thus, in contrast to intracellular SOD proteins, expression of SOD3 appears restricted to only a few cell types in specific tissues, such as alveolar type II cells, vascular smooth muscular cells, lung macrophages and few cultured fibroblast cell lines [76-77].

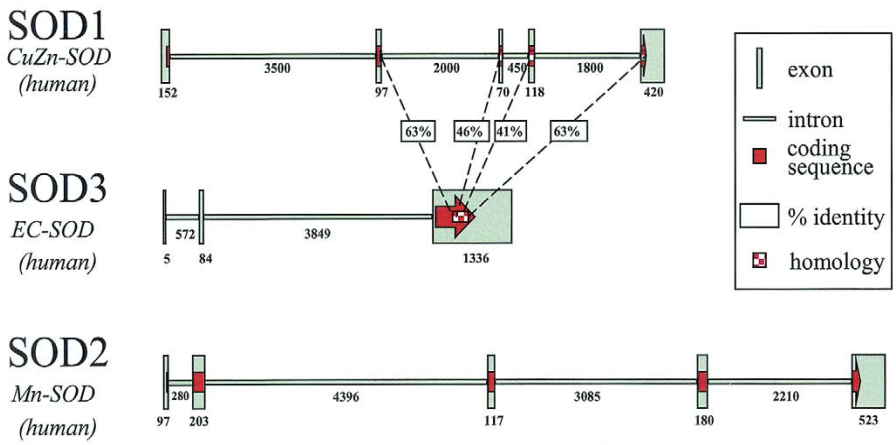

Fig 12 ***Genomic organization of human SOD genes***. SOD3 was placed in the middle in order to demonstrate areas of amino acid sequence homology between SOD1 and SOD3. SOD2 has no significant amino acid sequence homology with either SOD1 or SOD3. The size of each exon and intron, in base pairs, is shown in association with that fragment. Picture taken from [69].

1.3.3 Genomic organization of SOD1

The genomic organization of *sod1* gene shows a striking similarity among species. *Sod1* gene is characterized by five exons and four introns, a promoter containing TATA box, CCAAT box and several highly conserved GC-rich regions. Analysis of 5'-flanking sequence shows a high level of homology during evolution, assuming for this region a preserved key regulatory role for SOD1 expression. In addition, several putative binding sites for transcription factors have been found in *Sod1* promoter, such as sites for NF1, Sp1, AP1, AP2, GRE, HSF, and NF-κB [78].

The 3'-end of *sod1* gene is characterized by the presence of several poly(A) signal sequences that terminate the mRNA species with different lengths. To these, several consensus sequences, as YGTGTTYY and a G/T cluster, are associated, required for an efficient formation of 3'-termini.

As previously reported, *sod1* gene is located on chromosome 21, which has been studied intensely due to the association of the trisomy of 21 with Down's syndrome. Due to the presence of more copies of chromosome 21, the patients with Down's syndrome show around 50% of SOD1 activity increase; however, the role of SOD1 in pathologies, associated with this disease remains questionable, since no obvious implication in the development of the major symptoms was demonstrated [79]. Conversely, a well-known correlation was found between mutations in *sod1* gene and the onset of several familial form of *Amyotrophic Lateral Sclerosis* (*ALS*), a neurodegenerative disease characterized by the loss of motor neuron in brain stem and spinal cord. In 1993, 11 mutations in *sod1* were described for the first time and associated to ALS, providing the first molecular insight into the pathogenesis of this disease [80]. Today, over 150 mutations ALS-associated have been characterized. However, SOD1-mediated disease mechanism is not still clear. Involvement of SOD1 in ALS will be further discussed subsequently.

1.3.4 The structure of human SOD1

SOD1 protein is a homodimeric enzyme of 32 kDa formed by two subunit of 153 amino acids. The overall fold of the subunit consist in eight antiparallel β-strands connected by seven loops that form a flattened β-barrel with Greek key topology

[81]. A very important part of the single subunit is represented by the three external loops, which form a major structural element (Fig. 13).

Particularly, the loop IV includes a *Zn-binding region* involved in zinc coordination; the loop VII includes the *electrostatic loop,* which participates in electrostatic channel formation, through which superoxide is guided towards the active site. The electrostatic loop contains several charged residues, such as Arg143, that are directly involved in the electronic guidance of the substrate to the active site and contribute to the high specificity of SOD1 for the superoxide anion substrate. The smallest loop forms a Greek key connection across one end of the β barrel. The disulfide bond, which forms a left-handed spiral, covalently joins the largest loop to the beginning of the β-strand 8, representing another important structural element [82].

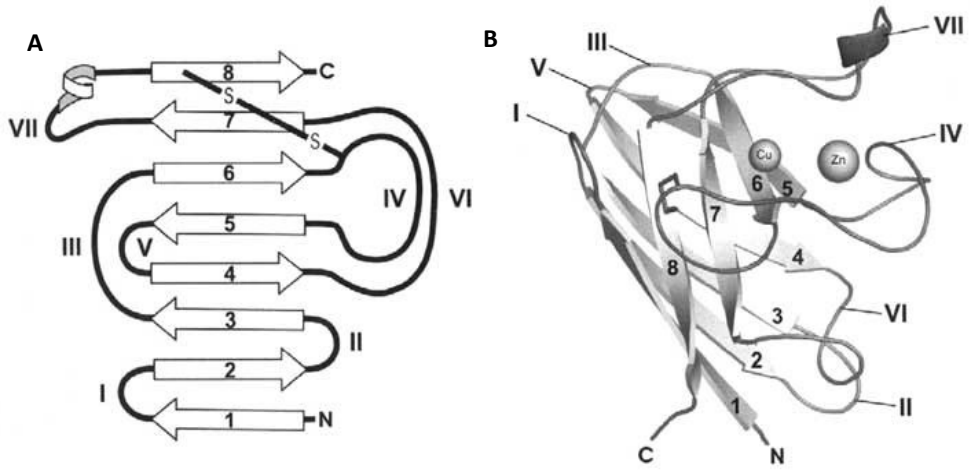

Fig 13 ***Structure of human SOD1 subunit.*** **A)** SOD1 subunit shows a secondary structure composed by eight β-strands antiparallel and seven loops. **B)** The tridimensional structure of the subunit. Picture taken from *Peter Doucette PhD Thesis, 2004, UCLA*.

The SOD1 active site contains one Cu (II) and one Zn (II) ions per subunit, which interact with polypeptide chain through non-covalent interactions. It was demonstrated that Zn ion has mainly a structural role, being necessary to stabilize the active site; anyway, it was observed that its removal decreases the redox potential of Cu and the catalytic abilities of the entire enzyme. Zn is coordinated to the protein due to the presence of three histidine residues, in position 61, 69 and 79, and an aspartic acid residue, in position 81. The Cu^{2+} ion, which represents the catalytic site, is coordinated by four imidazole of histidine residues, in position

44, 46, 61, 118 and a fifth axial coordination position exposed to solvent and represented by a molecule of water; the side-chain of His61 forms a bridge between the Cu and Zn [82-83].

For the correct positioning of the metal cofactors, as well as for the proper achievement of protein folding, the newly synthesized polypeptide chain undergoes several post-translational modifications, which make the protein functional. The post-translational modifications are supported by the presence of specific chaperones, called CCS, Copper Chaperone of SOD1 [84].

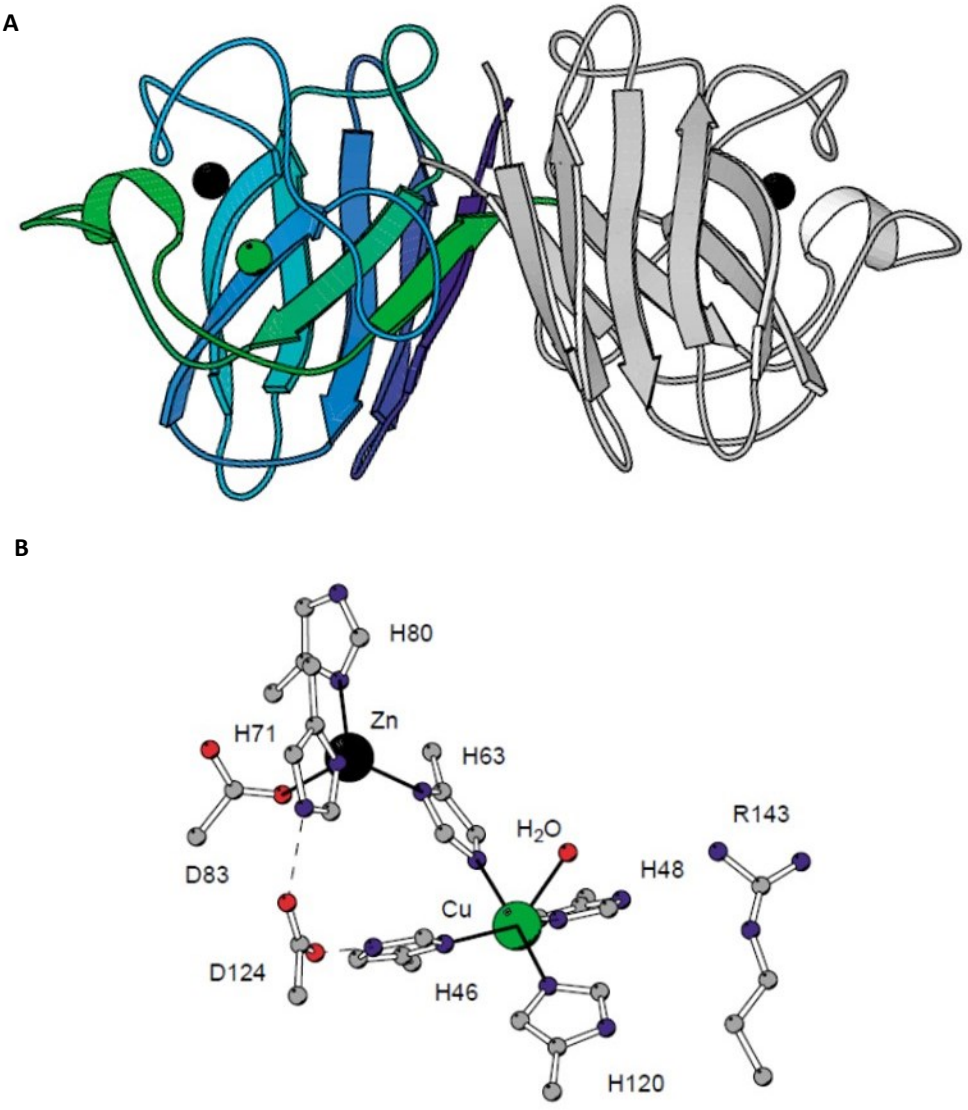

Fig 14 ***Structure of human SOD1 and its active site.*** **A)** The dimeric structure of human SOD1 formed by two identical subuinit of 16 kDa each. Each subunit shows eight antiparallel β-strands connected by seven loops that form a flattened β-barrel with Greek key topology. **B)** Schematic representation of the active site of the single subunit, which contain both zinc and copper ions. Zn ion is coordinated to the protein due to the presence of His61, 69 and 79, and an aspartic acid residue, in position 81. Cu ion is coordinated by four imidazole of histidine residues, in position 44, 46, 61, 118 and a fifth axial coordination position exposed to solvent and represented by a molecule of water; the side-chain of His61 forms a bridge between the Cu and Zn. Picture taken from [81].

The process starts with the hetero-dimerization between SOD1 monomer and CCS followed by coordination of Zn ion, transfer of Cu ion and the formation of a disulfide bond between cysteine residues 57 and 146 that stabilizes the structure. The process ends with the dimerization of two perfectly folded subunits [85]. The reaching of correct protein folding protein leads to the formation of a channel, due to the presence of positively charged amino acid residues; the amino acids disposal allows the formation of an electrostatic field that facilitates the approach and the subsequent association of the superoxide radical with the metal.

1.3.5 SOD enzymes in *S. cerevisiae*

As mammals, the budding yeast *S. cerevisiae* expresses two intracellular SOD isoforms: a cytosolic Cu,Zn-SOD, called SOD1 and the mitochondrial Mn-SOD, SOD2. SOD1 accounts for 90–95% of the total superoxide dismutase activity in *S. cerevisiae*: strains lacking SOD1 (*Δsod1*) show more severe defects than strains lacking SOD2 (*Δsod2*) [86]. In addition, SOD1 is considered essential for yeast survival during the stationary phase, which is characterized by high rate of respiration, thus more ROS production. Indeed, viability of Δsod1 strain significantly ameliorates by abolishing the mitochondrial respiration [87]: this underlines once again that SOD1 is involved in protection from oxidative stress promoted by respiration.

Therefore, function and activity of yeast enzymes is comparable to that performed by the homologous proteins of higher eukaryotes. In particular, yeast and human SOD1 share 70% homology and over 90% identity in their active-site residues, as showed by the followed sequence alignment:

```
hSOD1  MATKAVCVLKGDGPVQGIINFEQKESNGPVKVWGSIKG-LTEGLHGFHVHEFGDNTAGCT 59
ySOD1  -MVQAVAVLKGDAGVSGVVKFEQASESEPTTVSYEIAGNSPNAERGFHIHEFGDATNGCV 59
         .:**.*****. *.*:::*** ... *..*  .* *  .:. :***:***** * **.

hSOD1  SAGPHFNPLSRKHGGPKDEERHVGDLGNVTADKDGVADVSIEDSVISLSGDHCIIGRTLV 119
ySOD1  SAGPHFNPFKKTHGAPTDEVRHVGDMGNVKTDENGVAKGSFKDSLIKLIGPTSVVGRSVV 119
       ********:.:.**.*.** *****:***.:*::***. *::**:*.* *  .::**::*

hSOD1  VHEKADDLGKGGNEESTKTGNAGSRLACGVIGIAQ 154
ySOD1  IHAGQDDLGKGDTEESLKTGNAGPRPACGVIGLTN 154
       :*   ******..*** ******.* ******:::
```

The high level of sequence conservation allows the expression of an active human SOD1 in yeast, which significantly increases resistance to both oxidative and heat stress of yeast cells. Overexpression of hSOD1 increase up to 50% of cell survival after treatment with oxidizing agents, such as menadione or paraquat, or heat shock compared to the controls [88].

1.3.6 Distribution and localization of SOD1

SOD1 is constitutively expressed and shows widespread distribution in a large variety of cells, where it represents one of the most abundant protein of the entire cell. Here, SOD1 plays a key role in controlling steady-state levels of ROS and oxidative stress. Moreover, the regulation of *sod1* gene transcription may be subjected to control by both intra- and extra-cellular stimuli, such as heat shock, UV and X ray irradiation, increased levels of heavy metals or hydrogen peroxide [89], all cases in which SOD1 may help in oxidation control.

SOD1 is prevalently located into the cytosol [90], although under certain conditions SOD1 shows specific intra-organelles localization. For example, SOD1 was found in lysosomes and peroxisomes, even if the role of the enzyme in this compartment remains to be elucidated [91-92]. In yeast, a fraction of SOD1 localizes in IMS in association with its CCS, where it promotes prolonged survival in the stationary phase, diminishing the oxidative stress [93]; the redistribution of SOD1 in IMS was confirmed also in mammals [94].

1.3.7 Antioxidant-independent roles of SOD1

SOD1 is one of the most conserved enzymes throughout evolution due to its important antioxidant action. However, recent studies have suggested that the SOD1 role is much more extensive than its involvement in oxidative stress protection. For example, a series of metabolic alterations have been found in yeast cells devoid of endogenous SOD1 (*Δsod1*).

In presence of glucose, yeast cells grow in an exponential way using fermentation and repressing the expression of the respiratory machinery (catabolite repression), as long as the sugar is abundant. It was observed that *Δsod1* yeast cells exhibit an impaired aerobic growth under fermentative conditions, while they grow better

on non-fermentable carbon sources, such as lactate and pyruvate. In these conditions, *Δsod1* yeast shows also an increase in oxygen consumption and shorter survival times in stationary phase [86]. In addition, the mitochondrial mass in *Δsod1* yeast cells is approximately doubled compared to wild-type cells: this, in association with observed higher oxygen consumption when glucose is abundant, strongly indicates the presence of a defect in glucose repression [95].

Initially, the growth defect shown by *Δsod1* was attributed to an increased oxidative stress shown by the strain lacking endogenous SOD1; however, it has been shown that SOD1 plays a key role in respiration inhibition, independent of its antioxidant function, participating in the integration of signals from glucose and oxygen concentration [96].

Glucose activates a signal transduction pathway via the glucose-sensor on the plasma membrane, SNF3 and RTG2, which modulates the glucose sensing and the repression of respiration; activation of this pathway requires also the yeast homologous *casein kinase I* γ (CK1γ) YCK1 and its paralog YCK2 (Fig. 15A) [97]. YCK1/2 directly act on the detachment of the transcriptional repressor RGT1, coupled to MHR1, promoting its phosphorylation and subsequent degradation that results in RGT1 detachment and leads to the constitutive expression of glucose transporter HXT genes [98-99].

SOD1 protein is directly involved in maintenance the stability of YCK1 and YCK2 kinases, for respiratory repression. SOD1 binds to a specific YCK region, identified in residues 367–412, and prevents its degradation through a mechanism involving lysines at the YCK C-terminus (Fig. 15B). Particularly, the superoxide anions

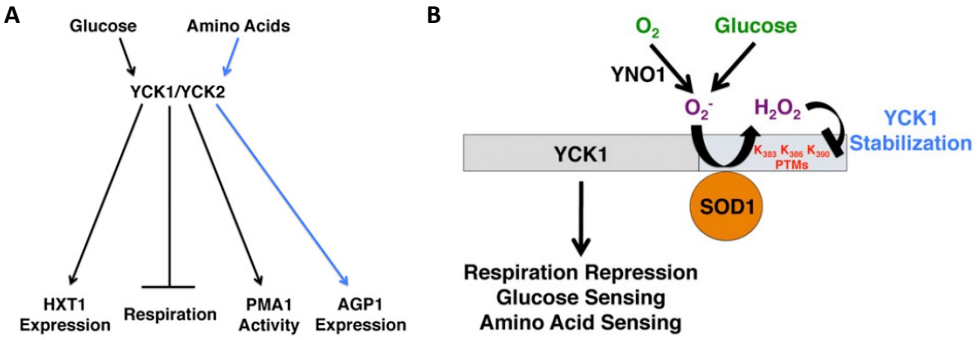

Fig 15 ***Role of YCK1/2 proteins in glucose metabolism.*** **A)** YCK1/2 proteins are directly involved in glucose sensing, repression of respiration, and in the extracellular amino acids signaling. **B)** SOD1 stabilizes YCK1/2 protein structure allowing to these proteins the activation of glucose metabolism. Pictures taken from [96].

generated during growth in the presence of glucose and oxygen feeds into cytosolic SOD1, and the concomitant production of hydrogen peroxide helps stabilizing the YCK kinases for nutrient signaling. In addition, SOD1 can maintain this function also for human CK1γ proteins, indicating that this mechanism is conserved through the evolution [96].

In a very recent work, it was shown in *S. cerevisiae* that the increase of oxidative stress induced by hydrogen peroxide or menadione promotes SOD1 translocation to the nucleus, where it is assumed that it plays a crucial role in DNA protection from oxidative damage. This change in SOD1 localization is specifically related to ROS increase, as demonstrated by the involvement of ATM/Mec1 kinase, a well known ROS sensor [100]. The activation of ATM pathway promotes the association of SOD1 with DUN1, that is responsible of specific phosphorylation of serine residues 60 and 99 of SOD1, conserved also in mammalian SOD1. Furthermore, once in nucleus, SOD1 acts as transcription factor: it directly binds promoters and regulates the expression of genes involved in ROS resistance and DNA damaging repair [101]. Mechanism is extensive explained in Fig. 16.

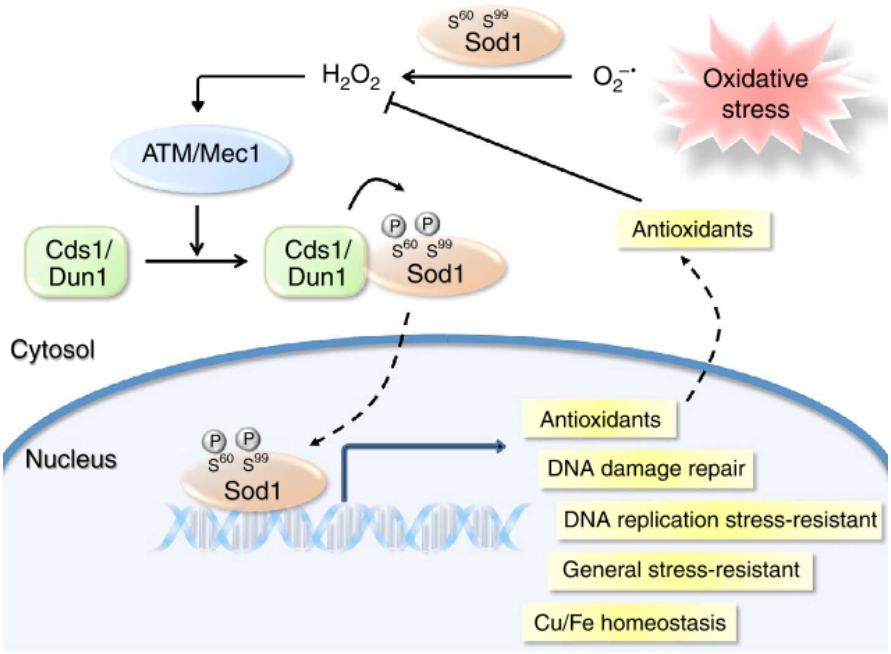

Fig 16 ***Proposed model of SOD1 traslocation into the nucleus.*** Hydrogen peroxide promotes SOD1 phosphorylation by ATM/Mec1 pathway activation, through SOD1 interaction with Dun1 kinase. Phosphorylated SOD1 traslocates to the nucleus where it acts a transcription factor involved in regulation of a set of gene that promote response to oxidative stress. Picture taken from [101].

Phosphorylation of SOD1 was found also in mammalian and human cells, suggesting that this SOD1 role is conserved through the evolution. The fact that this SOD1 function is regulated by the increase of H_2O_2 rather than its substrate superoxide anion, confirms the ability of SOD1 to act independently from its antioxidant role.

1.3.8 Relationship of SOD1 with VDAC1

Mitochondrion is considered the intracellular site of ROS production and then one of the main targets subjected to oxidative damage. It cannot be considered a coincidence that mitochondria possess a specific SOD isoform for the matrix (SOD2) and that a portion of cytosolic SOD1 is localized in the IMS. This massive presence of SOD in mitochondria is certainly correlated with the high necessity of oxidative stress protection in this organelle. In particular, one of the most common damage promoted by superoxide anion is the carbonylation of amino acid residues, a modification that can inactivates or irreversibly damage enzymes and proteins. In yeast, it has been demonstrated that SOD enzymes and specifically SOD1 are required for the protection of several proteins of OMM, such as POR1 [102].

Anyway, the relationship between SOD proteins and VDAC isoforms is more extensive. In yeast mutant strains *Δpor1* and *Δpor1Δpor2*, the activity and expression level of IMS-located SOD1 is changed compared to wild-type yeast: e.g., the absence of POR1 dramatically reduces SOD1 activity in the exponential phase, while it results increased during stationary phase, the opposite of what happens in normal conditions [103]. Many other interesting evidences on VDAC-SOD1 relationship were discovered in yeast strain devoid of endogenous SOD1. In *Δsod1* the probability of VDAC1 transition into low-conductance state is distinctly higher and the voltage-dependence of the POR1 is significantly less evident; moreover, the expression level of VDAC1 in this strain is lower than in wild-type, as well as, the level of other proteins of OMM such as the outer membrane translocase components Tom40 and Tob55 [104]. Taken together, these evidences underlined a mutual relationship between these two proteins.

1.4 The Amyotrophic Lateral Sclerosis

1.4.1 Clinical features of ALS

Amyotrophic lateral sclerosis (ALS), known also as *Lou Gehrig's disease*, is a neurodegenerative disease that affects specifically both upper and lower motor neurons of specific regions of the central nervous system (CNS), such as motor cortex, brain stem and spinal cord. Discovered in 1869 by Jean-Martin Charcot, ALS represents today one most common adult-onset disorder of motor neurons, with an incidence of approximately 1 in 100000 people [105].

Around 90% of incidences of ALS are sporadic and without an obvious genetic component, while approximately 10% are inherited in a dominant manner, and we refer to this condition as familial ALS (fALS). However, both sporadic and familial ALS produce similar pathological hallmarks. As consequence of motor neurons degeneration, patients have muscle weakness and atrophy, up to lose the ability to initiate and control the voluntary movement, which results in difficulty speaking, swallowing, and breathing; the patient's death is usually due to respiratory failure [106].

Although less commons, fALS forms are the most studied. Indeed, it is not excluded that the effects of specific mutations can promote mechanisms quite similar to those that occur in sporadic forms. To date, more than 10 different genes have been identified whose mutations are cause of as many forms of fALS [107]. In addition, several fALS forms are directly linked to the onset of other neurodegenerative disease as *Frontotemporal Dementia* (ALS-FTD) and both FTD coupled with *Parkinson's disease* (ALS-FTDP).

Mutations in the SOD1 gene are the most common form of inherited ALS (known as ALS1), accounting for around 20% of all the familial ALS forms and corresponding to 2% of all ALS cases.

In contrast, mutations in genes encoding for alsin (ALS2), angiogenin (ALS9), VAMPB (VAMP-associated protein type B) (ALS8), are extremely rare [108]. Recently, fALS has been associated with two structurally and functionally related genes, that encode respectively for the proteins TARDP (Transactive response DNA-binding protein of 43 kD) and FUS (fused in sarcoma). Over 30 mutations TARDP

and 13 mutations in FUS, were identified in respectively 1-3% and 2-5% of fALS patients [109].

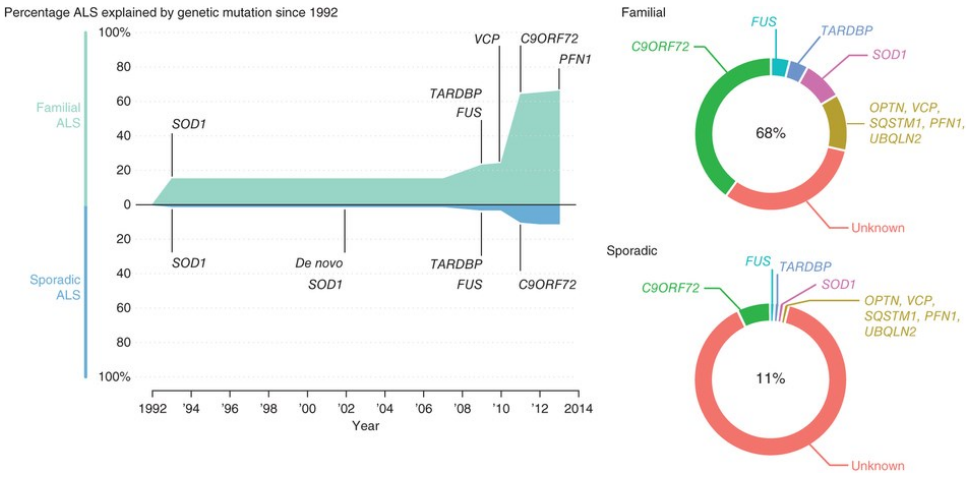

Fig 17 ***Involvement of genes in both sporadic and familial ALS.*** A schematization of genes involved in the onset of fALS and comparison with correlated protein dysfunctions in sporadic ALS. Picture taken from [107].

1.4.2 SOD1 mutations in ALS1

Involvement of SOD1 in ALS was discovered in 1993 as described by Rosen et al. [80]. Today, more than 150 mutations are considered responsible of the SOD1-mediated disease, distributed throughout all five exons encoding the 153 amino acid protein, with no region of the polypeptide escaping disease causing mutation. SOD1 mutations are mostly missense substitutions; furthermore, the frameshift deletion and insertion of respectively 8 and 5 bases, all located in exons 4 and 5, lead to a truncated form of the protein that can be involved in the pathology [110]. Both sporadic and familial ALS mediated by SOD1 mutant are clinically indistinguishable and affect the same neurons; however, in the familial forms, the time of onset and length of disease vary depending from the mutation. For example, one of the most frequent mutations, A4V (replacement of alanine with valine in position 4), shows lighter effects in affected motor neurons but, at the same time, an early onset of the disease at a young age. This aggressive phenotype of ALS is characterized by a rapid course, usually lasting of less than 12 months [110-111] and is shared by others less common mutations, such as C6F, C6G and G10V [112].

Over 20 years of research, the mechanism of SOD1-mediated toxicity has not yet been clarified. Initially, it was hypothesized that the cause of disease was dependent by the loss of the antioxidant activity of SOD1 as a result of mutation, with disastrous consequences for oxidative stress of affected motor neuron. However, experimental evidence indicates that most of the SOD1 mutants are active and partially folded as the wild-type protein. Consequently, the toxicity mediated by mutant SOD1 must be ascribed to other unknown characteristics. Many transgenic mice expressing the most common ALS-linked SOD1 mutants were generated throughout the years. For example, animals expressing dismutase active G37R and G93A, as well as less active G85R develop comparable disease pathologies similar to that seen in patients, confirming that onset of patology is independent from SOD1 activity [113].

A possible explanation of SOD1-mediated toxicity in ALS is related to the propensity of muntant and partially misfolded proteins to aggregate. Indeed, aggregation of misfolded proteins is a common feature of several neurodegenerative diseases, such as Alzheimer's and Parkinson's disease, and cytoplasmic aggregates are observed in both sporadic and familial ALS cases as well as in mutant SOD1 transgenic mice [114-115].

Although the toxicity of SOD1 aggregates remains to be established, it has been hypothesized that aggregates may act damaging several cellular compartments or promoting the inhibition of several cellular functions, as showed in Fig. 18. It has been proposed a direct involvement of SOD1 mutants in inhibition of other proteins function, due co-aggregation, and of proteasome machinery and chaperone activity, as well as in the deregulation of organelle function including Golgi, endoplasmic reticulum and mitochondria.

1.4.3 Impact of ALS-linked SOD1 mutants on mitochondria

Mitochondrial dysfunction has been observed in affected motor neurons of both sporadic and familial ALS patients. Morphological mitochondrial abnormalities, such as swelling and vacuolization, accompanied by a decreased mitochondrial activity have been reported [116]. Similar evidences were found in transgenic mice models expressing mutants SOD1, such as G93A.

The mutant G93A is one of the most prevalent mutations in patients with fALS. It is defined a wild-type like protein, due to its similarity of functional properties with those of wild-type. Furthermore, it is considered an excellent representative model for the study of ALS-linked SOD1 mutants [117]. It has been showed that SOD1 G93A co-localizes with the outer membrane of mitochondria in transgenic mice and a similar result was found for the mutant G85R [118]. Aggregation of misfolded SOD1 on cytosolic surface of mitochondria can partially explain the disruption of the physiological regulation of communication and exchange between mitochondria and cytosol. Accumulation of mutant SOD1 on mitochondria promotes an impairment of the mitochondrial respiratory chain, a reduction of both mitochondrial Ca^{2+} and buffering capacity of the organelle, a reduction of the import activity of mitochondrial proteins by translocates comples [119-121]. Moreover, SOD1 mutants appear to influence not only morphology and bioenergetics of mitochondria, but also axonal transport of mitochondria, that in affected cells is interrupted [122]. A schematization of SOD1 mutants impact on OMM is represented in Fig. 19.

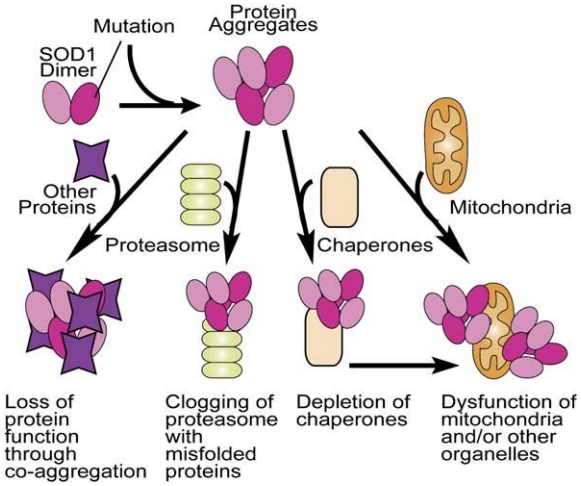

Fig 18 ***Proposed Toxicities of ALS-Causing SOD1 Protein Aggregates.*** Cell machinery that might be affected by misfolded, mutant SOD1 includes co-aggregation of essential cytoplasmic components, poisoning of the proteasome thereby inhibiting timely degradation of many cellular proteins, saturation of cytoplasmic chaperones that catalyze essential protein folding and refolding, and damaging mitochondria by aggregation onto the cytoplasmic surface and/or transport into the mitochondrial intermembrane space. Picture taken from [113].

Recently, it has been reported that several ALS-linked SOD1 mutants specifically binds the cytosolic surface of mitochondria using VDAC1 as docking site [123]. In

this work, it has been demonstrated that VDAC1 co-immunoprecipitates with several ALS-linked SOD1 mutants, such as G93A, H46R and G85R, in affected tissues from transgenic mice; on the contrary, no aggregation of wild-type SOD1 on mitochondria were detected. In addition, electrophysiological experiments have been showed that G93A and G85R SOD1 proteins are able to reduce the ionic conductance of VDAC1. These functional data suggest that, in the presence of mutant SOD1, VDAC1 can partially close, and that this conformational state has a negative impact on normal mitochondrial function [123].

From these works, a new hypothesis emerges: a mitochondrial channelopathy as a base for neurodegeneration of motor neurons affected by ALS [124]. Thus, ALS-linked SOD1 mutants would accumulate on the OMM through interaction with VDAC, an interaction can alter the functions of mitochondrial pore and consequently the same organelle function, strongly contributing to the degeneration of motor neurons.

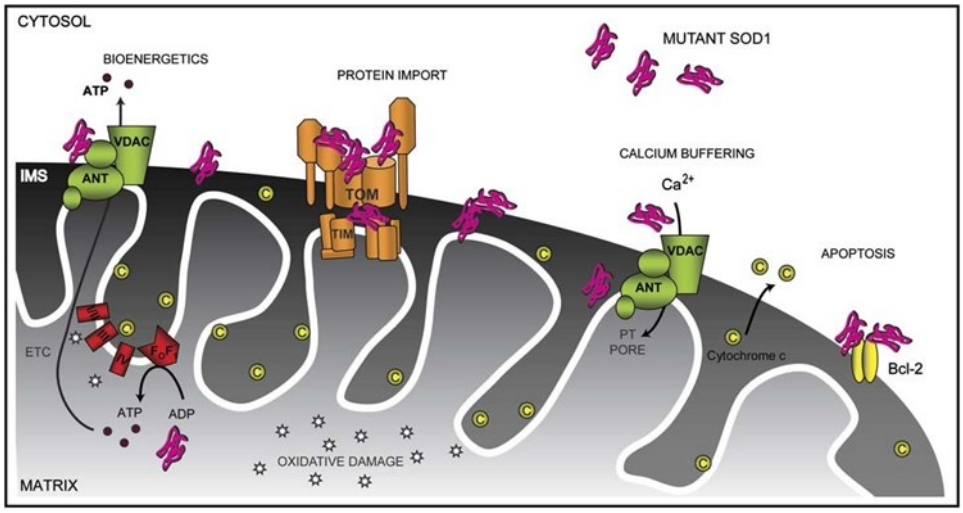

Fig 19 ***Mutant SOD1-Mediated Damage to Mitochondria.*** Accumulation of SOD1 mutants on cytosolic surface of mitochondria may interfere with the elements of the electron transport chain, disrupting ATP-generating oxidative phosphorylation. Mutants SOD1 may also disrupt mechanisms by which mitochondria buffer cytosolic calcium levels and may interfere with components of mitochondrial-dependent apoptotic machinery, such as Bcl-2, thereby triggering premature activation of an apoptotic cascade including cytochrome c release into the cytosol. Mutant SOD1 may indirectly affect similar pathways linked to mitochondria by physically blocking the protein import machines, TOM and TIM. Picture taken from [113].

2. AIM OF THE WORK

Although for basically different reasons, both VDAC1 and SOD1 represent two important proteins for mitochondrial functionality in both physiological and pathological conditions. VDAC proteins plays a key role in metabolism regulation, being the gate through which metabolites can reach mitochondria from cytosol and vice versa; in addition, VDAC regulate apoptosis, and thus life cycle of the cell, an aspect particularly relevant in case of pathology. SOD1 is directly involved in detoxification from superoxide anion, protecting cytosol and mitochondria from oxidative stress; however, many evidences suggest a more extensive role for this enzyme, which is independent from its antioxidant role.

The characterization of structural and electrophysiological features of VDAC proteins represents a crucial point in the understanding of them roles, in relation to the metabolism and to them involvement in neurodegeneration. For this reason, one of the aims of this work is the characterization of the less known human porin, VDAC3, as well as, the VDAC1 domains involved in the voltage gating.

Structure and function of SOD1 were fully characterized. However, recent works have shown that this protein play a key role in regulation of metabolism in yeast and gene expression under stress conditions. Thus, characterization of metabolic role of SOD1, in the absence of the main protagonist of mitochondrial metabolism, VDAC1, represents another aim of this work.

Finally, both proteins represent a crucial point for mitochondrial dysfunction in ALS. Characterization of molecular interaction between VDAC1 and ALS-linked SOD1 mutants can be considered fundamental for the understanding of molecular basis of ALS. Thus, preliminary analysis of interaction is another aim of this work.

3. MATERIALS AND METHODS

3.1 Cloning

3.1.1 Bacterial strain and growth condition

Propagation of the plasmid DNA and protein expression of recombinant proteins for *in vitro* studies were performed using the host bacterial cells *Escherichia coli*, respectively *XL10 gold* and *BL21 (DE3)* strains. Bacteria are grown in Luria-Bertani (LB) medium (0.5% yeast extract, 1% tryptone, 1% NaCl added of 2% agar for solid plates) containing the antibiotic ampicillin (100 µg/ml) for recombinant clones selection, at the temperature of 37°C under constant shaking.

BL21 (DE3) strain is widely used for the expression of proteins by the use of Isopropyl-1-thio-β-D-galactopyranoside (IPTG) in the culture medium that determines the induction of RNA T7 polymerase from promoter lacUV5, improving the expression of recombinant proteins.

3.1.2 Plasmids

For heterologous expression of proteins, vectors of *pET* series (*Novagen*) were used. The pET vectors (Fig. 20A) are widely used due to the possibility to add several tags to the sequence of the target gene, at both N- and C-terminal domain. Plasmids pET are characterized by the replication origin pBR322, able to confer a relatively high number of copies per cell, a gene encoding for the β-lactamase, that confers resistance to ampicillin and a multiple cloning site (MCS) flanked to T7 promoter upstream and T7 terminator downstream.

For protein expression in yeast, plasmid of *pYX* series (*Novagen*) were used. The pYX shuttle plasmids (Fig. 20B) allow the propagation of DNA in bacterial host and expression in yeast cells. Vectors pYX contain a bacterial replication origin *ColE1* and the Amp^r gene, which confers resistance to the antibiotic ampicillin; they also contain the yeast replication origin *2 µm* and the marker genes, which allows the expression of specific enzymes involved in biosynthesis pathway of auxotrophies. The expression of the target protein is under control of the housekeeping

promoter *TPI1*, normally involved in the expression of the catalytic enzyme Triose-Phosphate Isomerase 1.

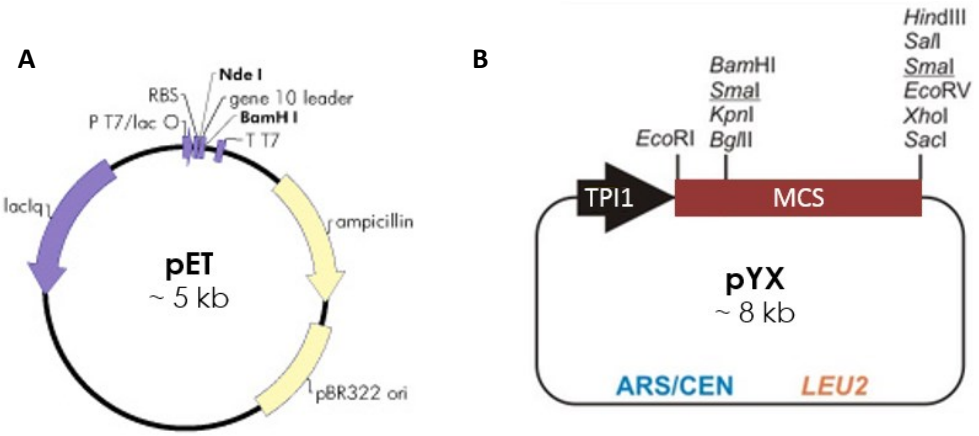

Fig 20 ***Plasmids general maps*****.** In this work, two different series of plasmids were used. **A)** General schematization of pET vector, which shows a length between 5.2 and 5.4 kb; **B)** General schematization of pYX plasmid, that shows a length of around 8 kb.

3.1.3 Cloning of human VDAC genes in pET-21a

The encoding sequences of human VDAC1 and VDAC3 were amplified by PCR using as template *in stock* plasmids. Primers were designed so as to incorporate in amplified DNA the restriction sites *NdeI* at 5'-end and *XhoI* at 3'-end. Amplified DNA was cloned in the pET-21a by digestion of both PCR products and plasmid with restriction enzymes NdeI and XhoI. For VDAC1 amplification, primers *VDAC1 NdeI FW* and *VDAC1 XhoI REV* were used; for VDAC3 amplification, primers *VDAC3 NdeI FW* and *VDAC3 XhoI REV* were used (for primers sequences see Table 1).

Sequences of VDAC genes were cloned in frame with the 6xHis tag at the C-terminal domain, which was used for further purification.

The PCR program used for amplification of both sequence was: denaturing step at 94°C 3 mins; 25 amplification cycles of 94°C 45 sec, 59°C 45 sec, 72°C 1 min; a final elongation step at 72°C 10 min.

3.1.4 Construction of VDAC1 deletion mutants

VDAC1 mutants were created starting from the encoding sequence of human VDAC1 by mutagenesis techniques based on PCR method as described in [125-126]. A general schematization of all VDAC mutants is reported in Fig. 21.

A

```
VDAC1          MAVPPTYADLGKSARDVFTKGYGFGLIKLDLKTKSENGLEFTSSGSANTETTKVTGSLET 60
N1-VDAC3       MAVPPTYADLGKSARDVFTKGYGFGMVKIDLKTKSCSGVEFSTSGHAYTDTGKASGNLET 60
               *************************::*:****** .*:**::** * *:* *.:*.***

VDAC1          KYRWTEYGLTFTEKWNTDNTLGTEITVEDQLARGLKLTFDSSFSPNTGKKNAKIKTGYKR 120
N1-VDAC3       KYKVCNYGLTFTQKWNTDNTLGTEISWENKLAEGLKLTLDTIFVPNTGKKSGKLKASYKR 120
               **:  :******:************: *::**.*****:*: * ******..*:*:.***

VDAC1          EHINLGCDMDFDIAGPSIRGALVLGYEGWLAGYQMNFETAKSRVTQSNFAVGYKTDEFQL 180
N1-VDAC3       DCFSVGSNVDIDFSGPTIYGWAVLAFEGWLAGYQMSFDTAKSKLSQNNFALGYKAADFQL 180
               : :.:*.::*:*::**:* *  **.:*********.*:****:::*.***:***: :***

VDAC1          HTNVNDGTEFGGSIYQKVNKKLETAVNLAWTAGNSNTRFGIAAKYQIDPDACFSAKVNNS 240
N1-VDAC3       HTHVNDGTEFGGSVYQKVNEKIETSINLAWTAGSNNTRFGIAAKYMLDCRTSLSAKVNNA 240
               **:**********:*****:*:**::*******..********** :*  :.:******:

VDAC1          SLIGLGYTQTLKPGIKLTLSALLDGKNVNAGGHKLGLGLEFQA 283
N1-VDAC3       SLIGLGYTQTLRPGVKLTLSALIDGKNFSARGHNVGLGFELEA 283
               ***********:**:*******:****..* **::***:*::*
```

β9

β9-β10

B

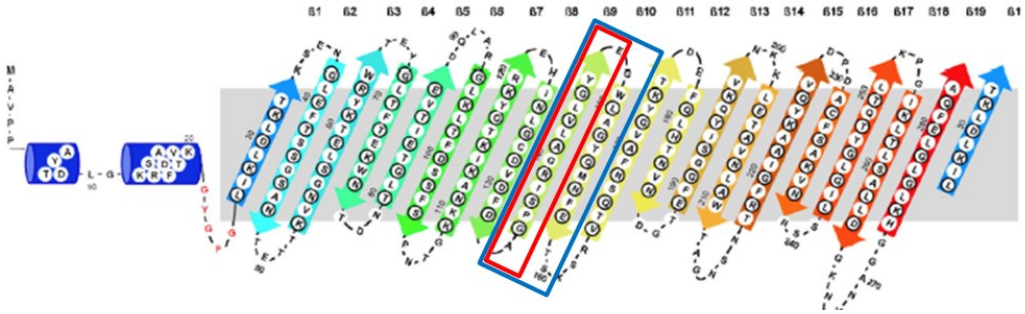

Fig 21 ***Features of the mutants used in this work***. **A)** Alignment of N1-VDAC3 with hVDAC1. Colored boxes indicate the sequences deleted in our experiments. **B)** Structure of VDAC according to the crystallographic structure of mVDAC1 as in [35]. β-strands 9-10 are highlighted by a box.

The mutant VDAC1 Δ136-147, carrying the deletion of β-strand 9, was created using two couples of primers that amplified respectively the regions corresponding to amino acids 1-136 and 147-282; similarly, the mutant VDAC1 Δ136-160, carrying the deletion of both β-strands 9 and 10, was created using an additional couples of primers that amplified the region corresponding to amino acids 160-282. Primers flanking the codons for amino acids 136 and 147 and the codons for amino acids 136 and 160 were used to delete the β-strands.

For construction of VDAC1 Δ136-147 mutant, two parallel PCR were performed. Amplification of 1-136 fragment was performed as follows: 94°C 3 min; 25 cycles of 94°C 45 sec, 52°C 45 sec, 72°C 1 min; 72°C 6 min. Reaction was performed using the primers VDAC1 NdeI FW and *VDAC1 Δ136-147 REV*.

Amplification of 147-288 fragment was performed as follows: 94°C 3 min; 25 cycles of 94°C 45 sec, 58°C 45 sec, 72°C 1 min; 72°C 6 min. Reaction was performed using the primers *VDAC1 Δ136-147 FW* and VDAC1 XhoI REV.

The PCR fragments obtained from the two reactions were purified and united in a new PCR reaction performed as follows: 94°C 3 min; 25 cycles of 94°C 45 sec, 62°C 45 sec, 72°C 90 sec; 72°C 10 min. Reaction was performed using the pimers VDAC1 NdeI FW and VDAC1 XhoI REV. A general scheme of the strategy construction of mutant lacking the β-strand 9 is described in Fig. 22.

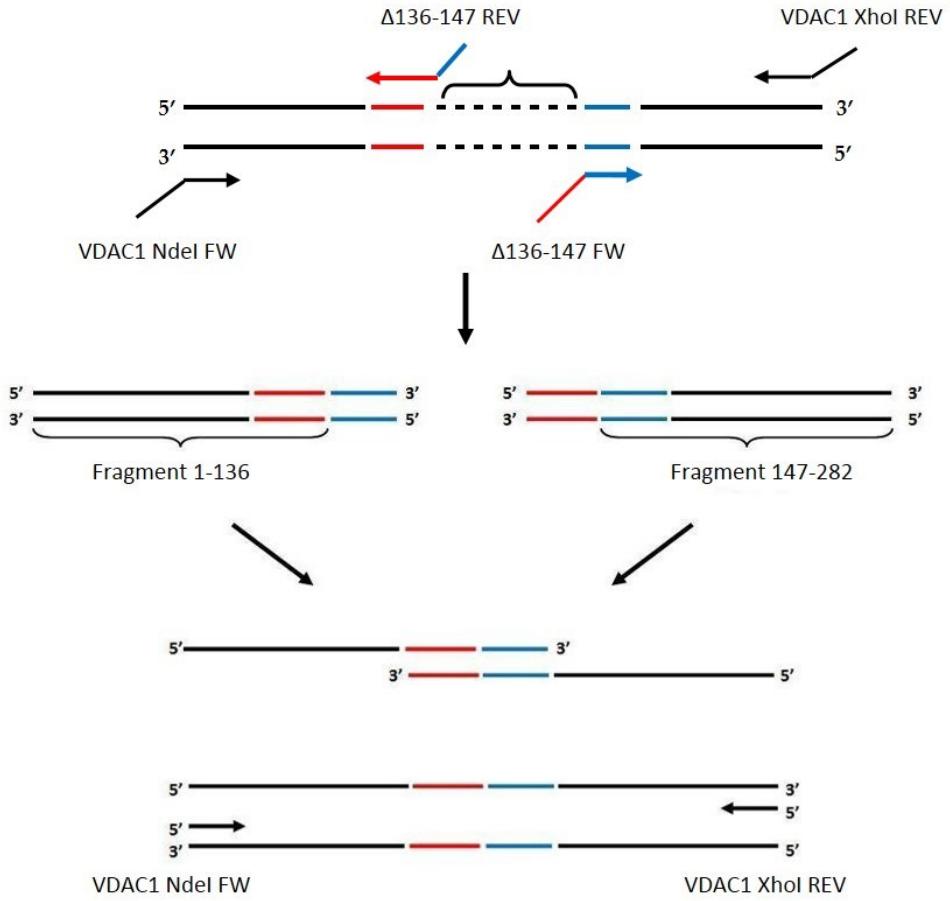

Fig 22 ***Construction of deletion mutants of VDAC1 by PCR.*** For mutant devoid of the β-strand 9, two different PCR were performed, amplifying two part of VDAC1 sequence so as to exclude the sequence encoding for deletion region. Then, a second PCR was performed to unify the two fragments. An identical strategy was used for construction of mutant deleted of both 9 and 10 β-strands.

To obtain the mutant VDAC1 Δ136-160 a PCR was performed for the amplification of the fragment 160-282, with the following parameters: 94°C 3 min; 25 cycles of 94°C 45 sec, 52°C 45 sec, 72°C 1 min; 72°C 6 min. The reaction was performed using

the primers *VDAC1 Δ136-160 FW* and VDAC1 XhoI REV. The fragment 160-282 was joined to fragment 1-136 by PCR, as described previously.

The sequences of human VDAC1, VDAC3 and the deletion mutants were confirmed by DNA sequencing.

3.1.5 Cloning of human VDAC genes in pYX212

The sequences coding the human VDAC1, VDAC3 and the chimera N1-VDAC3, (characterized by the switching of the whole β-barrel of VDAC1 with the corresponding barrel of isoform 3) were cloned in the yeast expression vector pYX212 as described in [61]. This plasmid contains URA3 marker, encoding for the enzyme orotidine 5'-phosphate decarboxylase (ODCase), which catalyzes a reaction in the synthesis of pyrimidine ribonucleotides.

3.1.6 Cloning of human SOD1 in pET-52b

The sequence coding the wild-type (WT) human SOD1 (hSOD1) was amplified by PCR using as template *in stock* plasmids. Primers were designed so as to incorporate in amplified DNA the restriction sites *SanDI* at 5'-end and *SalI* at 3'-end. Amplified DNA was cloned in the pET-52b by digestion of both PCR products and plasmid with the restriction enzymes SanDI and SalI. For hSOD1 amplification, primers *hSOD1 SanDI FW* and *hSOD1 SalI REV* were used (for primers sequences see Table 1). The sequence of hSOD1 gene was cloned in frame with the Strep-tag II at the N-terminal domain, and was used for further purification.

PCR cycles used to amplify the hSOD1 was: denaturing step at 94°C 3 mins; 25 cycles of 94°C 45 sec, 56°C 45 sec, 72°C 1 min; a final elongation step at 72°C 10 min.

3.1.7 Construction of ALS-linked SOD1 mutants

To generate single based mutations in WT hSOD1 sequence it was performed a site-directed mutagenesis, with the *Quick Change Mutagenesis Site-Direct kit* (Agilent). We produced the classical mutants G93A and G85R, the mutations most frequently associated with ALS. Primers used for mutagenesis are described in Table 2. All sequences were verified by sequencing.

3.1.8 Cloning of human hSOD1 in pYX142

The sequence coding the WT hSOD1 was amplified by PCR using as template *in stock* plasmids. Primers were designed so as to incorporate in amplified DNA the restriction sites *EcoRI* at 5'-end and *SalI* at 3'-end. Amplified DNA was subcloned in the pYX142 yeast expression vector by digestion of both PCR products and plasmid with restriction enzymes EcoRI and SalI. This plasmid contains LEU2 marker, which allows the expression of β-isopropylmalate dehydrogenase involved in leucine biosynthesis pathway. Primers used for hSOD1 amplification were *hSOD1 EcoRI FW* and *hSOD1 SalI REV*, and are showed in Table 1.

PCR cycles used to amplify SOD1: denaturing step at 94°C 3 mins; 25 cycles of 94°C 45 sec, 56°C 45 sec, 72°C 1 min; a final elongation step at 72°C 10 min.

VDAC1 NdeI FW	TTTCATATGGCTGTGCAACCCACGTAT
VDAC1 XhoI REV	TTTCTCGAGTGCTTGAAATTCCAGTCCTAG
VDAC3 NdeI FW	TTTCATATGTGTAACACACCAACGTACTG
VDAC3 XhoI REV	TTTCTCGAGAGCTTCCAGTTCAAATCCCAA
VDAC1 Δ136-147 FW	GACATTGCTGGGGGCTGGCTGGCCGGCTAC
VDAC1 Δ136-147 REV	GGCCAGCCAGCCCCCAGCAATGTCGAAATC
VDAC1 Δ136-160 FW	GACATTGCTGGGAAATCCCGAGTGACCCAG
VDAC1 Δ136-160 REV	CACTCGGGATTTCCCAGCAATGTCGAAATC
SOD1 SanDI FW	TTTGGGACCCATGGCCACGAAGGCCGTGTGCGTG
SOD1 SalI REV	TTTGAGCTCTTATTGGGCGATCCCAATTACACC
SOD1 EcoRI FW	TTTGAATTCATGGCCACGAAGGCCGTGTGCGTG
SOD1 SalI REV	TTTGAGCTCTTATTGGGCGATCCCAATTACACC

Table 1 ***Primers sequences*****.** Primers used in the amplification of both VDAC and SOD1 proteins for all plasmids used. In red are reported the sequences recognized by restriction enzymes, used for cloning.

SOD1 G93A FW	ACTGCTGACAAAGATGCTGTGGCCGATGTGTCT
SOD1 G93A REV	AGACACATCGGCCACAGCATCTTTGTCAGCAGT
SOD1 G85R FW	CATGTTGGAGACTTGCGCAATGTGACTGCTGAC
SOD1 G85R REV	GTCAGCAGTCACATTGCGCAAGTCTCCAACATG

Table 2 ***Primers sequences for mutagenesis*****.** Primers used in site-direct mutagenesis for the production of the two ALS-linked SOD1 mutants G93A and G85R. In red is showed the mutated codons.

3.1.9 Constructs pEGFP-N1

The vector pEGFP-N1 (Clontech) encoding WT hSOD1 linked at the C-terminus to the enhanced green fluorescent protein tag (eGFP), and mutant SOD1 G93A with the same tag, and vector encoding only the tag were donated by Dr. Adrian Israelson, Ben Gurion University of the Negev, Beer Sheva, Israel.

3.2 Expression and purification of recombinant proteins

3.2.1 Expression and purification of VDAC proteins in *E. coli*

The recombinant His-tagged human proteins VDAC1, VDAC3, VDAC1 Δ136-147 and VDAC1 Δ136-160 were expressed in *E. coli* BL21 (DE3). Cells transformed with pET-21a constructs were grown at 37°C under constant shaking up to an optical density (OD_{600}) of about 0.6. Protein expression was induced using 1 mM IPTG and incubating the cultures for 3 hours at 37 °C.

Cells were collected by centrifugation (30 min, 12000 x g) and resuspended in Buffer B (0.1 M NaH_2PO_4, 0.01 M Tris-HCl, 8 M urea, pH 8.0). To perform cell lysis, the suspension was incubated overnight at 4°C under constant shaking. The suspension was centrifuged (45 min, 12000 x g) to separate cell debris from clear lysate. Expression of each protein was verified by SDS-PAGE analysis, by comparison between not induced and induced samples.

Purification of recombinant His-tagged proteins was performed by affinity chromatography, using the nickel-nitrilotriacetic acid resin (Ni-NTA). Nickel ions show high affinity for histidine residues located at the C-terminus of the recombinant proteins, binding them specifically. Elution of His-tagged proteins was performed lowering the pH of Buffer B to 3.5.

Purified proteins were stored at -20°C.

3.2.2 Refolding VDAC1 and VDAC1 mutants

To fully restore the biological activity of VDAC proteins, the proteins purified in urea were refolded using a on-column procedure that utilizes an affinity chromatography [127]. For this purpose, a Talon resin (Clontech) was used. The Talon matrix is a cobalt-based resin that binds specifically His-tagged protein,

allowing the dilution of urea and the progressive folding of the protein whilst bound to the column [127]. This method was used for refolding the two deletion mutants and WT VDAC1 as control.

1 mL of Talon resin, pre-equilibrated with Buffer B, was used for each protein. The column was loaded with 2 mL of denatured protein supernatant (containing 3 mg of purified protein) and washed once with a mixture 1:3 of Buffer B and Buffer C (25 mM NaP_i, pH 7.0, 100 mM NaCl, 2% LDAO) supplemented of 10 mM imidazole. The resin was then washed twice with a mixture respectively of 1:7 and 1:15 of Buffer B and Buffer C1 (25 mM NaP_i, pH 7.0, 100 mM NaCl, 1% LDAO) with 10 mM imidazole. An additional wash was performed with 20 volumes of Buffer C2 (25 mM NaP_i, pH 7.0, 100 mM NaCl, 0.1% LDAO) with 10 mM imidazole. At the end the His-tagged protein was eluted with 5 volumes of Buffer C2 with 200 mM imidazole. The protocol was performed under gravity at 4°C.

Imidazole contained in Buffer C2 may interfere with further experiment, thus it was removed by dialysis against a 100X Buffer C2 without imidazole, overnight at 4°C. A Slide-A-Lyzer Dialysis Cassette (3.5K MWCO) (Thermo Scientific) was used to avoid any sample loss.

The protein purity was verified by 12% SDS–PAGE. When electrophysiological experiments had to be performed, the purified proteins were diluted 1:10 in 1% Genapol X-80 (Fluka, Buchs, Switzerland) to prevent aggregation and immediately used for further experiments.

3.2.3 Refolding of VDAC3

His-tagged VDAC3 refolding was not performed with the Talon resin, as described above, but with an alternative method. To have a positive control, also a sample of VDAC1 was treated in the same way. The denatured protein mixture was added drop-wise to a Refolding Buffer (25 mM TrisHCl, pH 7.0, 100 mM NaCl, 1 mM EDTA, 1% LDAO), allowing a ten-fold dilution of the urea concentration, and the mixture was gently stirred overnight at 4°C. The protein solution was then dialyzed against a 100 X buffer containing 0.1% LDAO overnight at 4 °C in Slide-A-Lyzer Dialysis Cassettes (3.5 K MWCO). The protein purity was controlled with 12% SDS-PAGE and Comassie staining. Purified samples were stored at 4°C until further use.

3.2.4 VDACs purification from yeast mitochondria

The pYX212 plasmid encoding for human VDAC1, VDAC3 and N1-VDAC3 were expressed in yeast *S. cerevisiae Δpor1* strain, and proteins were isolated from yeast mitochondria. The protocol for mitochondria isolation was performed as described in [128].

1 L of cell culture expressing VDAC proteins was grown in YPD medium, harvested by centrifugation (5 min, 3000 x g) and washed twice with water. The cell pellet was resuspended in DTT Buffer (100 mM Tris/H_2SO_4 pH 9.4, 10 mM DTT) and the cell suspension was rotated for 20 min at 30°C. After centrifugation the pellet was resuspended in Zymoliase Buffer (20 mM potassium phosphate, pH 7.4, 1.2 M sorbitol, Zymoliase 100 T) and rotated for 30 min at 30°C. Spheroplasts were centrifuged (8 min, 2200 x g) and resuspended in a homogenization buffer (10 mM TrisHCl pH 7.4, 0.6 M sorbitol, 1 mM EDTA, 0.2% BSA). The suspension was disrupted with a pestle and the obtained supernatant, containing the mitochondrial fraction, was centrifuged (15 min, 12000 x g) allowing the recovery of the mitochondria. Mutant and native VDAC proteins were released from the mitochondrial fraction by LDAO-extraction as described in [129], and were subsequently purified by chromatography using HTP/celite 2:1. Protein concentration was determined using the Bradford method.

3.2.5 Expression and purification of SOD1 proteins

The recombinant Strep-tagged human proteins WT SOD1 and mutant SOD1 G93A and G85R were expressed in *E. coli* BL21 (DE3). Cell transformed with pET-52b constructs were grown at 37°C under constant shaking up to an optical density (OD_{600}) of about 0.6. The protein expression was induced using 0.4 mM IPTG and incubating the cultures for 3-4 hours at 25°C. During induction, LB medium was enriched with 3 mM $CuSO_4$ and 30 µM $ZnSO_4$, to guarantee to the newly expressed proteins high levels of metal co-factors in the medium. Cells were harvested by centrifugation (30 min, 12000 x g) and the pellet cells were suspended in Lysis Buffer (10 mM Tris-HCl, pH 7.4, 150 mM NaCl, 20% Glycerol, 150 µM PMSF, 5 µg/ml Leupeptin). Cells were lysed by repeated sonication placing the cell suspension on ice between cycles. Cell lysate was clarified by centrifugation (12000 x g, 45 min).

The supernatant, containing the total soluble protein fraction, was temporarily stored at 4°C. The expression of each protein was verified by SDS-PAGE analysis, comparing induced and not induced samples.

Strep-tagged SOD1 WT and mutants proteins were purified by affinity chromatography using a pre-packed 5 ml StrepTrap HP column (GE Heathcare) in association with an AKTA PrimePlus (GE Heathcare) system, according with manufacturer's protocol. The elution profile was plotted using the measured OD_{280} for each fraction versus the elution time (or the corresponding fraction). Selected fractions were electrophoresed on SDS-PAGE to check for purity. Fractions containing our target proteins were dialyzed overnight at 4°C against 20 mM Tricine pH 7.4, 100 mM NaCl, 20% Glycerol, 200 µM $ZnSO_4$, 1 mM DTT. The protein solution was finally concentrated 10-fold using Amicon Ultra-4 Centrifugal Filter tubes (Millipore), snap-freezed in liquid nitrogen and then transferred to -80°C for long term storage.

3.3 *In vitro* analysis and characterization of recombinant proteins

3.3.1 Gel electrophoresis and Immunoblotting

SDS-PAGE was performed using 12 or 14% polyacrylamide gels. Gels were stained with Coomassie Brilliant Blue or electrotransferred onto nitrocellulose membranes for immunostaining. Membranes containing the transferred proteins were blocked with 5% nonfat dry milk and 0.1% Tween 20 in Tris-buffered saline and then incubated with polyclonal anti-hSOD1 (Santa Cruz Biotechnology, Inc.) antibodies, in dilution 1:1000, followed by incubation with HRP-conjugated anti-goat IgG secondary antibody, in dilution 1:10000. After treatment with the appropriate primary and secondary antibodies, enhanced chemiluminescence (Pierce) was performed.

3.3.2 Planar Lipid Bilayer

Planar Lipid Bilayer (PLB) is one of the most used method for electrophysiological characterization of pore-forming proteins. The method allows the reconstitution of a target protein on an artificial membrane, which reproduces a biological one.

The lipid bilayer is painted on a small aperture in a Teflon cuvette, and separates two chambers connected with two electrodes. The insertion of a protein forming a pore or a channel in the membrane allows the ions exchange across the membrane itself. Parameters such as conductance and ion selectivity, as well as the analysis of protein behavior at various voltage applied, can be monitored.
A schematization of PLB is represented in Fig. 23.

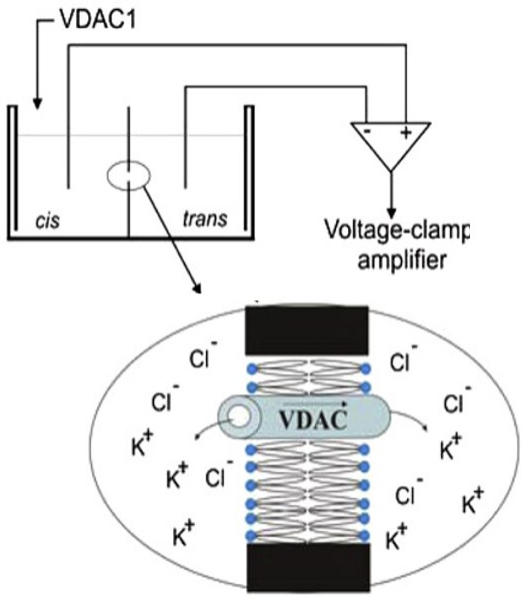

Fig 23 ***Schematic representation of a PLB*****.** Basic principle of PLB is the presence of a bilyer membrane located on a small pore of a Teflon cuvette, which separates two chamber. Any insertion of pore-forming protein allows the passage of ions.

The methods used for black lipid bilayer experiments have been described in [130]. Briefly, a Warner Instruments (Hamden) electrophysiological planar bilayer apparatus was used and bilayers were prepared using asolectin (Sigma) dissolved in n-decane (Sigma) containing 1% chloroform (Sigma) across a 250 µM hole in a polystyrene cuvette (Warner Instruments). Asolectin was partially purified by precipitation with cold acetone from a chloroform solution. The lipid membrane divided the trans and the cis compartments. When the bilayer membrane was formed, currents across the membrane elicited by different voltage pulses were measured and the membrane resistance could be determined. A bilayer membrane was considered to be satisfactory for further experiment if it exhibited a capacity of approximately 150–200 pF. The volumes of the cis and trans compartments were 3 ml. Solution in the chambers could be mixed through

stirring with a small magnetic bar. Both sides were connected to the electrodes via salt bridges (1 M KCl) in series with Ag/AgCl electrodes. All measurements were made at room temperature.

The standard experimental medium was 1 M KCl, 10 mM Hepes/pH 7.2. Otherwise, 1 M Kgluconate, 1 M Nagluconate or 500 mM $CaCl_2$ were used. Control experiments with an empty membrane or with the detergents used for the purification showed no activity in any of the above solutions. All voltages reported are those of the cis chamber, zero being assigned by convention to the trans (grounded) side. Currents are considered as positive when carried by cations flowing from the cis to the trans compartment.All experiments were performed at room temperature.

VDAC proteins were added from the 1 mg/mL protein stock solution, after the membrane had turned black (controlled by the capacity). At this point the single-channel conductance of the pores was measured. The stepwise increase in membrane conductance and the voltage dependency were determined as described [131].

3.3.3 SOD1 activity and oligomerization assay

Activity of purified WT and mutants SOD1 was tested by Riboflavin/NitroBlue Tetrazolium (RF/NBT) assay [132]. Several dilution of SOD1 proteins, such as WT SOD1 purchased from Sigma as a control, were loaded in 7.5% Native gel and the electrophoresis was performed under native conditions, for 1 h at 100 V. The gel was soaked in Riboflavin-NBT solution (1% Riboflavine, 2.5% NTB) for 15 min at RT in the dark, followed by 0.1% TEMED solution at the same condition. Then, the gel was then exposed to light until SOD1 white bands appears in the gel. Reaction was stopped soaking the gel in double distilled water.

The oligomeric state of purified hSOD1 proteins was measured by treatment with the cross-linker reagent Ethylene glycolbis (succinimidylsuccinate) (EGS). 2 µg of purified SOD1 proteins were treated with several concentration of EGS in 50% DMSO (0, 100, 200 mM), incubating the samples at 30°C for 15 mins. The reaction was stopped by addition of Laemmli sample buffer 4X and the samples were boiled at 70°C for 10 mins and stored. The samples were then analyzed by imunoblotting.

3.3.4 Microscale Thermophoresis

Microscale Thermophoresis (*MST*) is based on the molecules movement along temperature gradients, a function of hydration shell: changes in molecular structure/conformation promote changes in the shell. The molecules movements is measured by monitoring the fluorescence distribution inside a capillary of fluorescently-labeled molecules. A schematization of MST basic principle is represented in Fig. 24.

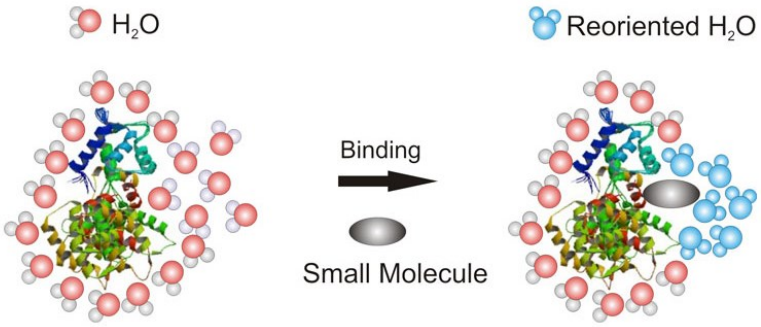

Fig 24 ***Basic principle of MST*.** MST is a sensitive technique that measures molecules movement along temperature gradients as a function of hydration shell. Any changes in molecular structure/conformation, due to an interaction, promote changes in the shell.

MST analysis was performed using the NanoTemper Monolith NT.115 apparatus, as recently described [133-134]. Purified VDAC1 was fluorescently labeled using the NanoTemper protein-labeling kit Green/Blue (NanoTemper Technologies, Munich, Germany). A constant concentration of labeled VDAC1 was incubated for 5 min at RT in the dark with different concentrations of wt and mutSOD1 (1.22 nM to 20 µM) in PBS containing 0.05% Tween 20. Afterward, the samples were loaded into a glass capillary (Monolith NT Capillaries), and thermophoresis analysis was performed (light-emitting diode 20%, IR laser 20 to 80%).

3.4 Yeast cellular biology

3.4.1 Yeast strain and growth conditions

In this work, the *Saccharomyces cerevisiae* yeast strains BY4742 wild-type (MATα, his3Δ1, leu2Δ0, lys2Δ0, ura3Δ0) and its mutant Δpor1 (MATα, his3Δ1, leu2Δ0,

lys2Δ0, ura3Δ0, por1::kanMX4), obtained from *EUROSCARF* (Frankfurt, Germany), were used.

Yeast strains were growth on rich medium YP (1% yeast extract, 2% peptone) added of 2% glucose (YPD) or minimal medium (0.67% yeast nitrogen base) supplemented with 2% of glucose (SD) or glycerol (SY), added of 10 µg/ml of according to the genotype of the strains. For solid plates, 2% agar was added.

For several experiments, YP plates were prepared using 2% glycerol, ethanol, potassium acetate, succinate or citrate. Yeast strains were growth on both liquid and solid media at 30 and 37°C. For liquid cultures, yeast growth was followed by measuring the optical density at 600 nm, using spectrophotometer.

Both WT and Δpor1 strain were transformed with pYX142 + hSOD1 using the litium acetate transformation method; selection of recombinant were performed on SD plate containing the appropriate nutritional requirements except leucine.

3.4.2 Complementation assay

The complementation assays allow determining if the expression of a heterologous protein in a mutant yeast strain is able to restore the wild-type phenotype. Complementation assay was performed by the preparation of serial dilutions, starting from same number of cells per sample, as described in Fig. 25.

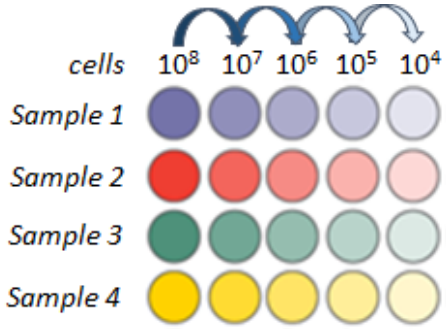

Fig 25 ***The serial dilution method.*** Around 10^8 cells per each samples were collected and resuspended in 200 µL of water; than, 20 µL of cells were added to 180 µL of water to obtain 10^7 cells. Same operation is repeated up to the last dilution.

Yeast samples were inoculated on liquid SD medium at 30 °C overnight under constant shaking.

Around 10^8 cells per sample were collected by centrifugation at 3000 rpm for 5 minutes, and resuspended in 200 µL of sterile water in a 96-well plate. Serial dilutions were prepared adding 20 µL of cell solution in 180 µL of water, repeating the dilution up to obtain 10^4 cells. 2 µL of each dilution was spotted on solid plates. In this work, complementation assay were performed using plates containing rich medium YPD, YPY, YPE, YP-Acetate, YP-Succinate and YP-Citrate incubating the plates for 1-2 days at 30°C, and on YPD and YPY incubating the plates for 3-4 days at the restrictive temperature of 37°C.

3.4.3 Flow Cytometry analysis

The Flow Cytometry is a laser-based technology employed in the analysis of the physical and biochemical features of cell populations. This technique allows the analysis of thousands of particles per second by suspending cells in a fluid stream that passes through an electronic detection apparatus: the diffraction signal gives information on cell volumes, while the intensity is proportional to cell dimension and shape. In addition, flow cytometry allows the fluorescence analysis due to the presence of specific fluorochromes conjugated to antibodies, probes and ligands and able to specifically bind to organelles, DNA, proteins and small molecules.

In particular, flow cytometry was used in this work for the evaluation of several parameters by the use of specific fluorescent probes.

The *CyFlow® ML flow cytometer* (Partec) system was used for all experiments. It is equipped with three laser sources and 10 optical parameters with dedicated filter setting and a high numerical aperture microscope objective (50× NA 0.82) for the detection of different scatter and fluorescence signals.

Around 20000 cells per sample were analyzed and each experiment was repeated at least twice in triplicate. The cells were excited by an air-cooled argon 488 nm laser and the signal from fluorescent probes was detected. Data obtained were acquired, gated, compensated, and analysed using the *FlowMax* software (*Partec*). Data were statistically analyzed by one-way ANOVA with Tukey's post hoc test. A value of $p < 0.05$ was taken as significant.

3.4.4 Determination of mitochondrial membrane potential

The fluorescent probe 3,3'-Dihexyloxacarbocyanine Iodide, known as *$DiOC_6(3)$* is widely used for determination of mitochondrial membrane potential ($\Delta\Psi_m$). $DiOC_6(3)$ is a cell-permeant, green-fluorescent, lipophilic dye that is selective for the mitochondria of live cells and was used in this work to evaluate the $\Delta\Psi_m$ of yeast samples. 5 x 10^6 cells were resuspended in 1 ml HEPES buffer (10 mM HEPES, pH 7.4) in presence 5% of glucose; then cells were treated with 40 nM of $DiOC_6(3)$ at 30°C for 30 mins. $\Delta\Psi_m$ was deermined by flow cytometry analysis, measuring the fluorescence signal of $DiOC_6(3)$.

3.4.5 Determination of total ROS

The dihydrorhodamine 123 (*DHR 123*) is a non fluorescent and uncharged molecule, that passively diffuses across membranes; the conversion to a fluorescent molecule exclusively depends on the presence of ROS and does not require any enzymatic catalysis: the DHR 123 is oxidized to the cationic molecule *rhodamine 123* that exhibits green fluorescence. In this work, DHR123 was used to evaluate the total ROS content of each yeast sample. Samples were treated with 5 µg/mL of culture of DHR 123 (Sigma) for 2 hours under constant shaking at 30°C. Total ROS content was determined by flow cytometry analysis, measuring the fluorescence signal of rhodamyne 123. .

3.4.6 Treatment of yeast cells with hydrogen peroxide

Hydrogen peroxide increases the oxidative stress of yeast cells; moreover, it represents a pro-apoptotic factor. Yeast cells were grown up to exponential phase and treated with 3 mM of hydrogen peroxide for 4 hours, directly added to the growth media. Not treated samples were prepared as controls. Treated and not treated samples were used for further analysis.

3.4.7 Yeast spheroplast preparation by glass beads

Yeast cells were collected by centrifugation and washed twice with sterile water. Cell pellets were resuspended in *spheroplast buffer* (100 mM Tris-HCl, pH 7.5, 5 mM EDTA, 150 mM NaCl), using 100 µL for each 10 mL of culture. Then, a same

weight of glass beads 425-600 µm (Sigma) was added. The cell pellets were vortexed at maximum speed for 1 minute and immediately incubated on ice for 1 minute, repeating this cycle for at least 10 times. Samples were centrifuged at 3000 rpm for 10 minutes at 4°C to precipitate glass beads and cell walls. Supernatant containing yeast spheroplast was used for further experiments.

3.5 Analysis of gene expression levels

3.5.1 Reverse Trascription PCR

Total RNA was extracted from yeast spheroplast samples using the *Trizol Plus RNA Purification Kit* (Life Technologies). This method combines the Trizol based lysis and nucleic acids extraction with the spin-column based RNA isolation technology.

Concentration of RNA samples were measured by spectrophotometer. RNA samples were treated with DNase I (*Invitrogen*) 1 µL for each µg of RNA that digests both single- and double-stranded DNA that can contaminate the RNA preparation. The sample volume was directly used for Reverse Trascription-PCR (RT-PCR).

RT-PCR is a variant of the classic PCR technique commonly used in molecular biology to detect RNA expression. The protocol provides two phases: the reverse transcription of RNA and the amplification of cDNA obtained in the first phase. For RT-PCR the *SuperScript II Reverse Transcriptase* (Invitrogen) was used. A 20 µL reaction was prepared in three different steps, according with manufacture's protocol. The obtained cDNA was stored at -20°C.

3.5.2 Quantitative Real-Time PCR

The *Real-Time PCR* is a PCR reaction that allows simultaneously detection and quantification of a target DNA molecule due to the presence of fluorescent dyes that intercalate with the DNA. In contrast to the standard PCR, in which the amplified product is detected at the end of the reaction, in Real-Time PCR the amplified DNA is detected as the reaction progresses. This allows to quantify the rate of generation of the amplified product at each PCR cycle.

The association between RT-PCR and Real-Time PCR is widely used for quantification of the expression levels of target genes, method known as

quantitative PCR (*qPCR*). Quantification is calculated plotting the fluorescence against the number of cycles on a logarithmic scale. A threshold for detection of fluorescence is previously set to remove background signal. The number of cycles at which the fluorescence exceeds the threshold is called threshold cycle (C_t); to normalize for variation in the amount and quality of RNA between different samples, the C_t of target gene is subtracted from the C_t of a housekeeping gene in the same sample, allowing to quantify the expression levels.

In our work, qPCR was used to analyze the expression levels of several target genes in both WT and Δpor1 yeast strains expressing or not hSOD1, using as templates the cDNA obtained by RT-PCR.

The expression levels of genes encoding for the mitochondrial porin *por2*, the subunit of mitochondrial translocator complex *tom40* and the subunit of mitochondrial sorting and assembly machinery of β-barrel proteins *sam50* were analyzed. The housekeeping *act1* gene, codifying for actin was used as normalizing control. Primers were specifically designed for Real-Time PCR experiments using *Primer3* software (biotools.umassmed.edu/bioapps/primer3_www.cgi). They were designed to specifically amplify a small gene portion of around 150 bp with a similar melting temperature. Primers are showed in Table 3.

Primer	Sequence	T_m	Length
qPCR Por2 FW	CCTGGTTGGAAAGGTGATGT	60	155 bp
qPCR Por2 REV	TGGCCCAAAGTAACACTTCC	60	155 bp
qPCR Tom40 FW	GTCTCCCGTGACGTGTTTTT	60	149 bp
qPCR Tom40 REV	AATGCGGAGAATGCGTACTT	60	149 bp
qPCR Sam50 FW	GGGCAGCTAGTGAAAAATGC	60	149 bp
qPCR Sam50 REV	ACTTCCATCAAAGGCACCAC	60	149 bp
qPCR Act1 FW	GCCTTCTACGTTTCCATCCA	60	153 bp
qPCR Act1 REV	GGCCAAATCGATTCTCAAAA	60	153 bp

Table 3 ***Primers used for qPCR*****.** List of primers used in Real-Time PCR created so as to amplified a specific portion of around 150 bp.

Real-Time PCR was performed using the *iCycler IQ* (Biorad) in 96-well plates. PCR cycle consist in a first step of PCR initial activation at 95°C for 5 minutes followed by a 2-step cycles of denaturation at 95°C for 30 seconds followed by combined

annealinig/extension step at 54°C for 30 seconds, repeated 35 times. A final step at 72°C for 10 minutes was performed. Three independent Real-Time PCR experiments were performed in triplicate.

3.5.3 Relative quantification of expression levels

The Ct values obtained by Real-Time PCR were used for the relative quantification of the expression level of analyzed genes, according to the method described in [135]. In this method, C_t value obtained from the amplification of a target gene was first normalized with C_t value obtained from amplification of the housekeeping gene (ΔC_t). Then, ΔC_t values obtained from two different samples, a reference sample, called *calibrator*, and the *target* sample were used for calculation of $\Delta\Delta C_t$. The fold change in the expression level of a specific gene (R) in a target sample compared to the calibrator sample is calculated using the followed equation: $\boldsymbol{R} = \mathbf{2}^{-\Delta\Delta \boldsymbol{C_t}}$. Data were statistically analyzed by one-way ANOVA with Tukey's post hoc test. A value of $p < 0.05$ was taken as significant.

3.6 Neuronal cell line

3.6.1 Maintenance of cell line and transfection

The neuronal *SH-SY5Y* cells were grown in Dulbecco's modified Eagle's medium-high glucose (DMEM), supplemented with 10% fetal bovine serum (FBS), 100 units/ml penicillin and 0.1 mg/ml streptomycin. Cells were maintained in at 37°C in presence of 5% CO_2. SH-SY5Y cells were transiently transfected with pEGFP-N1 encoding for SOD1 WT and G93A mutant, as well as the empty vector as control. The transfection reagent *Lipofectamine 2000* (Invitrogen) was used, according with manufacture's protocol.

3.6.2 Determination of mitochondrial membrane potential

Tetramethylrhodamine methyl ester (*TMRM*) accumulates in active mitochondria due its positive charge whereby the reduction of $\Delta\Psi_m$ leads to the release of TMRM. After 24h from transfection, SH-SY5Y adherent cells were washed with PBS and then incubated for 30 min at 37 °C with Krebs Ringer Buffered Saline (130 mM

NaCl, 3.6 mM KCl, 10 mM HEPES, 2 mM $NaHCO_3$, 0.5 mM NaH_2PO_4, 0.5 mM $MgCl_2$, 1.5 mM $CaCl_2$, 4.5 g/l glucose, pH 7.42) supplemented with 200 nM TMRM (Sigma). Cells were then detached by short treatment with trypsin–EDTA, re-suspended in the above buffer, supplemented with 1% FBS to neutralize the trypsin, and immediately analyzed using flow cytometry as previously described. The $\Delta\Psi_m$ of SH-SY5Y cells was estimated by gating cells with high red values (TMRM) characteristic of polarised mitochondria.

4.RESULTS

4.1 Electrophysiological characterization of human VDAC3

VDAC3 represents the less known of the three human isoforms. Although structure prediction, based on homology modelling, indicates a high similarity to VDAC1, the properties of VDAC3 might be different [136]. VDAC3 shows a slightly different tissue-dependent expression pattern, a variable abundance and a difference in cysteine content [27-29], compared to the others isoforms. Moreover, while transformation of *Δpor1* yeast cells with both human VDAC1 and 2 is able to restore the yeast growth defect, VDAC3 is just partially able to complement the absence of endogenous porin. In addition, an early report using VDAC3 purified from mitochondria of yeast transformed with the corresponding cDNA stated that no activity at all or very seldom pore insertion can be detected [30]. All these evidences have suggested that VDAC3 is not able to form pores.
In this part of the work, an electrophysiological characterization of VDAC3 was performed, using the human VDAC3 protein extracted from both yeast and bacteria.

4.1.1 Impact of human VDAC3 expression on *Δpor1* yeast cells

The yeast *Δpor1* strain is not able to grow on glycerol due to its mitochondrial defective metabolism. Transformation of *Δpor1* cells with pYX212 constructs expressing both human VDAC3 and VDAC1 was used to assay the complementation on non-fermentable carbon source.

As showed in Fig. 26, while VDAC1 is able to fully complement the growth defect on glycerol, VDAC3 is not able to give a comparable phenotype. Indeed, in presence of glycerol as unique carbon source yeast cells must use mitochondrial respiration and this allows only a very little growth on glycerol, that is aggravated at 37°C.

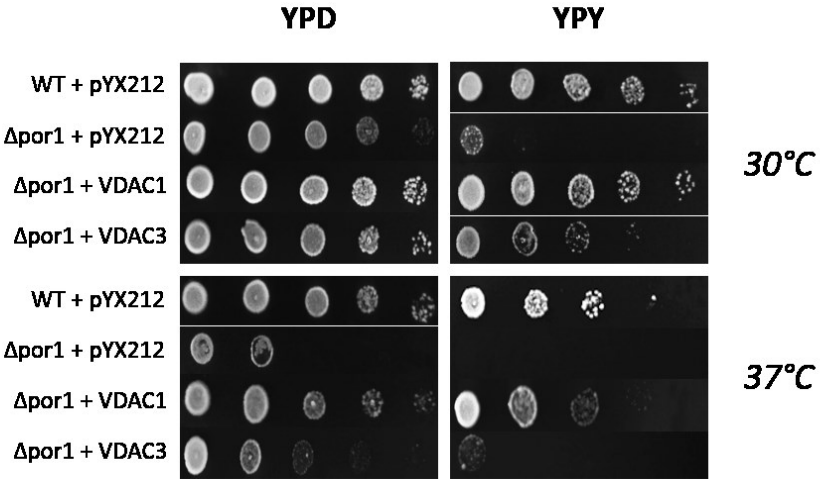

Fig 26 ***Complementation assay of human VDAC3 in Δpor1 yeast cells.*** Using the serial dilution method, complementation assay was performed using YPD and YPY. As expected, VDAC1 restore the yeast growth defect while isoform 3 just partially.

As expected, data showed here, perfectly overlap the data presented in literature, confirming an impaired role of VDAC3 in *Δpor1* complementation.

4.1.2 Purification of VDAC proteins from yeast

Human VDAC1, VDAC3 and N1-VDAC3 were expressed in *Δpor1* yeast strain and purified from yeast mitochondria. Purification was performed by chromatography using HTP/celite in ratio 2:1.

Aliquots of each eluate, containing purified proteins, were loaded on a 12% SDS-PAGE. As showed in Fig. 27, all proteins were successfully purified, as showed by the presence of single bands approximately of 32 kDa.

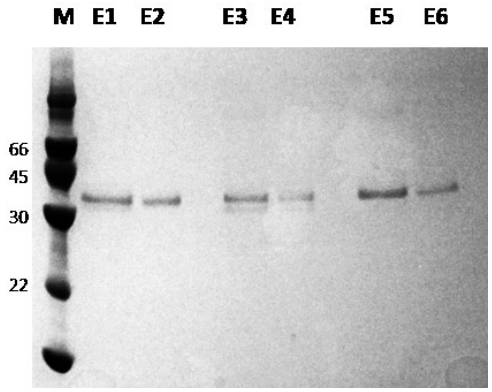

Fig 27 ***Electrophoretic analysis of VDAC proteins from yeast mitochondria.*** 12% SDS-PAGE of VDAC proteins expressed in yeast and purified from M: Mr Markers; E1-E2: fractions referred to VDAC1; E3-E4: fractions referred to VDAC3; E5-E6: fractions referred to N1-VDAC3.

4.1.3 Purification of VDAC proteins from *E. coli*

The His-tagged protein VDAC3 was expressed in *E. coli* BL21 strain and purified by affinity chromatography with Ni-NTA resin, as described in Methods. A specific purification procedure was used for getting the VDAC3 refolding, different from the protocol used for the others His-tagged VDAC proteins used. Previously, indeed, we found that the purification by Talon not allowed to obtain an appreciable amount of protein, for unknown reason. His-tagged VDAC1 was purified, as a control, using the same protocol.After Ni-NTA purification, small aliquots of each eluate containing the purified proteins were loaded on a 12% SDS-PAGE. As showed in Fig. 28, both VDAC1 and VDAC3 were obtained as pure proteins, as demonstrated by the presence of a single protein band of approximately 32 kDa.

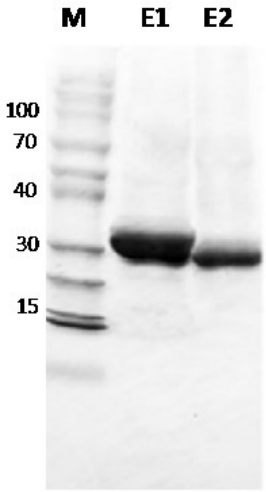

Fig. 28 ***Electrophoretic analysis of His-tagged proteins.*** 12% SDS-PAGE of his-tagged proteins expressed in E. coli and purified by Ni-NTA column. M: Mr Markers; E1: fractions containing VDAC1; E2: fraction containing VDAC3.

4.1.4 Electrophysiological characterization of human VDAC3 from yeast

As reported in literature, VDAC3 shows a reluctance for reconstitution in artificial membranes. The purified VDAC3 from yeast mitochondria was directly added to the PLB, as well as, VDAC1 purified by same protocol.

VDAC1 have shown easily ability to form pores of expected size and traces obtained from it insertion will be showed subsequently. The use of VDAC1 as control validates the method.

On the contrary, VDAC3 from yeast mitochondria preparation have shown pores just rarely; in addition, only very few channels were inserted after addition of 2 mM DTT. Trace recorded of VDAC3 is showed in Fig. 29. Due to an insufficient number of channels no additional analysis were performed.

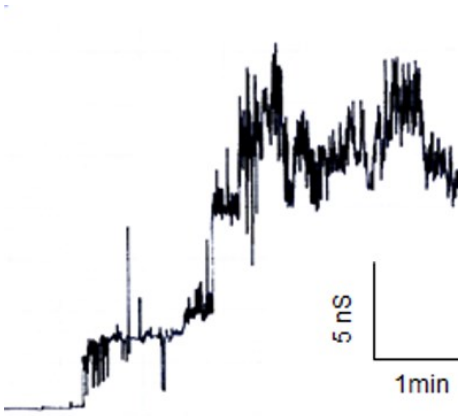

Fig 29 ***Electrophysiological analysis of VDAC3 from yeast mitochondria.*** Single-channel recording after the addition to the membrane of purified VDAC3 from yeast mitochondria. The aqueous phase contained 1 M KCl and 25 ng/ml protein. The membrane potential was 10 mV.

4.1.5 Electrophysiological characterization of recombinant human VDAC3

The His-tagged VDAC3 was expressed in *E. coli* and purified by affinity chromatography using Ni-NTA resin. Protein was refolded by drop-wise addition of the solution to the Refolding Buffer, as previously described. As control, VDAC1 was prepared, purified and refolded using same conditions. Both VDAC3 and VDAC1 were characterized using PLB, and the data obtained were used to compare the two isoforms.

The analysis of VDAC1 activity was comparable with the main characteristics described in literature for this protein: as expected, VDAC1 was able to form channels characterized by a conductance amplitude of 3.5 nS in 1 M KCl. In

addition, the protein displayed the typical voltage-dependent behavior, as showed in Fig. 30A. These data strongly validate the method used for preparation of recombinant protein.

Conversely, under same conditions, VDAC3 showed a very small activity as shown in Fig. 30B. The analysis of conductance in presence of different ions, such as KCl or K Gluconate, has revealed that VDAC3 has a main conductance at about 100 pS, thus 35-40 times less than isoform 1. This data may explain why VDAC3 activity has not been well characterized until now: its signal might have been previously overlooked because of this small conductance.

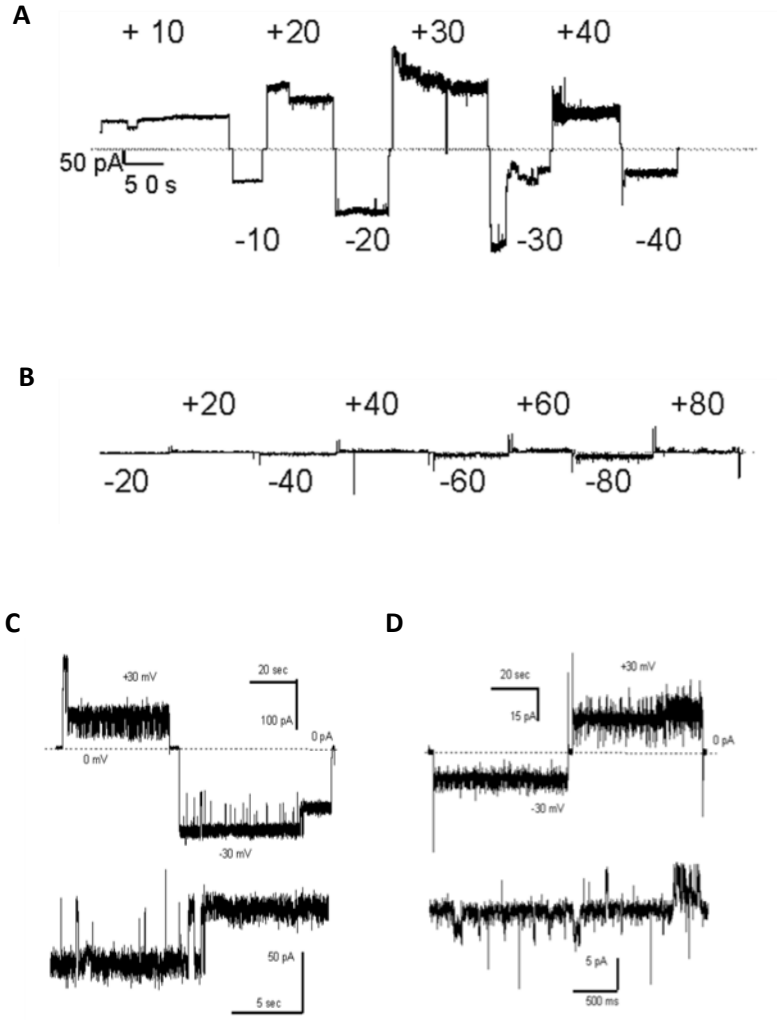

Fig 30 ***Electrophysiological analysis of VDAC1 and VDAC3.*** **A)** Recombinant human VDAC1 forms channels with typical biophysical characteristics. VDAC1 activity was recorded in 1 M KCl medium upon application of the indicated voltage pulses. Current steps corresponding to 3.5 nS conductance are observable. **B)** Activity of human recombinant VDAC3 obtained with the same purification protocol. The same scale was used for comparison. **C)** Current traces recorded in 1 M KCl medium at + and – 30 mV applied voltages (cis side) using purified VDAC1. The tendency to close at both potentials is clearly observable. **D)** VDAC3 activity recorded under the same conditions as C.

According to Laplace law, it is possible to estimate the diameter of the VDAC3 pore to be approx. 0.3 nm; same calculation for VDAC1 indicated a diameter of 2.5-3 nm. In contrast to VDAC1, that shows the typical tendency of adopting a partially closed state upon application of +/-30 mV, VDAC3 is characterized by the loss of this tendency, as showed in fig. 30C-D. Indeed, analysis of traces reveal that VDAC3 is active also at very high potentials, ranging up to 100 mV; at the same time, VDAC3 adopts lower-conductance states prevalently at positive voltages. This might be a peculiar property of VDAC3.

4.1.6 Conclusions

The sequence of human VDAC3 shows high homology to those of the others human isoforms; in addition, bioinformatics predictions indicate that secondary and tertiary structures of VDAC3 are similar to that of isoform 1 [136]. All these information have strongly prompted to consider VDAC3 as an additional pore-forming protein. However, VDAC3 behavior disproves this fact.

The complementation assay in the yeast *Δpor1* strain have revealed that VDAC3 is not able to fully recover the growth features of the yeast, at variance with VDAC1 and 2: as previously showed, VDAC3 allows a very scarce growth in conditions of strict oxidative metabolism. This means that, although VDAC3 is targeted to the yeast mitochondria, it is able to restore the bioenergetic metabolism very poorly.

Expression of VDAC3 in Δpor1 yeast and its purification from mitochondria did not result in an activity comparable to those of VDAC1. However, using the recombinant His-tagged protein, we report for the first time that VDAC3 is able to form small-conductance channels in 1 M KCl in a reproducible way. Becouse of its small conductance, VDAC3 activity might have been previously overlooked.

An estimation of VDAC3 pore size have been indicates a difference with VDAC1 in the range of one order of magnitude between the pores formed by the two proteins. The small pore diameter might well account for reduced metabolite flux across VDAC3, even if it has a predicted structural similarity to VDAC1. In addition, VDAC3 remains in a open state also at high voltages; however, the structural basis and the physiological significance of this phenomenon is unclear.

Concerning the tridimensional arrangement of VDAC3, in the absence of an experimental structure, it is possible to hypothesize that some domains of the protein can play a different role in VDAC3 with respect to VDAC1. In particular, in a previous work [61] it was demonstrated that the swapping of the N-terminal domain of VDAC3 with the same domain from VDAC1 fully restores the ability to complement the growth defect in *Δpor1* yeast. Thus, one possibility is that the structure/position of the N-terminal region of VDAC1 and VDAC3 are different, accounting for a partial occlusion of the pore.

As to the physiological function of VDAC3, one possibility is that this protein is not used routinely in the cell as a conduit for molecules, but it is specialized in other functions as well. The VDAC3 knock-out mouse show a peculiar phenotype: they are alive but suffer of male infertility. Such phenotype has been associated with a deficiency in the organization of the microtubules in the flagellum, possibly provoking reduced motility of the sperm [137]. Expression of VDAC3 in germinative tissues it has been shown to be associated to the mitochondrion, but also to other cytoskeletal structures like, for example the Outer Dense Fiber (ODF) [138].

In conclusion, this work presents an initial biophysical characterization of human VDAC3, previously suggested not to give rise to ion channel activity. Future structural and biophysical work is required to understand in detail the specific features of this isoform.

4.2 Electrophysiological characterization of VDAC1 mutated in domains possibly involved in voltage gating

The most important regulatory feature of VDAC proteins is the voltage dependence. Voltage dependence has been discovered in vitro, by the use of artificial bilayer. VDAC1 exists in a high conductive state, at applied voltage around 0 mV, while upon higher voltages, starting from 20-30 mV, it switches to lower conductance states.

It has been hypothesized that these states are associated with changes in the structural organization, modifying the permeability features of the pore. Despite the structural models of both human and mouse VDAC1 have been reported [33-35], structural details of this relevant feature is still missing. The three 3D structures agree on the location of the N-terminal inside the pore, even with some differences. It is generally accepted that N-terminal domain must play a key role in gating, since its deletion strongly affect the voltage dependency [43]. However, stabilizing contacts between the α-helix and the β-strands have been also attributed to hydrophobic interactions among the residues L10, V143 and V150, as reported in [60]. The identification and the possibility to interfere with the interactions between N-terminal and the pore walls are considered a crucial feature to understand how voltage-gating works.

In this part of the work, we studied the influence of the contacts between the N-terminal sequence and β-strands facing it. This influence was monitored by looking for difference in voltage-dependence and ion selectivity features of the protein. For this purpose, VDAC1 mutants were created by swapping the whole β-barrel of hVDAC1 with the homologous but not identical hVDAC3 barrel, and by removal of whole β-strand 9 or the hairpin of β-strands 9 and 10, thus removing the strands responsible of these contacts.

4.2.1 Impact of N1-VDAC3 expression on yeast *Δpor1* cells

Transformation of *Δpor1* cells with pYX212 constructs expressing both human VDAC3 and N1-VDAC3 was used to assay the complementation on non-fermentable carbon source. As previously reported in [61], the swapping of the N-terminus is sufficient to get a full activation of the normally poorly active isoform VDAC3. This occurs despite the alignment of human VDAC1 with N1-VDAC3 and VDAC3 shows strong similarity between isoform 1 and 3. In particular, differences in charged residues are very slight: VDAC1 has 29 acidic residues against 25 in both hVDAC3 and N1-VDAC3, while both have 35 positive amino acids. Result of complementation is showed in Fig. 31.

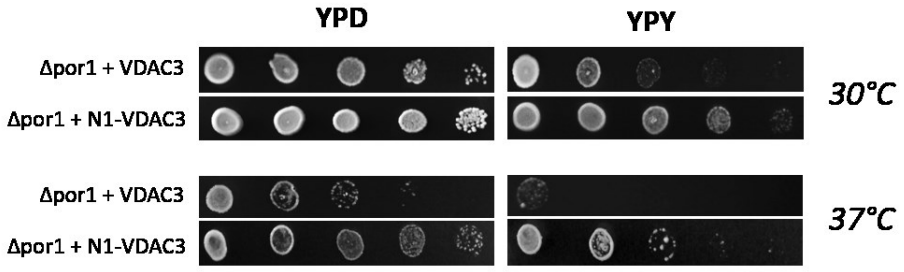

Fig 31 ***Complementation assay of human N1-VDAC3 in Δpor1 yeast cells.*** Using the serial dilution method, complementation assay was performed using YPD and YPY. As reported in [61], N1-VDAC3 restore the yeast growth defect.

4.2.2 Electrophysiological characterization of N1-VDAC3

The N1-VDAC3 chimera was purified from mitochondria obtained from the transformed Δpor1 yeast cell; also VDAC1 was obtained in the same conditions, to have a suitable positive control. N1-VDAC3 and VDAC1 purified from yeast mitochondria were added to PLB and studied by electrophysiological methods.

In a preliminary experiment the activity of VDAC1 obtained from purification of yeast mitochondria was compared to the activity of recombinant proteins coming from heterologous expression in *E.coli* and subsequent purification and refolding. It has been found that both VDAC1 preparations easily formed channels in a bilayer membrane, with almost undistinguishable features, as showed in Fig. 32.

The swapping of the N-terminal domain of VDAC3 with the same domain from VDAC1 confers electrophysiological properties largely overlapping those of VDAC1: as shown in Fig. 33, N1-VDAC3 easily formed channels in the bilayer membrane. In

addition, the conductance steps for both VDAC1 and N1-VDAC3 were quite uniform in size, with the most frequent single-channel conductance event of 4 nS.

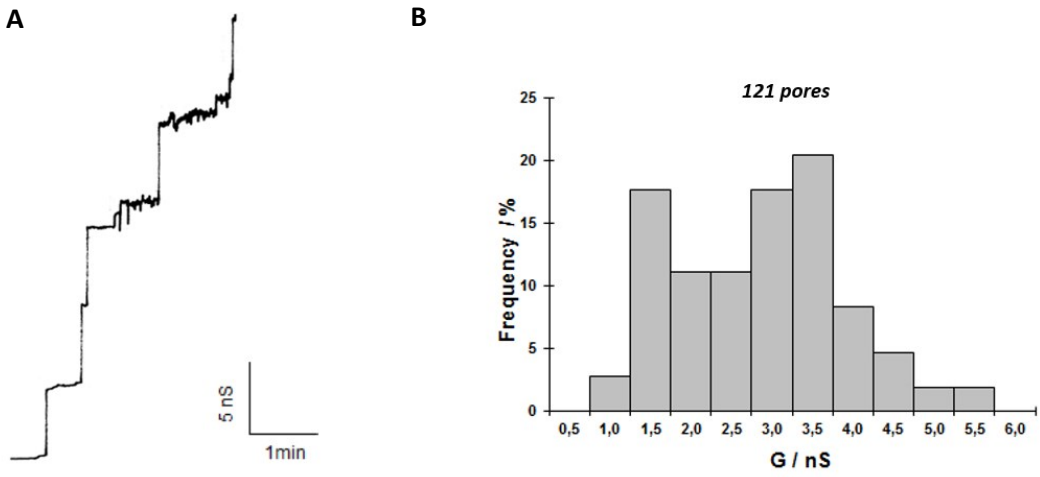

Fig 32 ***Electrophysiological characterization of hVDAC1*** **purified from yeast mitochondria**. A) Single-channel recording of a diphytanoyl phosphatidylcholine/n-decane membrane after the addition of hVDAC1 purified from mitochondria of *S.cerevisiae.* The aqueous phase contained 1 M KCl and 25 ng/ml protein. The applied membrane potential was 10 mV; *T* = 25°C. B) Histogram of the conductance steps measured after reconstitution of hVDAC1 into black lipid bilayer membranes. Conditions as in A. The most frequent single channel conductance was 4 nS.

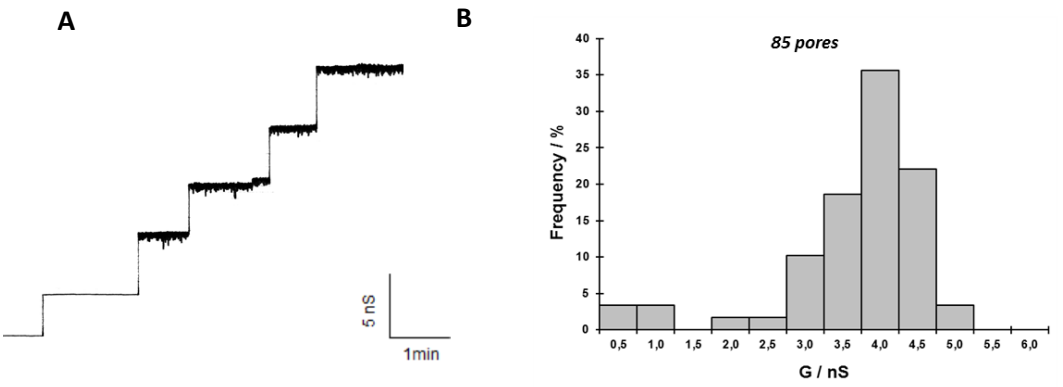

Fig 33 ***Electrophysiological characterization of N1-VDAC1*** **purified from yeast mitochondria**. A) Single-channel recording of a diphytanoyl phosphatidylcholine/n-decane membrane after the addition of N1-VDAC3 purified from mitochondria of *S. cerevisiae* in the same condition of VDAC1 B) Histogram of the conductance steps measured after reconstitution of N1-VDAC3 into black lipid bilayer membranes. Conditions as in A. The most frequent single channel conductance was 4 nS for 85 channels.

4.2.3 Voltage dependence analysis of N1-VDAC3

The voltage dependence of N1-VDAC3 protein purified from yeast mitochondria was analyzed and compared to VDAC1. The wild-type protein showed the normal voltage-dependent gating activity, characterized by the usual symmetrical

response to increasing voltage of opposite signs. Channel closure is evident at both positive and negative potentials starting from ± 30 mV. Conversely, N1-VDAC3 did not show the typical VDAC voltage dependence: three independent experiments have shown that until ± 90 mV the chimeric protein stays in an open state, and only at very high voltages of opposite signs the channel begins to close. The gating process of VDAC1 channels and of N1-VDAC3 in response to symmetrical voltage steps of linearly increasing amplitude is reported in Fig. 34A-B.

The comparison between the two proteins has been obtained by plotting the relative conductance G/G_0 as a function of the applied voltage (Fig. 34C). The plot clearly demonstrates the profound differences in term of gating dynamic between the two proteins.

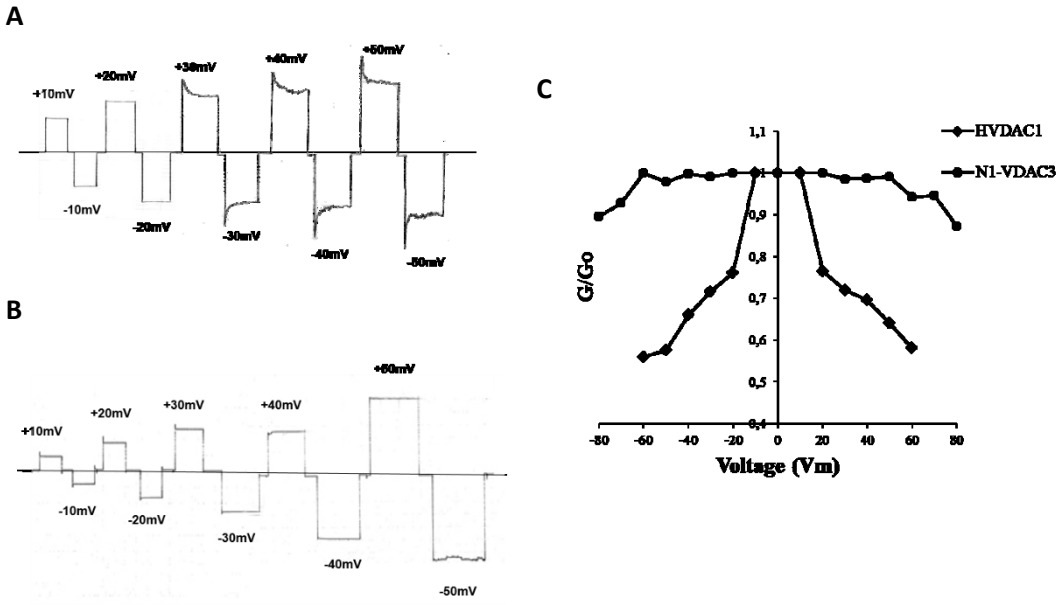

Fig 34 ***Voltage-dependence analysis of VDAC1 and N1-VDAC3.*** **A)** Voltage dependence of VDAC1. VDAC1 was added to the cis-side of a PC/n-decane membrane and few channels were incorporated. Next, increasing positive and negative voltages were applied to the membrane, and the current measured as a function of time. The aqueous phase contained 1 M KCl, T = 25°C. **B)** Voltage dependence of N1-VDAC3. Experimental procedure and conditions as in A. **C)** Analysis of VDAC1 and N1-VDAC3 voltage dependence. Ratio of the conductance G at a given membrane potential (Vm) divided by the conductance G_0 at 10 mV was plotted as a function of the membrane potential Vm. The curves show that hVDAC1 is voltage dependent (full squares) while the chimera N1-VDAC3 is not. The data shown are the average of three independent experiments.

4.2.4 Purification of VDAC1 deletion mutants from *E. coli*

The His-tagged proteins VDAC1 and the two deletion mutants, Δ136-147 and Δ136-160, were expressed in *E. coli* BL21 strain and purified by affinity

chromatography with Ni-NTA resin, as described previously. The refolding of these proteins was performed on-column with the Talon resin. Eluted proteins were visualized on a 12% SDS-PAGE.

As showed in Fig. 35, the recombinant proteins were completely purified, as demonstrated by the presence of a single protein band in the corresponding gel lanes.

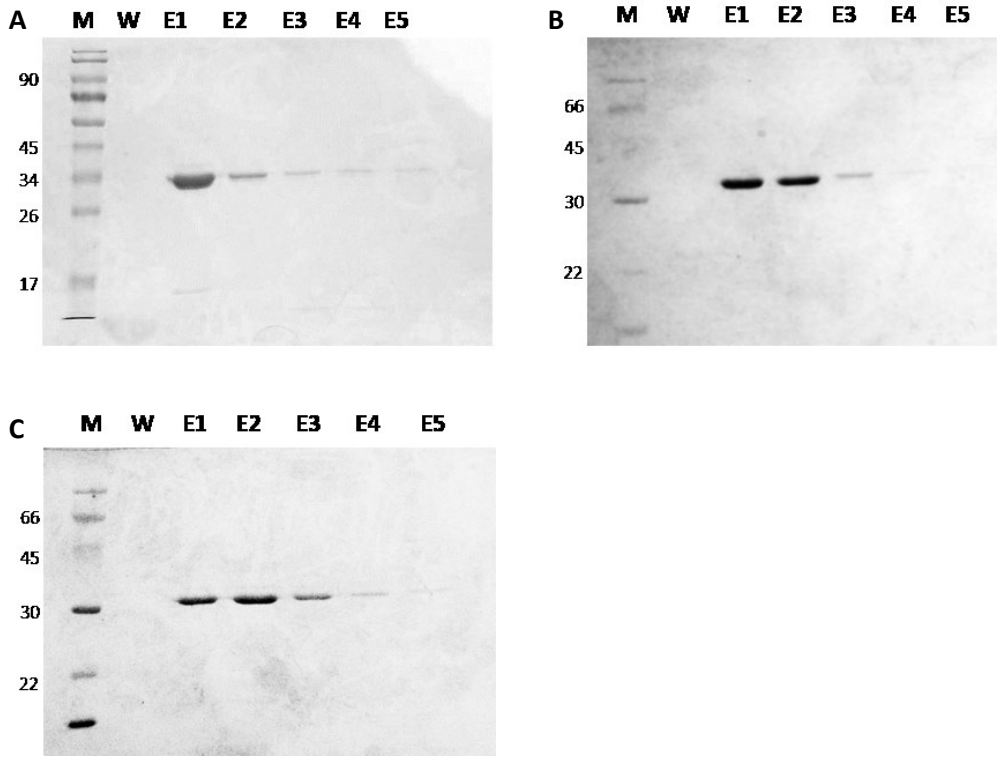

Fig 35 ***Electrophoretic analysis of His-tagged proteins.*** 12% SDS-PAGE of His-tagged proteins expressed in *E. coli* and refolded by a Talon column. M: Mr Markers; W: wash of the column; E1-E5: fractions collected from a Talon column showing the purity of each proteins. A) Purification of VDAC1; B) Purification of VDAC1Δ 136-147; C) Purification of VDAC1 Δ136-160.

4.2.5 Electrophysiological characterization of VDAC1 deletion mutants

Recombinant His-tagged proteins VDAC1 Δ136-147 and VDAC1 Δ136-160, as well as WT VDAC1 as control, were added to the aqueous phase bathing a lipid bilayer membrane. For VDAC1, most of the conductance steps had a single-channel conductance of 4 nS in 1 M KCl, a result that confirms existing data obtained by extraction of human VADC1 from yeast mitochondria. Moreover, experiments performed using 0.1 M KCl have confirmed that its single-channel conductance was a linear function of the aqueous salt concentration.

The single channel properties of both VDAC1 deletion mutants were completely different from those of wild-type protein (Fig. 36).

While the increase in VDAC1 conductance occurred in distinct steps, the deletion mutants showed “noisy” single channel behavior with fast fluctuations of the channels. The most frequent single channel conductance was 2 nS for VDAC1 Δ136-147 and 1.5nS for VDAC1 Δ136-160, as showed in Fig. 36. These results clearly indicate that the deletion of β-strands leads to proteins that form smaller pores, which are more instable than the wild-type ones.

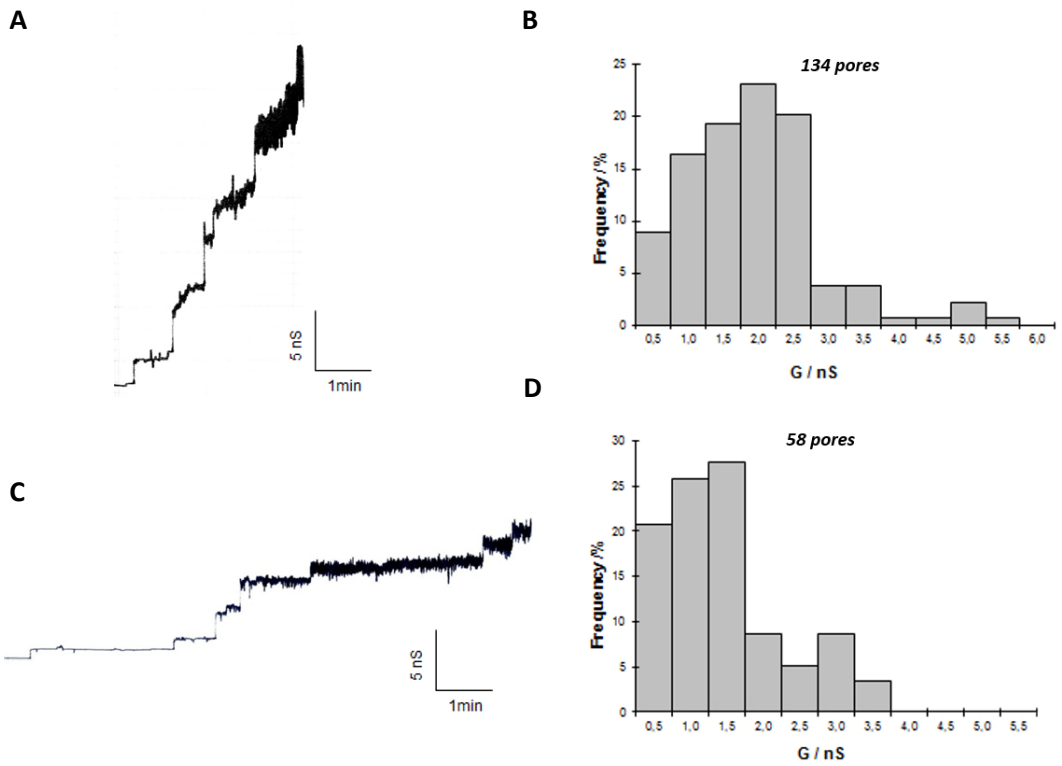

Fig 36 ***Characterization of VDAC1 deletion mutants***. **A)** Single-channel recording of a diphytanoyl phosphatidylcholine/n-decane membrane after the addition of his-tagged purified and refolded VDAC1 Δ136-147. The aqueous phase contained 1 M KCl and 25 ng/ml protein. The applied membrane potential was 10 mV; T = 25°C. **B)** Histogram of the conductance steps measured after reconstitution of VDAC1 Δ136-147 into black lipid bilayer membranes. Conditions as in A. The most frequent single channel conductance was 2 nS for 134 channels. **C)** Single-channel recording of a diphytanoyl phosphatidylcholine/n-decane membrane after the addition of his-tagged purified and refolded VDAC1 Δ136-160. The aqueous phase contained 1 M KCl and 25 ng/ml protein. The applied membrane potential was 10 mV; T = 25°C. **D)** Histogram of the conductance steps measured after reconstitution of VDAC1 Δ136-160 into black lipid bilayer membranes. Conditions as in A. The most frequent single channel conductance was 1.5 nS for 58 channels.

4.2.6 Voltage-dependence of VDAC1 deletion mutants

Voltage dependence analysis was performed for VDAC1 Δ136-147 and VDAC1 Δ136-160, as well as for VDAC1 as control. The voltage dependence of recombinant His-tagged VDAC1 was identical to that measured previously with the protein extracted from yeast mitochondria. Indeed, starting with 20-30 mV, the membrane current decreased for both positive and negative potentials, indicating a symmetrical response of the channels to the applied voltage. These results confirm that recombinant VDAC1 was successfully renatured and indicate that both proteins, prepared from yeast mitochondria or purified from bacteria show the same electrophysiological behavior.

The VDAC1 Δ136-147 showed a voltage-dependency similar to that of wild-type protein, although the membrane current decreased more at negative potentials (Fig. 37A). This asymmetry was even more pronounced in the mutant deleted of both β-strands. Most surprising VDAC1 Δ136-160 did not display any voltage dependence at positive voltages as clearly shown in Fig. 37B. This new functional feature is thus due to the absence of the β-hairpin 9-10.

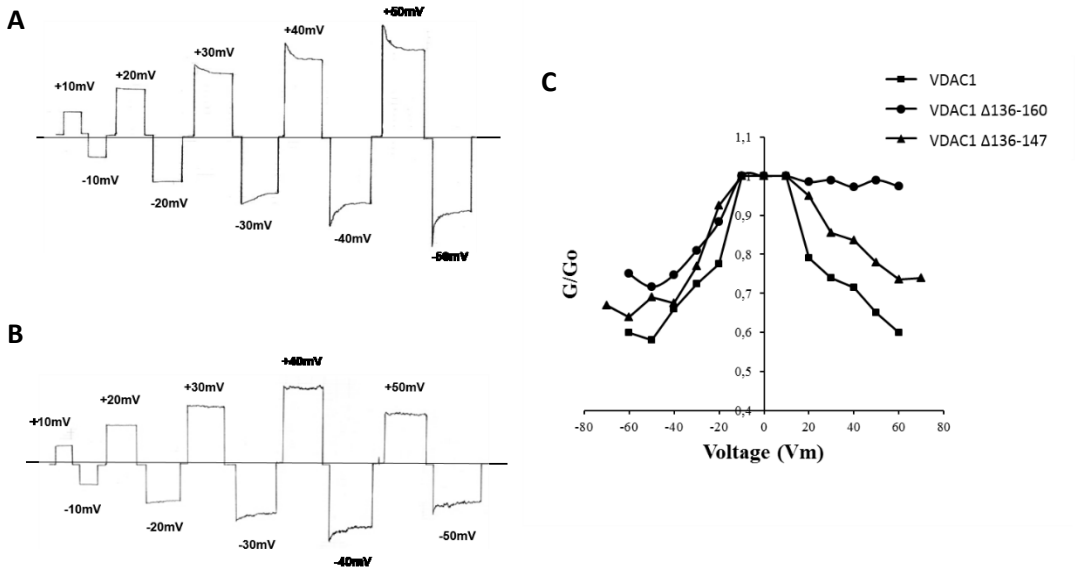

Fig 36 ***Voltage-dependency of VDAC1 deletion mutants.*** **A)** Voltage dependence of purified VDAC1 Δ136-147. Symmetrical voltage steps of linearly increasing amplitude were applied to the membrane, and the membrane current was measured as a function of time. The aqueous phase contained 1 M KCl, T = 25°C. **B)** Voltage dependence of purified VDAC1 Δ136-160. Conditions as in A. **C)** Analysis of VDAC1, VDAC1 Δ136-147 and VDAC1 Δ136-160 voltage dependence. Ratio of the conductance G at a given membrane potential (Vm) divided by the conductance G_0 at 10 mV as a function of the membrane potential Vm. The curves show that VDAC1 is voltage dependent (full squares) while Δ136-160 is asymmetrically voltage dependent, showing to be not sensitive to positive voltages applied to the cis side of the cell. VDAC1 Δ136-147 shows an intermediate behavior at positive voltages applied to the cis side. Data are the average of three independent experiments.

4.2.7 Ion selectivity analysis

Zero-current membrane potential experiments were performed and are presented in Table 4. VDAC1 showed preferential movement of anions through the channel, as widely reported in literature and in [53]. In the presence of N1-VDAC3 the pore became selective for cations over anions: this result cannot be simply explained with changes in the protein composition, with the ratio positive/negative that was reduced from 39 to 35. More interestingly, in the presence of a bulky anion, the cationic selectivity is further enhanced with respect to the control. This indicated that the screening properties of the pore changed as a consequence of the modifications of the residues exposed to the water-phase. The deletion of one β-strand or one β-hairpin in hVDAC1 produces similar consequences, with a preferential movement of cations in the presence of bulk anions. Also, in these mutants the screening features of hVDAC1 have been dramatically altered and the N-terminus defines a narrower section available to the ion flow. The deletion causes positive residues to approach and this might become a kind of trap for the bulkier anion acetate, thus slowing its movement, as it has been demonstrated by molecular dynamics simulation of the ion flow inside the pore [53]

	Pc/Pa		
Protein	***KCl***	***LiCl***	***KCH_3COO pH 7.0***
VDAC1	0.30 ± 0.02	0.35± 0.03	0.94 ± 0.016
N1-VDAC3	1.16 ± 0.05	0.57 ± 0.03	1.88 ± 0.17
VDAC1 Δ136-147	0.34 ± 0.04	0.42 ± 0.01	1.58 ± 0.01
VDAC1 Δ136-160	0.51± 0.05	0.43± 0.02	1.65 ± 0.01

Table 4 ***Zero-current analysis of ion selectivity.*** Zero-current membrane potentials, Vm, of diphytanoyl phosphatidylcholine/n-decane membranes in the presence of VDAC1, N1-VDAC3, VDAC1 Δ136-147 and VDAC1 Δ136-160 measured for a 10-fold gradient of different salts. Vm is defined as the difference between the potential at the dilute side (10mm) and the potential at the concentrated side (100 mm).

4.2.8 Conclusions

N-terminal domain of VDAC1 is considered one of the most interesting part of the protein, due to its strategic location and its possible flexibility. Based on structural models [33-35], N-terminal domain play a structural role, folding inside the pore, thus contributing to the rigidity of the structure. Moreover, it has been proposed

an interaction of the N-terminus with amino acid residues in the β-strands 9 and 10. The breakage of the hydrophobic interactions by application of higher voltages has been indicated as responsible for the removal of the N-terminus from inside the pore, reducing the pore diameter available for ion flux [139].

At the same time, N-terminal domain is involved in voltage gating: its removal, as reported in [43], strongly affects this VDAC feature, suggesting that N-terminal fragment is involved not only in the maintenance of the overall integrity of the incorporated channel, but also in its regulation. It is thus possible to state that also other structural components of the pore, interacting with the N-terminal sequence, might contribute to the regulation of the electrophysiological features of the pore.

To asses the involvement of these domains, we used a set of VDAC1 mutants. First mutant used in this work was a swapping mutant carrying the N-terminus of VDAC1 inserted on the VDAC3 barrel [61]. VDAC3 maintains both V143 and L150 and the N-terminal of VDAC1 still has in place L10. The swapping mutant has similar pore conductance but lost the voltage-dependence typical of hVDAC1. This can be interpreted as if more residues involved in the interactions between N-terminus and pore walls were changed and this fact de-sensitizes the moiety to move in/out of the pore. The whole electrostatic field due to the network of residues exposed to the hydrophilic inner side of the pore was changed. The voltage sensor has thus been modified so efficiently that it cannot exert its role anymore: this is confirmed by the finding that VDAC3 appears only poorly or not voltage-dependent, as previously reported.

Furthermore, we characterized the two VDAC1 mutants lacking respectively one or two β-strands (Δβ9 and Δβ9-β10) respectively missing V143 and both V143 and L150, thus their interactions with L10 were made impossible. In particular, the deletion of β-strands 9 and 10 can be seen as the deletion of a whole β-hairpin and this does not change the topology of the protein.

Although proteins were stable as predicted by modeling, electrophysiological characterization has indicated a reduced diameter. However, the most interesting result is the asymmetric decay of the voltage-dependence of these mutants. In

particular, the mutant missing the whole β-hairpin 9-10 has a fully asymmetric behavior, remaining insensitive to positive applied voltages.

An asymmetric behavior of voltage dependence has been rarely observed. One example is upon incubation of VDAC1 with a synthetic polyanion, which interacts with positive charges and is able to inhibit the single channel conductance of reconstituted pores [140]. Furthermore, the addition of this polyanion on the cis side, upon application of positive, but not negative, potential, resulted in the stabilization of the open state of the pore, and this result was interpreted as stabilization of the channel in the open state. In addition, is possible to hypothesize that deletion of the β9-10 hairpin strongly reduces the space available for N-terminus and probably hinders its movement toward outside the pore.

In conclusion, results obtained from our experiments showed that VDAC1 pore is stabilized by a network of interactions between the N-terminal and the pore-wall and confirms that interrupting them destroys the voltage-dependence property of this channel.

4.3 The hSOD1 expression in *S. cerevisiae* Δ*por1* strain: impact on the mitochondrial metabolism

Many evidences have indicated new roles for SOD1, which are independent from its antioxidant activity. In yeast S. cerevisiae is showed that SOD1 stabilizes YCK1 and 2, promoting the respiration repression in presence of glucose [95-96]. In addition, SOD1 is required to prevent VDAC carbonylation and to maintain the physiological levels of the mitochondrial proteins VDAC and TOM40 [102-104]. These evidences suggest an involvement of SOD1 in regulation of both fermentative and respiratory metabolism. To verify this hypothesis, in ths part of the work, the human SOD1 protein was expressed in yeast S. cerevisiae devoid of endogenous POR1, to assess SOD1 behavior in absence of the main protagonist of mitochondrial-mediated metabolism.

4.3.1 Expression of hSOD1 in *Δpor1* yeast cells

The human SOD1 (hSOD1) was expressed in *S. cerevisiae* BY4742 strain WT and mutant strain *Δpor1*. Yeast strains were transformed with the construct pYX142-hSOD1, as well as with the empty vector pYX142 as control, by the lithium acetate method. Selection of recombinant clones was performed on SD plate containing all nutritional requirements except leucine. It must be stressed that in both yeast strain tested here, the endogenous *sod1* gene was active.

4.3.2 Complementation assay of transformed *Δpor1* yeast cells on glucose and glycerol

The effect of hSOD1 expression in yeast cells on metabolism was evaluated by the complementation assay on both fermentable and non-fermentable carbon source. Indeed, *Δpor1* yeast shows difficult to grow on glycerol, due to the defects in the mitochondrial metabolism. Serial dilutions of WT and *Δpor1* yeast both transformed either with the empty vector pYX142 (as controls) or with the construct pYX142-hSOD1, were plated on the rich medium YP containing glucose (YPD) or glycerol (YPY) and incubated at 30 or 37°C respectively for 1-2 or 3-4 days. The results of complementation assay are showed in Fig. 37.

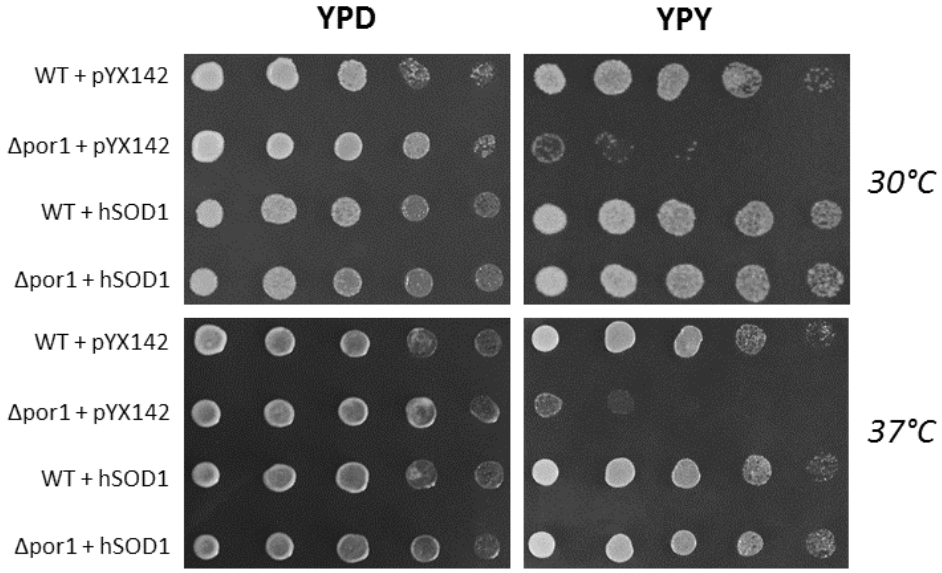

Fig 37 ***Complementation assay on glucose and glycerol.*** Yeast wild type or *Δpor1* strains transformed as described were plated on YPD and YPY and incubated at both 30 and 37°C respectively for 1-2 or 3-4 days. As showed, no major difference among the strains and the delivered constructs was detected on glucose. On glycerol, while *Δpor1* strain shows almost no growth, the addition of the plasmid expressing hSOD1 fully restores the yeast growth defect.

Glucose is the favorite fermentable carbon source for yeast, and normally it is metabolized via glycolysis. As expected, both WT and Δpor1 mutant strains do not exhibit any difference during the growth on glucose, both at 30 and 37°C. On the contrary, glycerol is a non-fermentable carbon source; its utilization provides a two-step process: the phosphorylation of glycerol, that occurs in cytosol, and the conversion of glycerol-3-phosphate in dihydroxiacetone, that occurs in mitochondria [141]. Due to a compromised mitochondrial functionality, *Δpor1* yeast strain transformed with the empty vector, exhibits an impaired growth on glycerol at 30°C, which is aggravated at the restriction temperature of 37°C.

However, the expression of hSOD1 in *Δpor1* strain restores the yeast growth defect, allowing the yeast to grow on the non-fermentable carbon source glycerol, at quantitative levels comparable to those of the WT strain. This surprising result indicates that the expression of hSOD1 in the defective strain *Δpor1* is able to improve mitochondrial utilization of glycerol, suggesting that hSOD1 is involved in restoring the mitochondrial functionality.

4.3.3 Complementation assay of transformed *Δpor1* yeast cells on mitochondrial substrates

In addition to glycerol, others non-fermentable carbon sources can be used by the yeast. We thus decided to assay other, commonly used, carbon sources that all needs a catabolic pathway involving the mitochondrion. Serial dilutions of WT and *Δpor1* yeast transformed as indicated were plated on YP rich medium added of 2% of ethanol, acetate, succinate and citrate, and incubated at 30°C for 1-2 days. The results of the complementation assays are showed in Fig. 38.

Ethanol is the final product of fermentation: in the absence of other nutrients, ethanol undergoes a series of reactions that convert it into Acetil-CoA; also acetate can be converted in Acetil-CoA and metabolized by TCA cycle in mitochondria. Citrate and succinate are metabolic intermediates of the TCA cycle. As expected, both WT strains, transformed or not to express hSOD1, did not show any defect in the growth on any substrate tested here. The *Δpor1* strain, instead, showed an impaired growth both on ethanol and acetate, and in the presence of the TCA cycle intermediates succinate and citrate.

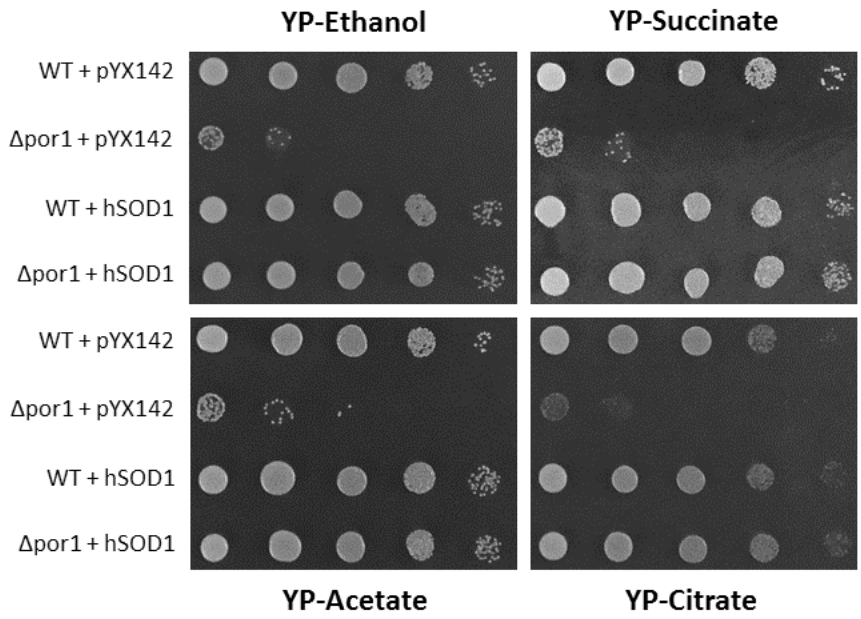

Fig 38 ***Complementation assay on non-fermentable carbon sources.*** Yeast transformants were plated on YP added of ethanol, acetate, succinate and citrate, and incubated at 30°C for 1-2 days. As showed, while Δpor1 strain shows difficult to grow in all substrates, the expression of hSOD1 in the strain restore the yeast growth defect, allowing the yeast to grow in a comparable way to WT strains.

Surprisingly, the presence of hSOD1 introduced in *Δpor1* yeast strain transformed by the suitable constructs, restored the growth defect of yeast plated on any tested substrates. This result suggests that the supplementation of hSOD1 in the yeast cell improves the mitochondrial functionality and this phenomenon is not limited to the glycerol metabolism but it is extended to other non-fermentable carbon sources.

4.2.4 Growth curves of transformed *Δpor1* yeast cells in glucose and glycerol

To quantitatively analyze the impact of hSOD1 on the yeast growth rate, yeast growth curves were produced. WT and *Δpor1* yeast were transformed either with empty plasmid pYX142 or with the construct pYX142-hSOD1, inoculated in liquid minimal medium containing glucose (SD) or glycerol (SY) at the starting OD_{600} of 0.01. The yeast growth was monitored by periodically measuring OD_{600}, till the stationary phase. OD_{600} values were plotted against time.

Fig. 39 shows the yeast concentration curves when they were grown in glucose. Although *Δpor1* yeast is able to use glucose as well as the WT strain, the curve in the minimal medium SD highlighted that its growth is slower than WT, but also that

it is able to reach a very similar saturation (maximum OD_{600} value at plateau phase). The expression of hSOD1 in this mutant strain improved, although minimally, the yeast growth rate, producing a curve that perfectly overlaps the WT curve. For unknown reason, the expression of hSOD1 in the yeast WT strain determines a minimum delay in the growth.

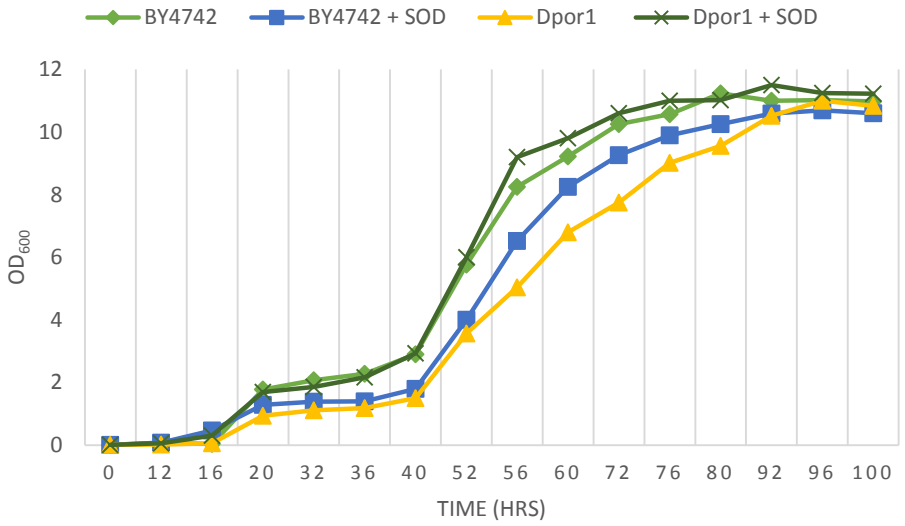

Fig 39 ***Yeast growth analysis on glucose.*** Curves of yeast concentration against time were obtained for the strains indicated in the panel upon growth in glucose. Yeast strain transformed with the empty plasmid or carrying hSOD1 were grown in SD liquid media and incubated at 30°C for up to 100 hours. Optical density was monitored every 4 hours (12 hours during nighttime). The expression of hSOD1 in *Δpor1* strain improves the growth of this defective strain, even if minimally.

Fig. 40 shows the yeast concentration curves when they were grown in glycerol. Although yeast strains have been previously made adapted to glycerol, all strains show a long lag phase compared to the growth in glucose: it was prolonged up to 36-40 hours for the WT yeast and up to 60 hours for the *Δpor1* yeast strain. According to the complementation assay, the mutant strain grew hard using glycerol as carbon source: both the growth rate and the maximum concentration (OD_{600}) reached after 100 hours are significantly lower than other strains. Surprisingly when *Δpor1* strain was transformed with a plasmid carrying the sequence of the human SOD1, the yeast growth rate significantly improved and almost overlapped the curve of the control WT yeast. The delay observed in the growth curve in glucose become much more evident in the growth in glycerol.

These results indicate that the expression of human SOD1, in addition to the endogenous yeast SOD1, can recover the cellular bioenergetic deficit due the absence of POR1.

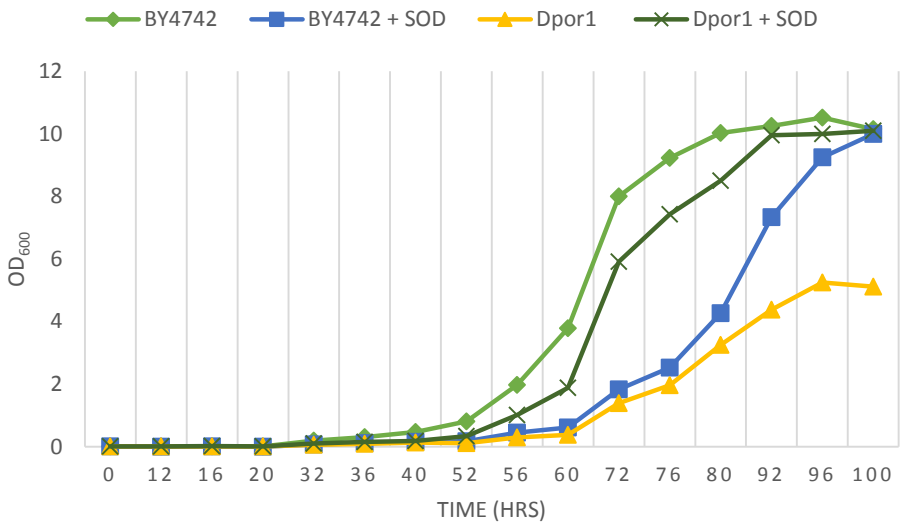

Fig 40 ***Yeast growth analysis on glycerol.*** Curves of yeast concentration against time were obtained for the strains indicated in the panel upon growth in glycerol. Yeast strain transformed with the empty plasmid or carrying hSOD1 were grown in SY liquid media and incubated at 30°C for up to 100 hours. Optical density was monitored every 4 hours (12 hours during nighttime). The expression of hSOD1 in *Δpor1* strain significantly improves the growth of this defective strain.

4.2.5 Measurement of mitochondrial membrane potential of transformed *Δpor1* yeast cells

The mitochondrial membrane potential ($\Delta\Psi_m$) is an important parameter of mitochondrial health. To track the membrane potential in yeast strains we used a fluorescence assay. The fluorescent probe $DiOC_6(3)$ is a cell-permeant lipophilic dye that binds mitochondria of live cells according with their $\Delta\Psi_m$. Its import in the organelle depends on the membrane potential, and fluorescence increases as more molecules are imported. The fluorescence was measured in all the transformed yeast strains, in the same estimated number of cells, to get a relative quantification. Yeast strains were growth in liquid SD up to 0.3-0.6 OD_{600} and treated with $DiOC_6(3)$ as previously described. The relative quantification of $\Delta\Psi_m$ was obtained measuring the fluorescence by flow cytometry and calculated using the WT as control strain (reference sample).

Analysis of $DiOC_6(3)$ fluorescence of WT strain has shown the presence of a unique fluorescence peak, indicating the presence of an homogeneous population of cells,

as showed in Fig. 41A. It can be assume that WT strain is characterized by cells carrying healthy and polarized mitochondria, thus, the fluorescence signal was taken as reference. On the contrary, the analysis of $DiOC_6(3)$ fluorescence in *Δpor1* strain has shown an enlarged peak and completely shifted towards lower fluorescence values, as showed by Fig. 41B. This indicates the presence of heterogeneous population of cells with increased percentage of cells carrying depolarized mitochondria.

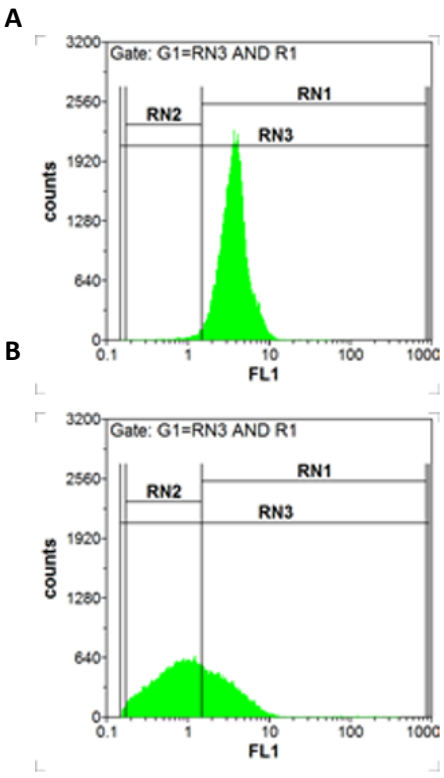

Fig 41 ***Distribution of DiOC₆(3) fluorescence.*** A representative image of fluorescence peak of $DiOC_6(3)$ signal obtained by flow cytometry analysis. **A)** Peak representative of WT cells. **B)** Peak representative of Δpor1 cells.

This analysis indicates that absence of endogenous POR1 dramatically affects the $\Delta\Psi_m$ of *Δpor1* cells. It was estimated that the percentage of depolarized mitochondria in *Δpor1* strain is around 40% of the total, with a more than 10 times increase of depolarized mitochondria in comparison with the WT, as showed in Fig. 42.

It was analyzed the impact of hSOD1 expression in *Δpor1* on $\Delta\Psi_m$; as showed in Fig. 42, hSOD1 drastically reduces the number of cells carrying depolarized mitochondria, indicating a positive effect on mitochondrial functionality. Interestingly, also the expression of hSOD1 in the wild type changes the pattern of mitochondria depolarization, raising the depolarization, albeit not dramatically.

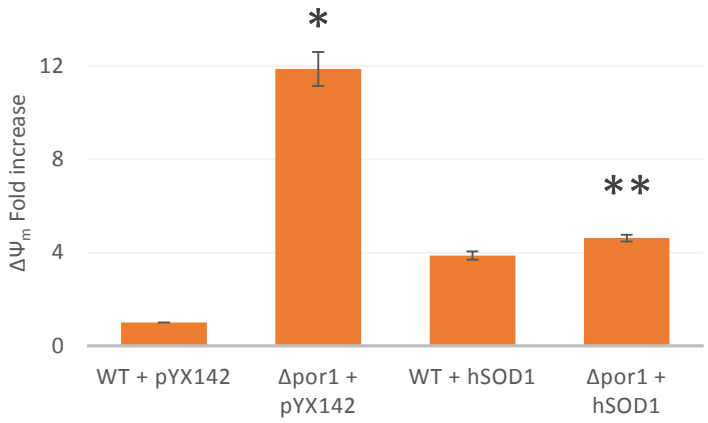

Fig 42 ***Relative depolarization of mitochondria in transformed yeast strains.*** The measurement of mitochondrial membrane potential was carried on with $DiOC_6(3)$. Mitochondria depolarization in the cell populations of each strain was quantified. As showed, the *Δpor1* strain shows the highest increase of depolarized mitochondria, with hSOD1 expression in the same strain significantly lowering this percentage.

* P<0,05 related to the WT + pYX142, ** P<0,05 related to *Δpor1* + pYX142

4.3.6 Determination of total ROS content in transformed *Δpor1* yeast cells

Mitochondria represent the most important intracellular source of ROS: this dangerous group of molecules in physiological condition can act as signaling molecules in specific pathways. Thus, production of ROS can be considered an indirect measurement of mitochondrial activity. Total ROS content in WT and in *Δpor1* yeast strains, transformed with the empty pYX142 or with pYX142-hSOD1, was measured. Yeast samples were growth in liquid SD up to 0.3-0.6 OD_{600} (early exponential phase), and treated with the fluorescent probe DHR 123, as described in Methods. The total content of ROS was detected by flow cytometry analysis by measuring the fluorescence emission of rhodamine. A relative quantification of ROS content was performed, using the WT strain transformed with the empty vector, as a control: the ROS content found in this sample was considered the physiological concentration, and used thereafter as reference.

Results showed in fig. 43 clearly indicate that the ROS level of *Δpor1* strain is significantly lower than the control, corresponding approximately to a fifth of the control. This apparently surprising result could be explained assuming that *Δpor1* strain, in term of mitochondrial metabolism is less active than the WT: the presence in *Δpor1* of an organelle less active than usual might have an impact also on the mitochondrial ROS production.

Although SOD1 is an antioxidant enzyme, the expression of hSOD1 in *Δpor1* strain increases the ROS content, restoring the physiological level of ROS as in the WT. This result indicates that, once again, hSOD1 in *Δpor1* strain acts as re-activator of the mitochondrial metabolism promoting the mitochondrial ROS production up to physiological levels

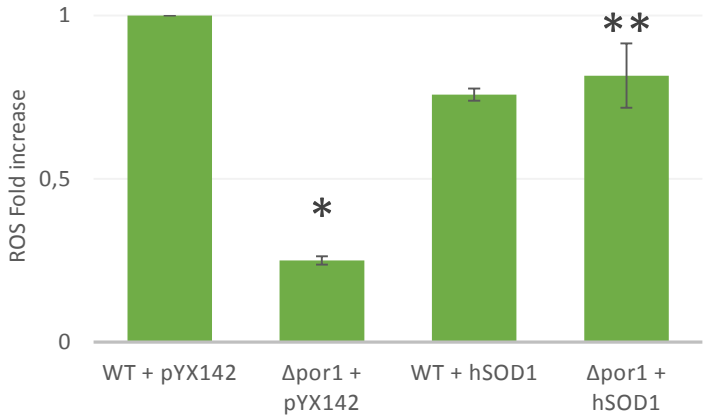

Fig 43 ***Relative ROS quantification.*** The total ROS content in yeast transformants were detected using DHR 123 as probe and flow cytometry. Results are showed as fold increase in ROS content compared to the reference strain wt + pYX142. *Δpor1* shows low levels of ROS, probably due to a less active mitochondria, but the expression of hSOD1 restores the growth level to the level of wt strain.

* P<0,05 related to the WT + pYX142, ** P<0,05 related to Δpor1 + pYX142

4.3.7 Resistance to hydrogen peroxide of transformed *Δpor1* yeast cells

Hydrogen peroxide (H_2O_2) is a ROS mainly produced in the cells from the dismutation of the superoxide anion catalyzed by SOD1. It has been demonstrated that H_2O_2 acts as a pro-apoptotic factor for yeast cells and that *Δpor1* yeast strain is much more sensitive to H_2O_2 than the WT [61].

We analyzed the effect of H_2O_2 on the ROS content in the yeast strains under investigation. The cells were grown in liquid media SD up to OD_{600} of 0.3-0.6, and then incubated with 3 mM H_2O_2 for 4 hours. Cells were then treated with DHR 123. Results are shown in fig. 44, as percentage of ROS increase compared to not treated samples.

As expected, *Δpor1* strain showed a 91% increase in the total ROS content in comparison to the untreated sample. On the contrary, the increase of ROS in wt strain after H_2O_2 treatment was around 43%. These data perfectly match the information in the literature.

Despite H_2O_2 is a product, and not a substrate, of the reaction catalyzed by SOD1, the presence of hSOD1 in the *Δpor1* strain promotes a meaningful decrease of the ROS after H_2O_2 incubation till 50%: this value is comparable to that of the wt strain, suggesting that hSOD1 protects the Δpor1 yeast cells against oxidative stress promoted by H_2O_2.

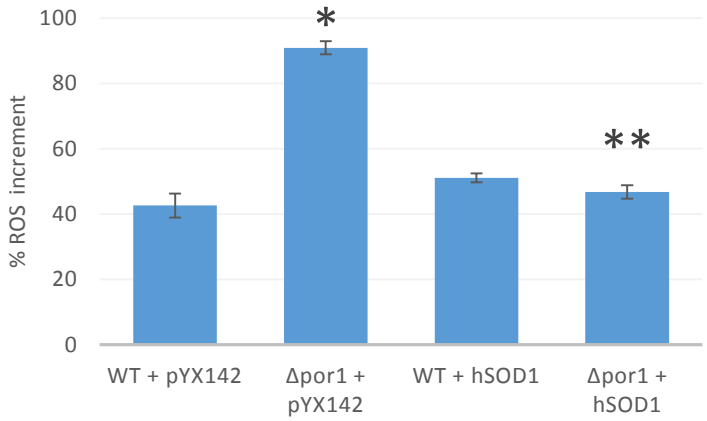

Fig 44 *ROS increase after hydrogen peroxide treatment.* The measurement of total ROS content was obtained after treatment of hydrogen peroxide and compared with the not treated samples. *Δpor1* strain shows the highest increase in ROS, while hSOD1 expression in the same strain significantly lowers this percentage.

* P<0,05 related to the WT + pYX142, ** P<0,05 related to *Δpor1* + pYX142

4.3.8 Real-Time PCR analysis of the expression of genes for mitochondrial proteins in cDNA from transformed *Δpor1* yeast cells

According to previous data, we hypothesized that hSOD1 promotes the re-activation of the mitochondrial metabolism by acting on gene expression of specific genes. Several genes are possible candidates in such a process.

Por2 encodes for the mitochondrial porin isoform 2. This protein has never been purified and it has been showed not to be able to form pores in reconstituted systems [55]. Neverthless a 49% sequence identity with porin1 makes it a natural candidate to substitute the isoform 1 and explain the recovery of mitochondrial functionality in *Δpor1* strain as a result of hSOD1 expression. In addition, also others mitochondrial proteins can be involved in this process; for this reason we have investigated the expression levels of the *sam50* and *tom40*. In particular, *sam50* encodes for a subunit of SAM complex, directly involved in the import and

assembly of β-barrel proteins across OMM. Although it has not been demonstrated, it can be hypothesized that porin2 can be imported into the mitochondria through the SAM complex, thus a change in *por2* expression can be linked to changes in *sam50* expression. TOM40, a subunit of the TOM complex, allows the mitochondrial proteins synthesized in cytosol to reach mitochondrial membranes, with a mechanism different from SAM complex. In addition, beyond its activity as translocator, TOM40 shows a β-barrel structure reminding VDAC organization: therefore, it cannot be excluded that, in an emergency situation TOM40 can partially compensate the lack of VDAC.

Total RNA was extracted from yeast wt and *Δpor1* strains transformed with pYX142 empty or expressing hSOD1 after growth in SD medium up to the exponential phase. The cDNA obtained from each sample was used as template, to perform quantitative Real-Time PCR with specific couples of primers. As internal control, the *act1* gene encoding for actin was used.

The results indicate that these genes show changes in the expression, as hypothesized. A relative quantification was performed.

4.3.8.1 Relative quantification of *por2* expression

C_t values obtained from Real-time PCR experiments were analyzed and relative quantification of *por2* expression was analyzed by using double samples each time. First, we compared the expression levels of *por2* gene in *Δpor1* strain with WT strain, both transformed with the empty pYX142. As showed in Fig. 45A, *Δpor1* shows 50% less *por2* transcripts than the WT. This result could be due to a reduced amount of mitochondria in the porin1-less strain or to mitochondria in a metabolically less active state, or to a combination of both aspects.

To evaluate the effect of hSOD1 expression in healthy mitochondria, we have analyzed the changes in *por2* expression levels in WT yeast strain supplied with hSOD1, comparing it with the same WT strain as a control. As showed in Fig. 45B, the presence of hSOD1 in WT strain significantly improves the level of *por2* expression of around 3.5 times, compared to control. This result indicates that supplementation of hSOD1 in the cell is able to increase *por2* gene transcription.

Furthermore the hSOD1 impact on *por2* transcription is enhanced in the presence of a mitochondrial stress. The expression level of the *por2* gene in *Δpor1* expressing hSOD1 increased about 15 times in comparison with the *Δpor1* strain and more than twice in comparison with the wt strain transformed with the same hSOD1 construct (Fig. 45C-D).

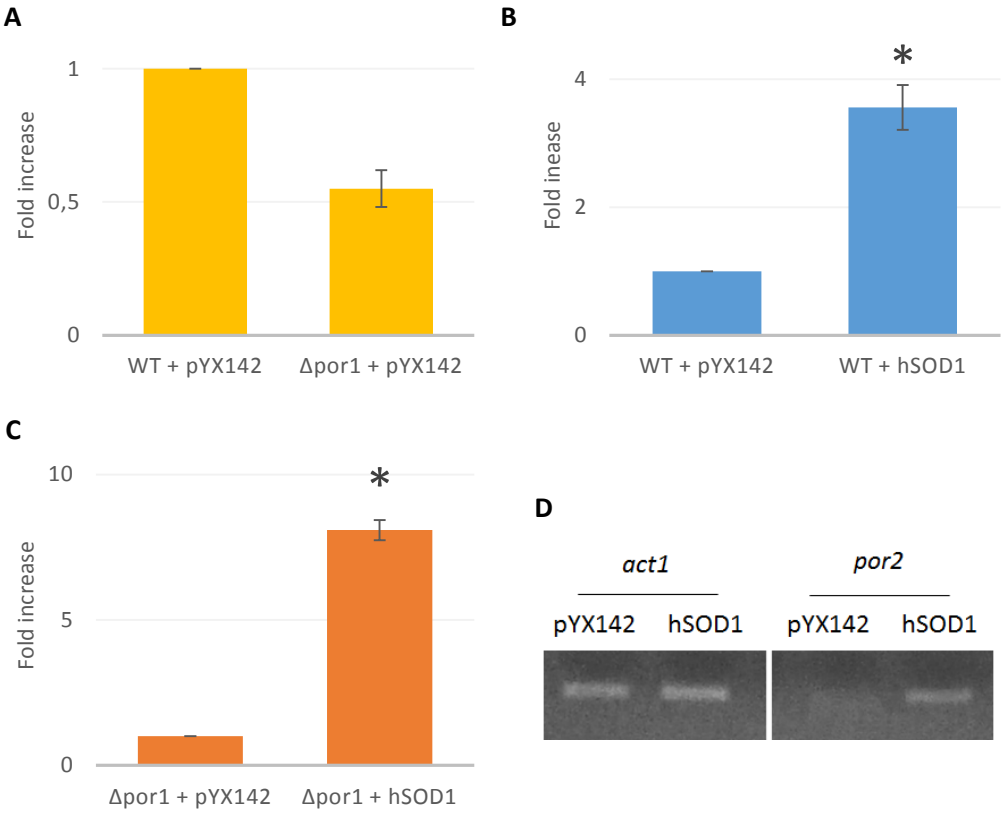

Fig 45 ***Relative quantification of por2 expression levels.*** **A)** Quantification of the expression level of *por2* gene in yeast Δpor1 respect to WT, both transformed with pYX142. **B)** Quantification of por2 level in WT + hSOD1 compared with WT. **C)** Quantification of por2 level in Δpor1 + hSOD1 respect to Δpor1 transformed with pYX142. **D)** Semi-quantitative PCR that shows the different amplifications of por2 transcripts in Δpor1 strain.

* P<0,05 related to the WT + pYX142.

Taken together, these results suggest that the overexpression of SOD1 in the yeast cell has additional effects to the detoxifying one, possibly confirming the ability to act as modulator of the expression of target genes. These data strongly explain how hSOD1 acts in promoting mitochondrial stress relief.

4.3.8.2 Relative quantification of *sam50* expression

Sam50 expression level was quantified as previously described.

In basal condition, *Δpor1* strain shows a slight decrease of *sam50* expression, comparable to the decrease showed for *por2* gene (Fig. 46A).

The incidence of hSOD1 expression was first analyzed in WT strain.

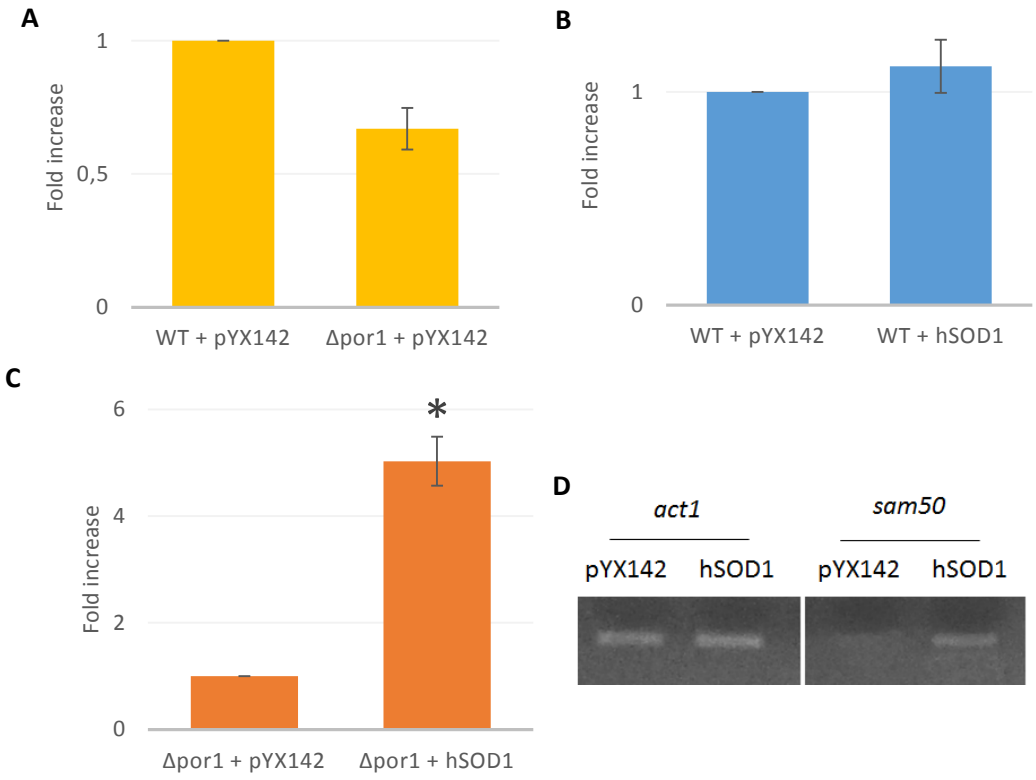

Fig 46 ***Relative quantification of sam50 expression levels.*** **A)** Quantification of the expression level of sam50 gene in Δpor1 yeast with respect to wt, upon transformation with pYX142. **B)** Quantification of sam50 in wt supplemented with hSOD1 in comparison with control. **C)** Quantification of sam50 in Δpor1 + hSOD1 in comparison with Δpor1 transformed with pYX142. **D)** Semi-quantitative PCR that shows different amplification of sam50 gene in Δpor1 strain.

* P<0,05 related to the WT + pYX142.

As showed in Fig. 46B, hSOD1 does not have any significant effect on *sam50* expression levels: indeed, the level of *por2* transcripts remains almost unchanged in WT expressing hSOD1 compared to control. Conversely, in *Δpor1* strain supplemented with hSOD1, the expression level of *sam50* is strongly increased: it was found that hSOD1 promotes an increase of *sam50* transcripts of around 5 times respect to the *Δpor1* control strain, as showed in Fig 46C-D.

These results indicate that in *Δpor1* strain expressing hSOD1 the levels of both *por2* and *sam50* are increased with respect to *Δpor1*. The increase in *sam50* may

be due to a biosynthetic stimulus, used to improve the import of POR2 (and other) proteins with an appropriate level of SAM50.

4.3.8.3 Relative quantification of *tom40* expression

Analysis of *tom40* expression has revealed that no differences were found in the expression between WT and *Δpor1* strain, as showed in Fig. 47A. However, it was found that both WT and *Δpor1* expressing hSOD1 double the concentration of *tom40* in comparison, respectively, to the WT control (Fig. 47B) and to the *Δpor1* control (Fig. 47C-D).

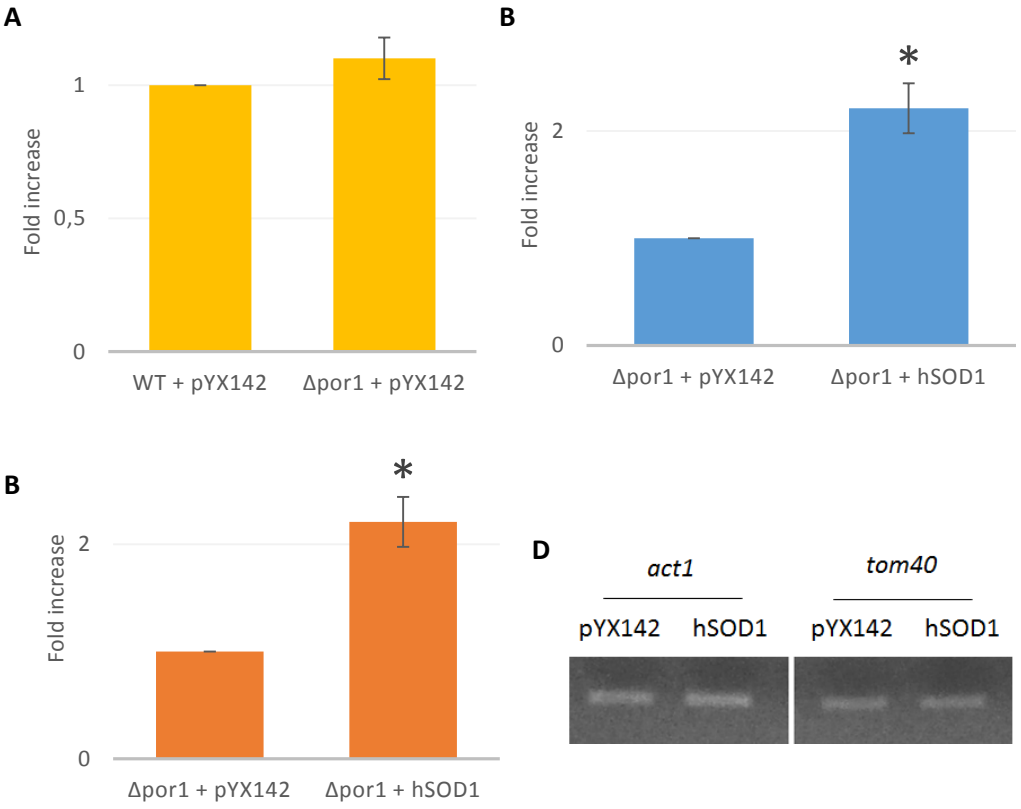

Fig 47 ***Relative quantification of tom40 expression levels.*** **A)** Quantification of the expression level of tom40 gene in yeast Δpor1 respect to WT, both transformed with pYX142. **B)** Quantification of tom40 level in WT + hSOD1 compared with WT. **C)** Quantification of tom40 level in Δpor1 + hSOD1 respect to Δpor1 transformed with pYX142. **D)** Semi-quantitative PCR that shows different amplification of tom40 gene in Δpor1 strain.

* P<0,05 related to the WT + pYX142.

4.3.9 Conclusion

The evidences collected in last years have underlined many new properties of SOD1, independent from its antioxidant role. Although the main activity of SOD1

remains the dismutation of superoxide anions, it was shown in yeast that it is required for the regulation of fermentative metabolism [95-96] and in the VDAC protection from carbonylation [102]. Undoubtedly, the most surprising property showed by SOD1 is its involvement in the regulation of gene expression under particular stress condition, as demonstrated recently by Tsang et al. In response to the canonical function of oxidation of dangerous radicals, SOD1 is translocated to the nucleus where it acts as transcription factor, mediating the cellular response to the oxidative stress [101]. A prerequisite for SOD1 translocation into the nucleus is the phosphorylation of the conserved serine residues 60 and 99 by DUN1; this phosphorylation mechanism is conserved up to mammals. Both human and yeast SOD1 share more of 70% of sequence identity, and it has been demonstrated that hSOD1 in yeast is perfectly active. Moreover, residues Ser60 and Ser99 are conserved and the translocation of SOD1 to the nucleus was observed also for human SOD1 [101].

In our work, the expression of hSOD1 was performed in the mitochondrial defective yeast strain *Δpor1*, which shows a strong impairment of growth in the presence of non-fermentable carbon sources. The utilization of this strain has allowed the analysis of the hSOD1 behavior in response to a mitochondrial stress, due to POR1 absence. As VDAC1 for mammals, POR1 is the main mitochondrial porin of OMM in yeast, directly involved in the metabolic exchange between cytosol and mitochondria. Surprisingly, we have found that the expression of hSOD1 in *Δpor1* strain fully restores the yeast growth defect, allowing the yeast to growth in any non-fermentable carbon sources tested here, such as glycerol, ethanol and acetate; all these nutrient sources, indeed, require a perfectly active mitochondria to be metabolized. Moreover, hSOD1 increases the *Δpor1* growth rate also on glucose, where it is normally able to grow but slower than WT yeast. These data are a strong evidence that hSOD1 is involved in restoring the mitochondrial functionality, and are supported by the concomitant analysis of mitochondrial ΔΨm and cellular ROS, that indicate that hSOD1 significantly decreases the percentage of *Δpor1* cells containing depolarized mitochondria and restores the physiological ROS content as in WT.

All these data can be explained as a re-activation of mitochondrial metabolism. We hypothesize that the lack of POR1 has the same effect of a stress factor, and since in stress situations SOD1 is translocated into the nucleus, it thus can stimulate the expression of proteins involved in recovery of mitochondrial metabolism.

To prove this we have studied the modifications in the expression of other genes that could be involved in the response due to the POR1 lacking. In particular we studied the second porin isoform (POR2), two transmembrane proteins used by the cell for the import of nuclearly encoded mitochondrial proteins (TOM40) and for the assembly of OMM proteins like POR1 itself (SAM50). These last two proteins, containing β-barrel structure might contribute to vicariate the lack of the porin-pore in OMM.

The *S. cerevisiae* genome encodes for a POR1 paralog, POR2, classified as a putative porin. In fact, doubts exist about the ability of POR2 to form pores in OMM: its physiological expression in *Δpor1* is not sufficient to complement the absence of POR1, and previous studies have reported that POR2 does not form pores in artificial membranes [55].

Our qPCR experiments, however, indicate that the expression of hSOD1 in *Δpor1* promotes a significant increase of *por2* transcription and, proportionally, of *sam50*, that codify for a protein involved in β-barrel protein assembly and import to mitochondria. Although POR2 shows less than 50% of sequence identity with POR1, a preliminary analysis of POR2 hydropathic profiles suggests that its sequence is compatible with other β-barrel proteins, such as POR1.

Another feature described in [55] is the lower activity of POR2 promoter, in comparison with the promoter of POR1, which could explain the paucity of this protein. These evidences not only suggest that POR2 could form pores in mitochondrial membrane but also that POR2 could complement the absence of POR1, when overexpressed. It is thus tempting to speculate that hSOD1 can stimulate an improvement in the activity of *por2* gene, producing enough protein to vicariate the lack of POR1.

To confirm this hypothesis some new experiments should be devised. The transformation with hSOD1 of another yeast strain showing the same phenotype

of mitochondrial defect, i.e. the reduced growth when fed with a not fermentable carbon source could explain whether the adaptation by hSOD1 is a general pathway used to rehabilitate the organelle or it is specific for porin. The transformation of a yeast strain devoid of both porins (*Δpor1Δpor2*) with hSOD1, should indicate how much connected and coordinated are the two expression pathways, and whether other putative pore-forming proteins can vicariate the porin family. This last experiment is in progress thanks to a double mutant strain kindly provided by H. Kmita (Poznan, Poland). At the end the direct characterization of purified POR2 in planar lipid bilayer experiments has now become an important issue, and it will be pursued either obtaining POR2 as a recombinant and refolded protein and by a direct purification from mitochondria of yeast overexpressing *por2*. These experiments will allow to present a conclusive picture about the interconnections between porin genes and other genes directly involved in the mitochondria integrity. Presently it can not be excluded that hSOD1 can also act on the regulation of genes involved in mitochondrial biogenesis, in tubulation and fission, all mechanisms able to act on the abundance and quality of mitochondria. These aspects may also contribute to explain the recovery of mitochondrial functionality.

Although further analyses have to be made, our work shows how strongly the fate of VDAC is evidently linked to SOD1, and vice versa.

4.4 Interaction between VDAC and ALS-linked SOD1 mutants: molecular characterization

Mutations in SOD1 gene represent the first cause of familial ALS. Although more than 150 mutants have been discovered, the SOD1-mediated toxicity remains unclear. From a molecular point of view, ALS affected motor neurons show aggregation of misfolded proteins and mitochondrial dysfunction, aspects that partially explain the neurodegeneration of these cells. Many evidences have shown that the most diffused SOD1 mutants, G93A and G85R, were found linked to the cytosolic surface of mitochondria, using VDAC1 as a docking site, as demonstrated by Israelson et al. In addition, electrophysiological measurements have indicated that this interaction can partially influence the VDAC1 conductivity: this phenomenon can be considered the beginning point of mitochondrial dysfunction. In this work, a preliminary characterization of VDAC1-SOD1 ALS-linked mutants was performed, analyzing the effect of these mutants on mitochondria functionality. WT and mutants SOD1 were expressed in vitro, characterized and used from several analysis; in addiction, expression of both WT and mutant SOD1 in neuronal cell were analyzed.

4.4.1 Expression of hSOD1 proteins

The sequences encoding the human SOD1 WT and its ALS-linked mutants SOD1 G93A (from now simply G93A) and SOD G85R (from now simply G85R) were cloned into the bacterial expression vector pET-52b in frame with a Strep-tag at the N-terminal domain. Protein expression was performed in BL21 (DE3) strain after induction with IPTG.

The WT SOD1 is a cytosolic and soluble protein, while the mutant forms tend to form insoluble aggregates. To increase the solubility of these proteins, the protein expression was performed at lower temperature (25°C). After the expression, cell lysis was performed and small aliquots of not induced and induced bacterial extracts were analyzed by SDS-PAGE. The result is showed in Fig. 48.

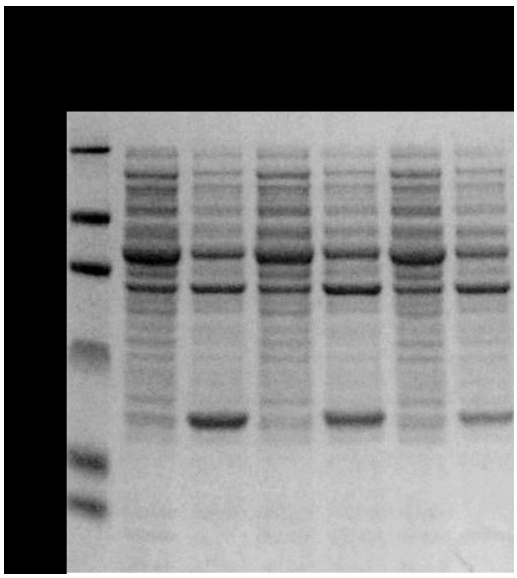

Fig 48 ***Electrophoretic analysis of recombinant hSOD1 proteins expression.*** Lysates from not induced (NI) and induced (I) samples were loaded an a 12% gel and analyzed by SDS-PAGE. An additional band is evident in each induced samples. **M** indicates Mr markers.

The expression of both WT and mutants proteins were successfully obtained, as showed by the presence of a strong additional band in each induced samples, of about 22-23 kDa; indeed, although SOD1 monomer Mr is 16 kDa, it is well known that its electrophoretic mobility corresponds to a band of apparent Mr 20 kDa. In addition, although this was not a quantitative assay, it is apparent that the both mutants, and particularly for G85R, are expressed at lower levels than the WT SOD1.

4.3.2 Purification of hSOD1 proteins

The expression of the proteins was performed in 1 L cultures supplemented with with 0.4 mM IPTG for 3-4 hours at 25°C. Cells were then collected and lysed as described, and the clear lysates corresponding to the soluble fraction were used for the purification of Strep-tagged proteins, by affinity chromatography as described in Methods. Fractions containing the eluted SOD1 protein were loaded on a gel and analyzed SDS-PAGE, as showed in Fig. 49.

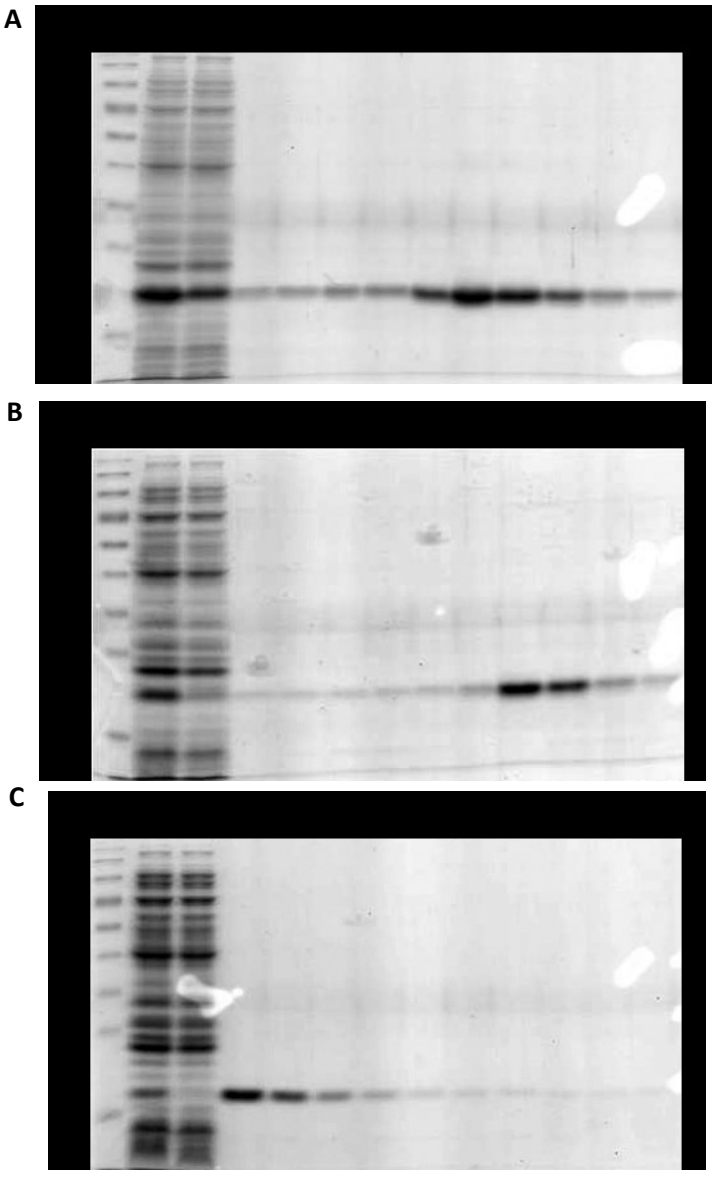

Fig 49 ***Electrophoretic analysis of eluted proteins.*** Fractions containing the purified Strep-tagged proteins were analyzed in 14% gel. **A)** Purification of SOD1 WT. **B)** Purification of G93A. **C)** Purification of G85R. **M** indicates Mr markers, **L** is the lysate, **FT** is the flow through. .

Purification of Strep-tactin proteins were successfully performed. Although the wt isoform is the most abundant, due to its higher solubility, the expression of mutants is however appreciable. Fractions containing the proteins were pulled and dialyzed. Purified proteins were then used for further analysis.

4.4.3 Functional characterization of purified proteins

The functional properties of purified recombinant hSOD1 proteins were analyzed. As reported in the literature, most part of ALS-linked SOD1 mutants, such as G93A, maintain the enzymatic activity and the ability to form a dimeric structure. To confirm the functionality of recombinant hSOD1 proteins we tested the presence of superoxide dismutation activity using the in gel Riboflavine/Nitro Blu Tetrazolium assay as in [132]. In presence of a superoxide anions source, the active hSOD1 shows its activity by causing achromatic zones on dark-blue native gel, caused by the inhibition of NBT salt reduction. As showed in Fig. 50A, both wt and mutant hSOD1, G93A and G85R, resulted active as well as the positive control hSOD1 protein (enzyme obtained from Sigma). In Fig. 50B, as a loading control, an immunoblot of the same samples with anti-SOD1 antibody, is showed

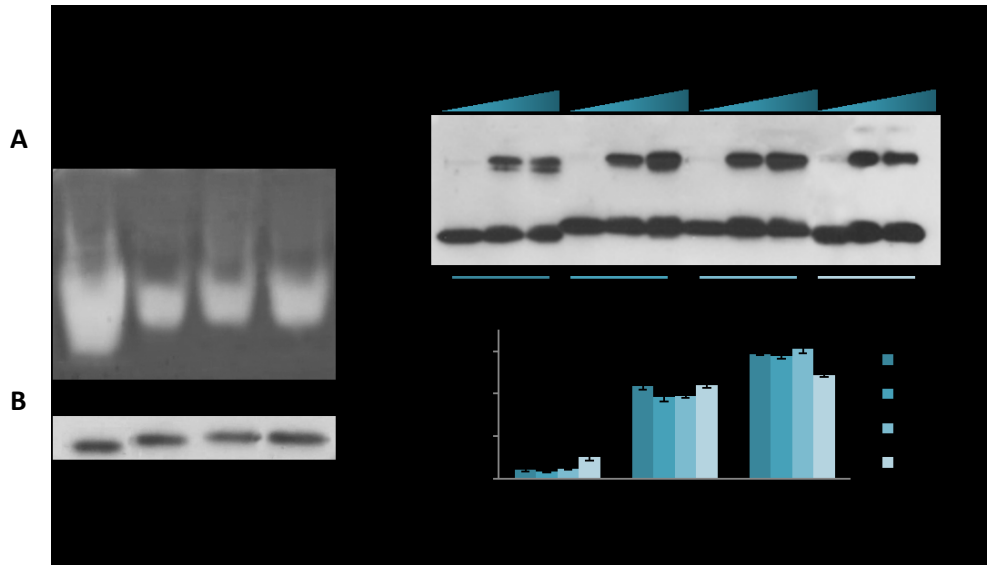

Fig 50 ***Functional characterization of recombinant hSOD1 proteins***. **A)** Measurement of superoxide dismutase activity of hSOD1 (CTRL, WT, G93A, G85R) by in gel Riboflavin/NBT assay. **B)** Relative amount of each protein tested by immunoblotting. **C)** Oligomerization analysis by cross-linking with EGS reagent. **D)** Quantitative analysis by ImageJ software.

In addition, we verified the oligomerization ability of recombinant hSOD1 proteins, studying the levels of dimers formation after the treatment with the cross-linker

reagent EGS. As expected, the oligomerization ability of recombinant WT and of mutant G93A was comparable to the positive control (fig. 50 C-D): without the cross linker reagent, the amount of dimers was really low (around 3-4% of the total) while, after the treatment with 100 and 200 mM of EGS the amount of dimers significantly raised up to 40-60% of the total. On the contrary, the mutant G85R shows higher level of dimers formation without EGS (around 15%) that increase with the addition of EGS. This can be easily explained: the mutation G85R leads to a misfolded protein that can form aggregates much more easily than the WT-like mutations (e.g. G93A).

4.4.4 VDAC1-SOD1 interactions by Microscale Thermophoresis

The interaction among VDAC1 and the SOD1 mutants G93A and G85R was previously described by Israelson et al. [123]. To support these data, we performed a quantitative analysis of interaction using the Microscale Thermophoresis (MST), a sensitive protein-protein interaction assay. MST detects changes in the hydration shell of a fluorescent-labeled protein that occurs as a result of interaction with other molecules. This alteration affects the thermal migration behavior of the protein and it is used to accurately determine the binding affinity coefficient (Kd), obtained by fluorescence depletion curves measured as a function of increasing interactor concentrations [133-134].

Purified rat VDAC1 was prepared as in [142] and labeled with NT.115 Blue/Green dye and incubated with increasing concentrations of purified WT and G93A (1,22 nM to 20 μM) and the analysis performed using a NanoTemper Monolith NT 115 apparatus. The curve was fitted on the data points using the GraphPad Prism software by plotting the percentage of change in normalized fluorescence (F Norm %) as a function of SOD1 sample concentrations.

The results, showed in Fig. 51, clearly show that, at the concentration tested, no interaction with VDAC1 was detected using SOD1 WT. On the contrary, high affinity interaction was detected for the mutant SOD1 G93A, as demonstrate also by the estimated dissociation constant of 5 μM.

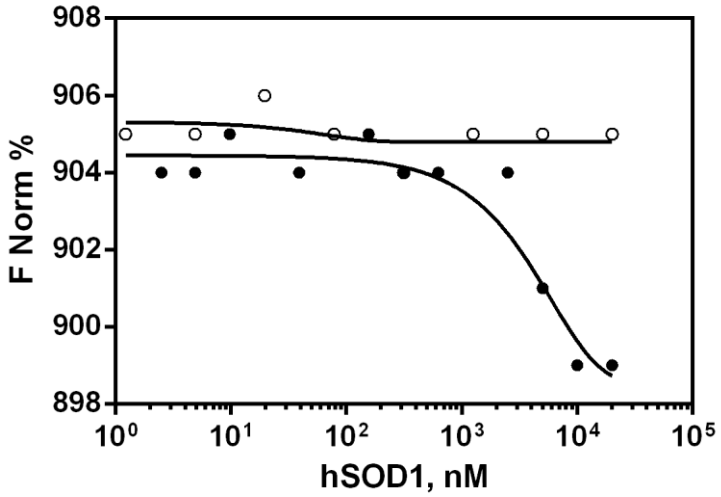

Fig 51 ***Binding of SOD1 to rVDAC1 by MST.*** VDAC1 was fluorescentlyl labeled using the NanoTemper protein-labeling kit Green/Blue. The assay was performed in PBS buffer with 0.005% Tween 20. The concentration of wtSOD1 and mutSOD1 G93A was varied from 1.22 nM to 20 µM, whereas the concentration of the labeled rVDAC1 was kept constant. Interaction between VDAC1 and mutant G93A (•) was detected, while no interaction was detected using wtSOD1 (o).

4.4.5 The influence of SOD1 proteins on the mitochondrial swelling

The mitochondrial swelling is induced by several factor, such as the addition of calcium phosphate that can promote the mitochondria permeability transition pore (MPTP) opening. 25 µM of purified SOD1 WT, G93A and G85R, was added to the purified mitochondria from rat liver, and the effect of these protein on the swelling was monitored by the change in the absorbance at 520 nm in the mitochondrial suspension. Each sample was then treated with 100 µM calcium phospate, to induce the swelling. No protein sample was added in the control.

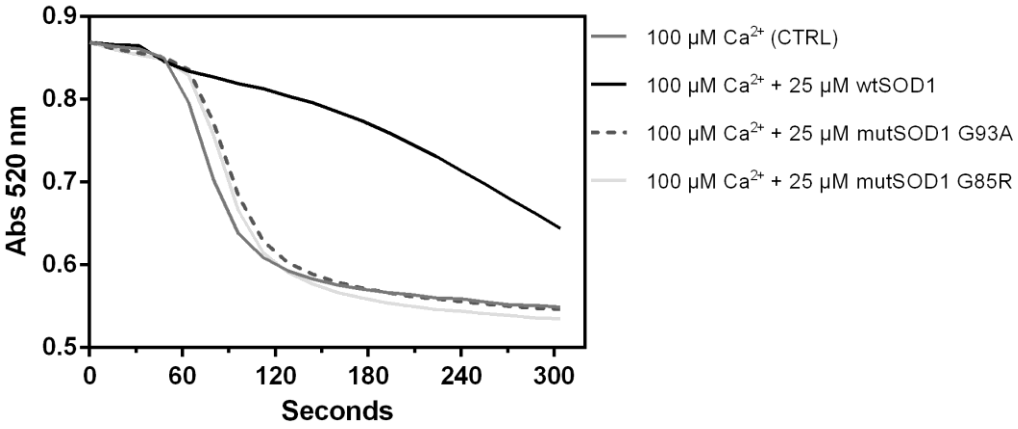

Fig 52 ***Mitochondrial swelling.*** Induction of mitochondrial swelling in isolated hepatic mitochondria from mice. Swelling effect was monitored as the decrease of absorbance at 520 nm of a mitochondria suspension after addition of Ca^{2+}, and wt or mutSOD1.

As showed in Fig. 52, while in the presence of SOD1 WT the swelling was inhibited, the addition of G93A and G85R had no effect and did not change the swelling curves due to the addition of calcium. This means that SOD1 has an influence effect on the mitochondria permeability, and this effect is lost by the mutated SOD1.

4.4.6 The influence of SOD1 proteins on the mitochondrial membrane potential

The cells SHSY-5Y were transfected with increasing concentration of pEGFP-N1 expressing both SOD1 WT and G93A mutant, in the range from 100 to 1000 ng. As a control, transfection with the empty plasmid expressing GFP was performed. After 24h, cells were treated with 200 nM TMRM for 20 minutes at 37°C, then they were collected and analyzed by flow cytometry.

The histograms in Fig. 53 represent the percentage of transfected cells with depolarized mitochondria. As shown, raising the amount of plasmids used in the transfection, the cell population with depolarized mitochondria increases and this is true both for SOD1 WT and G93A. Furthermore, the depolarization is much more evident for the mutant SOD1, also at low concentrations.

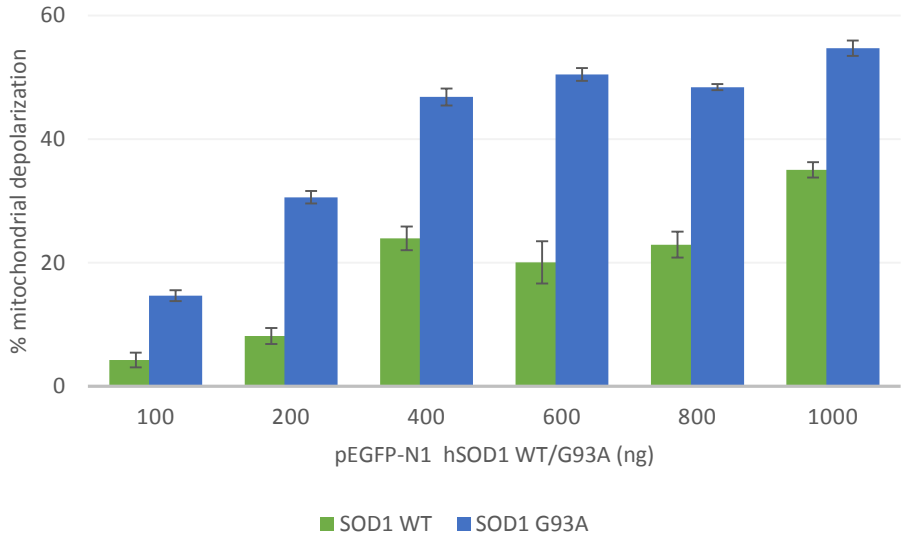

Fig 53 ***Effect of SOD1 WT and G93A on SH-SY5Y mitochondria*** Increasing concentrations of plasmid pEGFP-N1 encoding for SOD1 WT and G93A, as well as the empty vector (expressing the GFP) were used to transfect the cells. As shown, the G93A promotes mitochondrial depolarization, more than overexpression of WT proteins.

4.4.7 Conclusion

ALS is a neurodegenerative disease that affects motor neurons of specific regions of the central nervous system. Although in 90% of cases ALS is sporadic, in the remaining 10% of cases it is genetically inherited, and mutations in SOD1 genes represent the first cause of fALS. However, toxicity mediated by ALS-linked SOD1 mutants is not well understood. It has been proposed that aberrant SOD1 proteins can form toxic aggregates in affected motor neurons, promoting dysfunction of several organelles, such as mitochondria [113]. Recently it was proposed that mitochondrial impairment may be promoted by accumulation of SOD1 mutants on the cytosolic surface of mitochondria [116-118]. As reported by Israelson et al, SOD1 mutants G93A and G85R use VDAC1 as mitochondrial docking site, partially inhibiting VDAC1 conductance. This event could explain the mitochondrial degeneration of affected cells [123].

To better understand the molecular basis of this interaction, in our work we have successfully produced the WT SOD1 and two of its most often ALS-linked SOD1 mutants, G93A and G85R, using heterologous expression in *E. coli*. The expressed proteins resulted to be active enzymes, showing all the typical features reported in the literature, from the enzymatic activity to the subunit dimerization.

We also perfomed interaction analysis between hSOD1 and mutants with VDAC1 by Microscale Thermophoresis and we found that SOD1 G93A mutant has high affinity for VDAC1.

Israelson et al have hypothesized that the interaction of G93A promotes the inhibition of VDAC1 conductance, resulting in a drastic reduction of OMM permeability for metabolites such as ATP, ADP, NADH, Pi; this slows down the ATP production via ATP synthase, and in turn decreases the mitochondrial membrane potential. We tried to verify this hypothesis through the transformation with increasing concentration of plasmids carrying SOD1 of the neuronal cell line SH-SY5Y. This experiment has clearly shown that the accumulation of mutant SOD1, and minimally of SOD1 WT, affects the $\Delta\Psi m$.

However, some additional and brand new information about SOD1 mutant interaction with mitochondria were obtained by further results presented here. In

ALS affected tissues, mitochondria increased in volume, aggregated, swollen and vacuolated were found; in addition, dysfunction in Ca^{2+} homeostasis and increase of oxidative stress were associated to structural damages [143]. In particular, using purified mitochondria, we tested the effect of both WT and mutants SOD1, studying the modifications in the mitochondrial swelling. Our results indicate that WT SOD1 protects mitochondria from swelling after calcium phosphate addition, while no similar effect was reported using both SOD1 mutants G93A and G85R. The mitochondrial swelling is a physiological phenomenon due to an osmotic imbalance of mitochondria in suspension. The mitochondria become more "transparent" upon swelling and the absorbance decreases. The lack of swelling in the presence of WT SOD1 and the physiological swelling upon addition of mutant SOD1 could indicate that SOD1 act with some mechanism to hinder the flow of ions and water toward the mitochondrial inside. This mechanism could involve VDAC (porin in yeast), decreasing the ion flow through the pore: but this conclusion does not fit with the evidence that WT SOD1 does not bind VDAC (porin).WT SOD1 should thus interact with some other protein or in some other way with the machinery involved in the swelling, for example by influencing the inner mitochondrial carriers transporting the calcium or the phosphate inside. The lack of this "protective" action of WT SOD1 should provoke the usual swelling of mitochondria. Thus the SOD1 mutations could change this specific function of the WT SOD1 and also the potentially pathological mechanism could be due to the lack of inhibition of swelling.

A possible mechanism candidate to a functional interaction of WT SOD1 with mitochondria could be the mitochondrial permeability transition pore (MPTP). MPTP has been found to be critical in neurodegeneration and its activation in the mitochondrial transition represents one of the major causes of cell death in a variety of conditions. For example, cells exposed to toxic amounts of Ca^{2+} ionophores undergo MPTP formation and death by necrosis [144]. In the mitochondrial transition a direct linkage between the matrix and the cytosol is realized. Such linkage in some way has to overcome the outer membrane. In former times VDAC was considered heavily involved in the MPTP: unfortunately no molecular prove of such involvment was discovered and even the K.O. of VDAC

gene did not hinder the permeability transition [145], thus weakening its opportunities to be part of the MPT pore. A purely speculative hypothesis can thus propose that WT SOD1 binds a protein in the outer membrane that influence VDAC while the SOD1 mutants studied here abolish such link by binding directly to VDAC. Again, other experiments are needed to clarify this point. If WT SOD1 has a protective effect on permeability transition, a PT assay in the presence of an excess of WT SOD1 (but not of mutant SOD1) should show it. This conclusion could have very profound consequences on our view of permeability transition and on the causes of ALS.

These conclusions do not contrast with the data by Israelson et al [123] that stated that the binding of the mutant SOD1 to VDAC1 is responsible of the organelle inactivation: in the perspective offered by our experiments the hypothesis is that a more sophisticated chain of events than the simple block of the VDAC permeation should be at the basis of ALS and also of other connected pathologies.

5. DISCUSSION

The Voltage-Dependent Anion Channel represents the most important family of pore-forming proteins of the outer mitochondrial membrane. VDAC proteins are mainly involved in the metabolic exchange between cytosol and mitochondria: through VDAC, ions, ATP, ADP and small molecules can cross the OMM. Moreover, VDAC proteins play a key role in calcium homeostasis and in regulation of apoptosis, through the interaction with Bcl-2 family proteins. For their centrality in mitochondrial homeostasis, VDAC proteins can be considered among the most important players in both physiology and pathology of mitochondria.

As most chordates, in humans, three different VDAC isoforms are expressed, that show high level of sequence conservation but, at the same time, different physiological features. VDAC1 is the most abundant and studied isoform, and its tridimensional structure was completely solved in 2008.

It has been shown that VDAC1 is characterized by a large β-barrel channel, which is associated to a N-terminal domain structured as α-helix. The N-terminus is considered one of the most interesting domains of the protein, since it plays a key role in regulation of the main VDAC feature, the voltage gating. Many studies have indicated that the N-terminal domain is a mobile part of the protein: protruding to the cytosol could allow VDAC1 interaction with others molecules. At the same time, N-terminus has been found localized into the pore's lumen, interacting with specific residues of β-strands and conferring stability to the whole protein in the solved crystal structure. The formation and breakage of these links are considered the key to fully understand the voltage gating mediated by the N-terminal domain.

Conversely, VDAC3 is the least characterized isoform. Although structural predictions based on VDAC1 strongly indicates a similar conformation, the ability of VDAC3 to form pores has been questioned. VDAC3, indeed, is not able to complement the lack of endogenous POR1 in yeast *S. cerevisiae* on glycerol (as in *Δpor1* strain), a substrate metabolized exclusively through mitochondria, while

both human VDAC1 and 2 totally restore the yeast growth defect. A possible explanation is that the conformation assumed by VDAC3 determines the formation of a smaller pore compared to VDAC1. Once again, the N-terminal domain might play a key role for reaching this conformation, as well as the peculiar content of cysteine residues showed by VDAC3. Indeed, in a previous work it was demonstrated that the swapping of the N-terminal domain of VDAC3 with the corresponding sequence of VDAC1 (N1-VDAC3 chimera) allows the total recovery of *Δpor1* growth on glycerol.

In this work, we reported for the first time an electrophysiological characterization of VDAC3. Our data indicates that under physiological pH condition, VDAC3 forms pores with an average conductance of 100 pS, thus much smaller than VDAC1, which is characterized by pores of 3.5-4 nS. Interestingly, in electrophysiological experiments, the swapping of VDAC3 N-terminus with the VDAC1 N-terminus (chimera N1-VDAC3) shows that the canonical pore of 4 nS, thus comparable to VDAC1, is reactivated. This result means that the N-terminal domain has a fundamental role in the pore activity; in addition it explains why N1-VDAC3 is able to complement POR1 lack in yeast strain *Δpor1.*

NMR analysis has suggested that the contact between N-terminal domain and the β-barrel of VDAC1 is based on the interaction between Leu10, located on the N-terminal and Val143 and Leu150, located on the opposite side of the β-barrel, respectively on the β-strands 9 and 10. To assess the importance of these residues in the physical contacts between the two parts of the protein, in our work we have created a set of mutants in which the β-strand 9 or both strands 9 and 10 were deleted; in another approach, the whole β-barrel of the protein was swapped with the homologous but not identical domain of VDAC3 (N1-VDAC3). Our work has showed that, although all mutant proteins were able to form pores in artificial membranes, the removal or substitution of specific β-strands strongly affect the voltage-dependence of VDAC1. It was found that, although the chimera N1-VDAC3 maintains all three residues presumably involved in the interaction (VDAC3 barrel has Val143 and Leu150 and the N-terminus of VDAC1 has Leu10), the protein totally loose the voltage dependence. This indicates that also other residues are involved in the interaction between the N-terminus and the barrel wall. In

addition, mutants lacking the β-strand 9 and the β-harpin 9-10 show an asymmetrically response to voltage: at positive voltage they partially lose the voltage-dependence, and it is completely abolished for the mutant lacking both β-strands 9-10. These results indicate that VDAC1 pore is stabilized by a network of interactions between the N-terminal and the pore-wall, and confirm that interrupting them destroys the voltage-dependence property of this channel, especially when the whole β-barrel is changed with that of VDAC3.

VDAC proteins are expressed also in yeast. In particular, *S. cerevisie* encodes for two mitochondrial porins, called POR1 and POR2. POR1 shares with human VDAC1 most part of the structure and the electrophysiological features. POR2 is less characterized and, as for VDAC3, no evidence indicates that it is able to form pores. The yeast model lacking the endogenous POR1, the *Δpor1* strain, was used in this work to investigate the relationships between VDAC and the antioxidant enzyme Superoxide Dismutase I. Indeed, many evidences have shown that SOD1 can act as a regulator of metabolism in yeast: e.g., SOD1 regulates the fermentative metabolism of glucose by repressing respiration, and it is required for protection of VDAC from oxidative stress damages, as carbonylation. We have hypothesized a wider role for SOD1 in metabolism mediated by its relation to VDAC and, for this reason, we expressed the human SOD1 in *Δpor1* yeast strain, that, as previously reported, shows an impaired growth on glycerol.

Results presented here strongly demonstrate that the expression of hSOD1 in *Δpor1* yeast promotes a total restoration of mitochondrial functionality when the yeast is cultured on any tested non-fermentable carbon sources, which require mitochondria to be metabolized. In addition, our qPCR experiments indicate that hSOD1 promotes a significant increase of *por2* transcription and, proportionally, of *sam50*, codifying for a protein involved in the β-barrel protein assembly and import to mitochondria. This suggests that POR2 overexpression could be involved in the substitution of POR1 activity to restore the mitochondrial functionality.

The results not only suggest that POR2 could form pores in mitochondrial membrane but also that this protein can complement the absence of the main POR1. Although more experiments will be necessary, the results indicate that,

under stress condition, SOD1 acts as transcription factor promoting the response to the stress factor.

Anyway, the relationship between VDAC1 and SOD1 is much more extensive. In familial ALS type 1, mutant and misfolded SOD1 proteins directly bind cytosolic surface of mitochondria through VDAC1. This fact could have dramatic consequences for mitochondrial metabolism, since it was demonstrated that binding of mutant SOD1 G93A and G85R promotes the inhibition of VDAC1 conductance. In our work, we have demonstrated that the affinity between VDAC1 and SOD1 G93A mutant is really high and that expression of the same mutant in the neuronal cell line SH-SY5Y promotes the mitochondrial membrane potential drop. However, some additional and brand new information about SOD1 mutant interaction with mitochondria were obtained by mitochondrial swelling experiments. The WT SOD1 protects mitochondria from swelling after calcium phosphate addition; on the contrary, no similar effect was reported using SOD1 mutants. This fact could indicate that in physiological conditions, SOD1 interact with some other protein or with a machinery involved in the swelling, preventing this phenomenon, while SOD1 mutants involved in ALS lose this ability. Indeed, one of the most documented mitochondrial dysfunction related to ALS is the mitochondrial swelling and these evidences can provide a preliminary explanation to the phenomenon.

In conclusion we have produced an original piece of work on the way toward the comprehension of the regulatory interconnections between mitochondria, genome and the metabolic network of the cell. Also with the utilization of our data we expect new, exciting progress in a very close future.

.

6. BIBLIOGRAPHY

[1] Goffeau A., Barrell B.G., Bussey H., Davis R.W., Dujon B., Feldmann H., Galibert F., Hoheisel J.D., Jacq C., Johnston M., Louis E.J., et al. *Life with 6000 genes*. Science (1996), 274, 546.

[2] Botstein D., Chervitz S.A., Cherry M.J. *Yeast as a Model Organism.* Science (1997), 277(5330), 1259–1260.

[3] Zlotnik H., Fernández M.P., Bowers B., Cabib E. *Saccharomyces cerevisiae mannoproteins form an external cell wall layer that determines wall porosity.* J Bacteriol (1984), 159, 1018–1026.

[4] Kawai A., Nishikawa S., Hirata A., Endo T. *Loss of the mitochondrial Hsp70 functions causes aggregation of mitochondria in yeast cells*. J Cell Sci (2001), 114 (19), 3565-3574.

[5] Zörgö E., Chwialkowska K., Gjuvsland A.B., Garré E., Sunnerhagen P., Liti G., Blomberg A., Omholt S.W., Warringer J. *Ancient evolutionary trade-offs between yeast ploidy states.* PLoS Genet (2013), 9 (3), e1003388.

[6] Faria-Oliveira F., Puga S., Ferreira C. *Yeast: World's Finest Chef*. Food Industry (2013), Chapter 23, ISBN 978-953-51-0911-2.

[7] Rintala E., Wiebe M., Tamminen A., Ruohonen L., Penttilä M. *Transcription of hexose transporters of Saccharomyces cerevisiae is affected by change in oxygen provision*. BMC Microbiol (2008), 8 (1), 53.

[8] Lagunas R. *Sugar transport in Saccharomyces cerevisiae*. FEMS Microbiol Rev (1993), 10, 229–242.

[9] Blank L.M., Sauer U. *TCA cycle activity in Saccharomyces cerevisiae is a function of the environmentally determined specific growth and glucose uptake rates*. Microbiology (2004), 150, 1085–1093.

[10] Gancedo J. *Carbon catabolite repression in yeast*. Eur J Biochem (1992), 206, 297–313.

[11] Gancedo J.M. *The early steps of glucose signalling in yeast*. FEMS Microbiology Reviews (2008), 32 (4), 673-704.

[12] Crabtree H.G. *Observations on the carbohydrate metabolism of tumours*. Biochem J (1929), 23 (3), 53.

[13] Gray J.V., Petsko G.A., Johnston G.C., Ringe D., Singer R.A., Werner-Washburne M. "*Sleeping beauty": quiescence in Saccharomyces cerevisiae*. Microbiol Mol Biol Rev (2004), 68,187–206.

[14] Rodrigues F., Ludovico P., Leão C. *Sugar metabolism in yeasts: an overview of aerobic and anaerobic glucose catabolism*. Biodiversity and ecophysiology of yeasts (2006), 101-121.

[15] Brown G.C. *Control of respiration and ATP synthesis in mammalian mitochondria and cells*. Biochem J (1992), 284 (1), 1–13.

[16] Brighton C.T., Hunt R.M. *Mitochondrial calcium and its role in calcification*. Clinical Orthopaed Rel Res (1974), 100 (100), 406–416.

[17] Wang C., Youle R.J. *The role of mitochondria in apoptosis*. Annu Rev Genet (2009), 43, 95-118.

[18] Yang J., Kim J., Park S., Jeon J., Shin Y., Kim S. *Spatial and functional organization of mitochondrial protein network.* Scientific Reports (2012), 3, 1403.

[19] Cooper G.M. *The Cell: A Molecular Approach*. Mitochondria (2000), Sunderland (MA), Sinauer Associates, 2nd edition.

[20] Alberts B., Johnson A., Lewis J., et al. *The Transport of Proteins into Mitochondria and Chloroplasts.* Molecular Biology of the Cell, 4th edition (2002), New York: Garland Science.

[21] Schein S.J., Colombini M., Finkelstein A. *Reconstitution in planar lipid bilayers of a voltage-dependent anion-selective channel obtained from paramecium mitochondria*. J Membr Biol (1976), 30, 99-120.

[22] Cowan S.W., Schirmer T., Rummel G., Steiert M., Ghosh R., Pauptit R.A., Jansonius J.N., Rosenbusch J.P. *Crystal structures explain functional properties of two E. coli porins*. Nature (1992), 358, 727-733.

[23] Yamashita E., Zhalnina M.V., Zakharov S.D., Sharma O., Cramer W.A. *Crystal structures of the OmpF porin: function in a colicin translocon*. EMBO J (2008), 27 (15), 2171–2180.

[24] Delcour A.H, Martinac B., Kung C., Adler J. *Voltage-sensitive ion channel of Escherichia coli*. J Membr Biol (1989), 112, 267–275.

[25] Benz R. *Permeation of hydrophilic solutes through mitochondrial outer membranes: review on mitochondrial porins*. Biochim Biophys Acta (1994), 1197, 167-196.

[26] Young M.J., Bay D.C., Hausner G., Court D.A. *The evolutionary history of mitochondrial porins*. BMC Evol Biol (2007), 7, 31.

[27] Messina A., Reina S., Guarino F., De Pinto V. *VDAC isoforms in mammals*. Biochim Biophys Acta (2012), 1818, 1466-1476.

[28] Majumder S., Fisk H.A.*VDAC3 and Mps1 negatively regulate ciliogenesis*. Cell Cycle (2005), 12 (5), 849-858.

[29] De Pinto V., Guarino F., Guarnera A., Messina A., Reina S., Tomasello F.M., Palermo V., Mazzoni C. *Characterization of human VDAC isoforms: a peculiar function for VDAC3?* Biochim Biophys Acta (2010), 1797, 1268-1275.

[30] Xu X., Decker W., Sampson M.J., Craigen W.J., Colombini M. *Mouse VDAC isoforms expressed in yeast: channel properties and their roles in mitochondrial outer membrane permeability*. J Membr Biol (1999), 170, 89–102.

[31] Checchetto V., Reina S., Magrì A., Szabò I., De Pinto V. *Recombinant Human Voltage Dependent Anion Selective Channel Isoform 3 (hVDAC3) Forms Pores with a Very Small Conductance*. Cell Physiol Biochem (2014), 34, 842-853.

[32] Casadio R., Jacoboni I., Messina A., De Pinto V. *Hypothesis: A 3D model of the voltage-dependent anion channel (VDAC)*. Febs Lett (2002), 520, 1-7.

[33] Bayrhuber M., Meins T., Habeck M., Becker S., Giller K., Villinger S., Vonrhein C., Griesinger C., Zweckstetter M., Zeth K. *Structure of the human voltage-dependent anion channel*. Proc Atl Nat Sci (2008), 105 (40), 15370-15375.

[34] Hiller S., Garces R.G., Malia T.J., Orekhov V.Y., Colombini M., Wagner G. *Solution Structure of the Integral*
Human Membrane Protein VDAC-1 in Detergent Micelles. Science (2008), 32, 1206-1210.

[35] Ujwal R., Cascio D., Colletier J.P., Faham S., Zhang J., Toro L., Ping P., Abramson J. *The crystal structure of mouse VDAC1 at 2.3 Å resolution reveals mechanistic insights into metabolite gating*. Proc Natl Acad Sci USA (2008), 105 (46), 17742-17745.

[36] De Pinto V., Tomasello F.M., Messina A., Guarino F., Benz R., La Mendola D., Magrì A., Milardi D., Pappalardo G. *Determination of the Conformation of the Human VDAC1 N-Terminal Peptide, a Protein Moiety Essential for the Functional Properties of the Pore*. Chem bio chem (2007), 8 (7), 744-756.

[37] Song J., Midson C., Blachly-Dyson E., Forte M., Colombini M. *The Topology of VDAC as Probed by Biotin Modification*. J Biol Chem (1998), 273, 24406-24413.

[38] Wojtkowska M., Jakalski M., Pienkowska J.R., Stobienia O., Karachitos A., Przytycka T.M., Weiner J. 3rd, Kmita H.,Makalowski W. *Phylogenetic Analysis of Mitochondrial Outer Membrane β-Barrel Channels*. Genome Biol Evol (2012), 4, 110-125.

[39] De Pinto V., Ludwing O., Benz R ., Krause J., Palmieri F. *Porin pores of mitochondrial outer membranes from high and low eukaryotic cells: biochemical and biophysical characterization*. Biochim Biophys Acta (1987), 894, 109-119.

[40] Colombini M. *Structure and mode of action of a voltage dependent anion-selective channel (VDAC) located in the outer mitochondrial membrane*. Ann NY Acad Sci (1980), 341, 552–563.

[41] Gincel D., Silberberg S.D., Shoshan-Barmatz V. *Modulation of the Voltage-Dependent Anion Channel (VDAC) by Glutamate1*. J Bioenerg Biomembr (2000), 32 (6), 571–583.

[42] Hodge T., Colombini M. *Regulation of metabolite flux through voltage-gating of VDAC channels*. J Membr Biol (1997), 157 (3), 271–279.

[43] Abu-Hamad S., Arbel N., Calo D., Arzoine L., Israelson A., Keinan N., Ben-Romano R., Friedman O., Shoshan-Barmatz V. *The VDAC1 N-terminus is essential both for apoptosis and the protective effect of anti-apoptotic proteins*. J Cell Sci (2009), 122 (11), 1906–1916.

[44] Törnroth-Horsefield S., Neutze R. *Opening and closing the metabolite gate*. Proc Natl Acad Sci USA (2008), 105 (50), 19565–19566.

[45]Szabò I., Zoratti M. *Mitochondrial Channels: Ion Fluxes and More*. Physiol Rev (2014), 94 (2), 519-608.

[46] Blachly-Dyson E., Forte M. *VDAC Channels*. IUBMB Life (2001), 52, 113–118.

[47] Shoshan-Barmatz V., Zakar M., Rosenthal K., Abu-Hamad S. *Key regions of VDAC1 functioning in apoptosis induction and regulation by hexokinase.* Biochim Biophys Acta (2009), 1787 (5), 421–430.

[48] Bryson J.M., Coy P.E., Gottlob K., Hay N., Robey R.B. *Increased hexokinase activity, of either ectopic or endogenous origin, protects renal epithelial cells against acute oxidant-induced cell death*. J Biol Chem (2002), 277 (13), 11392–11400.

[49] Pedersen P.L. *Voltage dependent anion channels (VDACs): a brief introduction with a focus on the outer mitochondrial compartment's roles together with hexokinase-2 in the ''Warburg effect" in cancer*. J Bioenerg Biomembr (2008), 40 (3), 123–126.

[50] Gross A., Jockel J., Wei M.C., Korsmeyer S.J. *Enforced dimerization of BAX results in its translocation, mitochondrial dysfunction and apoptosis*. Embo J (1998), 17 (14), 3878–3885.

[51] Abu-Hamad S., Zaid H., Israelson A., Nahon E., Shoshan-Barmatz V. *Hexokinase-I protection against apoptotic cell death is mediated via interaction with the voltage-dependent anion channel-1: mapping the site of binding*. J Biol Chem (2008), 19, 13482–13490.

[52] Zalk R., Israelson A., Garty E., Azoulay-Zohar H., Shoshan-Barmatz V. *Oligomeric states of the voltage-dependent anion channel and cytochrome c release from mitochondria*. Biochem J (2005), 386, 73–83.

[53] Forte M., Guy H.R., Mannella C.A. *Molecular genetics of the VDAC ion channel: structural model and sequence analysis*. J Bioenerg Biomembr (1987), 19 (4), 341-50.

[54] Dihanich M., Suda K., Schatz G. *A yeast mutant lacking mitochondrial porin is respiratory-deficient, but can recover respiration with simultaneous accumulation of an 86-kd extramitochondrial protein*. EMBO J (1987), 6, 723–728.

[55] Blachly-Dyson E., Song J., Wolfgang W.J., Colombini M., Forte M. *Multicopy suppressors of phenotypes resulting from the absence of yeast VDAC encode a VDAC-like protein.* Mol Cell Biol (1997), 17, 5727–5738.

[56] Blachly-Dyson E., Zambronicz E.B., Yu W.H., Adams V., McCabe E.R., Adelman J., Colombini M., Forte M. *Cloning and functional expression in yeast of two human isoforms of the outer*

mitochondrial membrane channel, the voltage-dependent anion channel. J Biol Chem (1993), 268, 1835–1841.

[57] Sampson M.J., Lovell R.S., Craigen W.J. *The murine voltage-dependent anion channel gene family. Conserved structure and function*. J Biol Chem (1997), 272 (30), 18966-18973.

[58] Arzoine L., Zilberberg N., Ben-Romano R., Shoshan-Barmatz V. *Voltage-dependent anion channel 1-based peptides interact with hexokinase to prevent its anti-apoptotic activity*. J Biol Chem (2009), 284, 3946–3955.

[60] Hiller S., Wagner G. *The role of solution NMR in the structure determinations of VDAC-1 and other membrane proteins*. Curr Opin Struct Biol (2009), 19, 396–401.

[61] Reina S., Palermo V., Guarnera A., Guarino F., Messina A., Mazzoni C., De Pinto V. *Swapping of the N-terminus of VDAC1 with VDAC3 restores full activity of the channel and confers anti-aging features to the cell*. FEBS Letters (2010), 584, 2837–2844.

[62] Kopp R.E., Kirschvink J.L., Hilburn I.A., Nash C.Z. *The Paleoproterozoic snowball Earth: A climate disaster triggered by the evolution of oxygenic photosynthesis*. Proc Natl Acad Sci USA (2005), 102 (32), 11131–11135.

[63] Davies K.J. *Oxidative stress: the paradox of aerobic life*. Biochem Soc Symp (1995), 61, 1-31.

[64] Liochev S.I., Fridovich I. *Superoxide and iron: partners in crime*. IUBMB Life (1999), 48, 157–161.

[65] Turrens J.F. *Mitochondrial formation of reactive oxygen species*. J Physiol (2003), 552.2, 335–344.

[66] Richter C., Park J.W., Ames B.N. *Normal oxidative damage to mitochondrial and nuclear DNA is extensive*. Proc Natl Acad Sci USA (1988), A85, 6465–6467.

[67] Rubbo H., Radi R., Trujillo M., Telleri R., Kalyanaraman B., Barnes S., Kirk M., Freeman B.A. *Nitric oxide regulation of superoxide and peroxynitrite-dependent lipid peroxidation. Formation of novel nitrogen-containing oxidized lipid derivatives*. J Biol Chem (1994), 269, 26066–26075.

[68] Stadtman E.R., Levine R.L. *Protein oxidation*. Ann N Y Acad Sci (2000), 899, 191–208.

[69] Mukherjee P.K., Marcheselli V.L., Serhan C.N., Bazan N.G. *Neuroprotecin D1: A docosahexanoic acid-derived docosatriene protects human retinal pigment epithelial cells from oxidative stress*. Proc Natl Acad Sci (2004), 101 (22), 8491–8496.

[70] Floyd R.A. *Neuroinflammatory processes are important in neurodegenerative diseases: An hypothesis to explain the increased formation of reactive oxygen and nitrogen species as major factors involved in neurodegenerative disease development*. Free Rad Biol Med (1999), 26(9–10), 1346–135.

[71] McCord J.M., Fridovich I. *Superoxide dismutase. An enzymic function for erythrocuprein (hemocuprein)*. J Biol Chem (1969) 244 (22), 6049-6055.

[72] Grace S.C. *Phylogenetic distribution of superoxide dismutase supports an endosymbiotic origin for chloroplasts and mitochondria*. Life Sci (1990) 47(21), 1875-1886.

[73] Zelko I.N., Mariani T.J., Folz R.J. *Superoxide Dismutase multigene family: a comparison of the CuZn-SOD (SOD1), Mn-SOD (SOD2), and Ec-SOD (SOD3) gene structures, evolution and expression*. Free Rad Biol Med (2002), 33 (3), 337–349.

[74] Lebovitz R.M., Zhang H., Vogel H., Cartwright J.Jr., Dionne L., Lu N., Huang S., Matzuk M.M. *Neurodegeneration, myocardial injury, and perinatal death in mitochondrial superoxide dismutase-deficient mice*. Proc Natl Acad Sci USA (1996), 93, 9782–9787.

[75] Marklund S.L., Holme E., Hellner L. *Superoxide dismutase in extracellular fluids*. Clin Chim Acta (1982), 126, 41–51.

[76] Folz R.J., Guan J., Seldin M.F., Oury T.D., Enghild J.J., Crapo J.D. *Mouse extracellular superoxide dismutase: primary structure, tissue-specific gene expression, chromosomal localization and lung in situ hybridization*. Am J Respir Cell Mol Biol (1997), 17, 393–403.

[77] Stralin P., Karlsson K., Johansson B.O., Marklund S.L. *The interstitium of the human arterial wall contains very large amounts of extracellular superoxide dismutase*. Arterioscler Thromb Vasc Biol (1995), 15, 2032–2036.

[78] Kim H.T., Kim Y.H., Nam J.W., Lee H.J., Rho H.M., Jung G. *Study of 5'-flanking region of human Cu/Zn superoxide dismutase*. Biochem Biophys Res Commun (1994), 201, 1526–1533.

[79] De La Torre R., Casado A., Lopez-Fernandez E., Carrascosa D., Ramirez V., Saez J. *Overexpression of copper-zinc superoxide dismutase in trisomy 21*. Experientia (1996), 52, 871–873.

[80] Rosen D.R., Siddique T., Patterson D., Figlewicz D.A., Sapp P., Hentati A., Donaldson D., Goto J., O'Regan J.P., Deng H.X., Rahmani Z., Krizus A., et al. *Mutations in Cu/Zn superoxide dismutase gene are associated with familial amyotrophic lateral sclerosis*. Nature (1993), 362, 59–62.

[81] Bordo D., Djinovic K., Bolognesi M. *Conserved patterns in the Cu,Zn superoxide dismutase family*. J Mol Biol (1994), 238, 366–386.

[82] Tainer J.A., Getzoff E.D., Beem K.M., Richardson J.S., Richardson D.C. *Determination and analysis of the 2 Å structure of copper, zinc superoxide dismutase*. J Mol Biol (1982), 160, 181–217.

[83] Miller A.F. *Superoxide dismutases: active sites that save, but a protein that kills.* Curr Op Chem Biol (2004), 8, 162–168.

[84] Furukawa Y., Torres A.S., O'Halloran T.V. *Oxygen-induced maturation of SOD1: a key role for disulfide formation by the copper chaperone CCS*. EMBO J (2004), 23, 2872–2881.

[85] Banci L., Bertini I., Cantini F., Kozyreva T., Massagni C., Palumaa P., et al. *Human superoxide dismutase1 (hSOD1) maturation through interaction with human copper chaperone for SOD1 (hCCS)*. Proc Natl Acad Sci USA (2012) 109, 13555–13560.

[86] Longo V.D., Gralla E.B., Valentine J.S. *Superoxide dismutase activity is essential for stationary phase survival in Saccharomyces cerevisiae: mitochondrial production of toxic oxygen species in vivo.* J Biol Chem (1996), 271, 12275–12280.

[87] Guidot D.M., McCord J.M., Wright R.M., Repine J.E. *Absence of electron transport (Rho 0 state) restores growth of a manganese-superoxide dismutase-deficient Saccharomyces cerevisiae in hyperoxia. Evidence for electron transport as a major source of superoxide generation in vivo*. J Biol Chem (1993), 268, 26699–26703.

[88] Yoo H.Y., Kim S.S., Rho H.M. *Overexpression and simple purification of human superoxide dismutase (SOD1) in yeast and its resistance to oxidative stress*. J Biotechnol (1999), 68 (1), 29-35.

[89] Yoo H.Y., Chang M.S., Rho H.M. *The activation of the rat copper/zinc superoxide dismutase gene by hydrogen peroxide through the hydrogen peroxide-responsive element and by Paraquat and heat shock through the same heat shock element*. J Biol Chem (1999), 274, 23887–23892.

[90] Crapo J.D., Oury T., Rabouille C., Slot J.W., Chang L. *Copper,zinc superoxide dismutase is primarily a cytosolic protein in human cells*. Proc Natl Acad Sci USA (1992), 89, 10405-10409.

[91] Geller B.L., Winge D.R. *Rat liver Cu, Zn-superoxide dismutase. Subcellular location in lysosomes*. J Biol Chem (1982), 257, 8945–8952.

[92] Islinger M., Li K.W., Seitz J., Völkl A., Lüers G.H. *Hitchhiking of Cu/Zn superoxide dismutase to peroxisomes–evidence for a natural piggyback import mechanism in mammals*. Traffic (2009), 10, 1711–1721.

[93] Sturtz L.A., Diekert K., Jensen L.T., Lill R., Culotta V.C. *A fraction of yeast Cu,Zn-superoxide dismutase and its metallochaperone, CCS, localize to the intermembrane space of mitochondria. A physiological role for SOD1 in guarding against mitochondrial oxidative damage.* J Biol Chem (2001), 276 (41), 38084-38089.

[94] Okado-Matsumoto A., Fridovich I. *Subcellular distribution of superoxide dismutases (SOD) in rat liver: Cu,Zn-SOD in mitochondria.* J Biol Chem (2001), 276, 38388–38393.

[95] Sehati S., Clement M., Martins J., Xu L., Longo V.D., Valentine J.S., Gralla E.B. *Metabolic alterations in yeast lacking copper–zinc superoxide dismutase.* Free Rad Biol Med (2011), 50, 1591–1598.

[96] Reddi A.R., Culotta V.C. SOD1 *Integrates Signals from Oxygen and Glucose to Repress Respiration*. Cell (2013), 152, 224–235.

[97] Moriya H., Johnston M. *Glucose sensing and signaling in Saccharomyces cerevisiae through the Rgt2 glucose sensor and casein kinase I*. Proc Natl Acad Sci USA (2004), 101, 1572–1577.

[98] Holsbeeks I., Lagatie O., Van Nuland A., Van de Velde S., Thevelein J.M. *The eukaryotic plasma membrane as a nutrient-sensing device*. Trends Biochem Sci (2004), 29, 556–564.

[99] Liu Z., Thornton J., Spı´rek M., Butow R.A. *Activation of the SPS amino acid-sensing pathway in Saccharomyces cerevisiae correlates with the phosphorylation state of a sensor component, Ptr3*. Mol Cell Biol (2008), 28, 551–563.

[100] Carter C.D., Kitchen L.E, Au W.C., Babic C.M., Basrai M.A. *Loss of SOD1 and LYS7 sensitizes Saccharomyces cerevisiae to hydroxyurea and DNA damage agents and downregulates MEC1 pathway effectors*. Mol Cell Biol (2005), 25, 10273-10285.

[101] Tsang C.K., Liu Y., Thomas J., Zhang Y., Zheng X.F.S. *Superoxide dismutase 1 acts as a nuclear transcription factor to regulate oxidative stress resistance.* Nature Comm (2014), 5, article number 3446.

[102] O'Brien K.M., Dirmeier R., Engle M., Poyton R.O. *Mitochondrial Protein Oxidation in Yeast Mutants Lacking Manganese- (MnSOD) or Copper- and Zinc-containing Superoxide Dismutase (CuZnSOD)*. J Biol Chem (2004), 279, 51817–51827.

[103] Budzinska M., Galganska H., Wojtkowska M., Stobienia O., Kmita H. *Effects of VDAC isoforms on CuZn-superoxide dismutase activity in the intermembrane space of Saccharomyces cerevisiae mitochondria*. Biochem Biophys Res Comm (2007), 357, 1065–1070.

[104] Karachitos A., Galganska H., Wojtkowska M., Budzinska M., Stobienia O., Bartosz G., Kmita H. *Cu,Zn-superoxide dismutase is necessary for proper function of VDAC in Saccharomyces cerevisiae cells*. FEBS Lett (2009), 583, 449-455.

[105] Yoshida S., Mulder D.W., Kurland L.T., Chu C.P., Okazaki H. *Follow-up study on amyotrophic lateral sclerosis in Rochester, Minn., 1925 through 1984*. Neuroepidemiology (1986), 5, 61–70.

[106] Logroscino G., Traynor B.J., Hardiman O., Chio' A., Couratier P., Mitchell J.D., Swingler R.J., Beghi E. *Descriptive epidemiology of amyotrophic lateral sclerosis: new evidence and unsolved issues.* J Neurol Neurosurg Psychiatry (2008), 79 (1), 6–11.

[107] Renton A.E., Chiò A., Traynor B.J. *State of play in amyotrophic lateral sclerosis genetics*. Nature Neurosci (2014), 17, 17–23.

[108] Mandrioli J., Faglioni P., Merelli E., Sola P. *The epidemiology of ALS in Modena, Italy*. Neurology (2003), 60, 683–689.

[109] Millecamps S., Salachas F., Cazeneuve C., Gordon P., Bricka B., Camuzat A., Guillot-Noel L., Russaouen O., Bruneteau G., Pradat P.F., et al. *SOD1, ANG, VAPB, TARDBP, and FUS mutations in familial amyotrophic lateral sclerosis: genotype-phenotype correlations*. J Med Genet (2010), 47, 554–560.

[110] Cudkowicz M.E., McKenna-Yasek D., Sapp P.E., Chin W., Geller B., Hayden D.L., Schoenfeld D.A., Hosler B.A., Horvitz H.R., Brown R.H. *Epidemiology of mutations in superoxide dismutase in amyotrophic lateral sclerosis*. Ann Neurol (1997), 41 (2), 210-221.

[111] Juneja T., Pericak-Vance M.A., Laing N.G., Dave S., Siddique T. *Prognosis in familial amyotrophic lateral sclerosis: progression and survival in patients with glu100gly and ala4val mutations in Cu,Zn superoxide dismutase*. Neurology (1997), 48, 55-57.

[112] Morita M., Aoki M., Abe K., Hasegawa T., Sakuma R., Onodera Y., Ichikawa N., Nishizawa M., Itoyama Y. *A novel two-base mutation in the Cu/ Zn superoxide dismutase gene associated with familial amyotrophic lateral sclerosis in Japan.* Neurosci Lett (1996), 205, 79-82.

[113] Boillèe S., Vande Velde C., Cleveland D.W. *ALS: A Disease of Motor Neurons and Their Non neuronal Neighbors.* Neuron (2006), 52, 39–59.

[114] Bruijn L.I., Becher M.W., Lee M.K., Anderson K.L., Jenkins N.A., Copeland N.G., Sisodia S.S., Rothstein J.D., Borchelt D.R., et al. *ALS-linked SOD1 mutant G85R mediates damage to astrocytes and promotes rapidly progressive disease with SOD1-containing inclusions*. Neuron (1997), 18, 327–338.

[115] Watanabe M., Dykes-Hoberg M., Culotta V.C., Price D.L., Wong P.C., Rothstein J.D. *Histological evidence of protein aggregation in mutant SOD1 transgenic mice and in amyotrophic lateral sclerosis neural tissues*. Neurobiol Dis (2001), 8, 933–941.

[116] Xu Z., Jung C., Higgins C., Levine J., Kong J. *Mitochondrial Degeneration in Amyotrophic Lateral Sclerosis*. Bioenerg Biomembr J (2004), 36 (4), 395-399.

[117] Higgins C.M., Jung C., Ding H., Xu Z. *Mutant Cu, Zn superoxide dismutase that causes motor neurondegeneration is present in mitochondria in the CNS*. J Neurosci (2002), 22 (6), RC215.

[118] Vande Velde C., Miller T.M., Cashman N.R., Cleveland D.W. *Selective association of misfolded ALS-linked mutant SOD1 with the cytoplasmic face of mitochondria*. Proc Natl Acad Sci USA (2008), 105 (10), 4022–4027.

[119] Borthwick G.M., Johnson M.A., Ince P.G., Shaw P.J., Turnbull D.M. *Mitochondrial enzyme activity in amyotrophic lateral sclerosis: implications for the role of mitochondria in neuronal cell death*. Ann Neurol (1999), 46, 787–790.

[120] Jung C., Higgins C.M., Xu Z. *A quantitative histochemical assay for activities of mitochondrial electron transport chain complexes in mouse spinal cord sections*. J Neurosci Methods (2002), 114, 165–172.

[121] Carri M.T., Ferri A., Battistoni A., Famhy L., Gabbianelli R., Poccia F., Rotilio G. *Expression of a Cu,Zn superoxide dismutase typical of familial amyotrophic lateral sclerosis induces mitochondrial*

alteration and increase of cytosolic Ca^{2+} concentration in transfected neuroblastoma SH-SY5Y cells. FEBS Lett (1997), 414, 365–368.

[122] Bowling A.C., Schulz J.B., Brown R.H. Jr., Beal M.F. *Superoxide dismutase activity, oxidative damage, and mitochondrial energy metabolism in familial and sporadic amyotrophic lateral sclerosis*. J Neurochem (1993), 61, 2322–2325.

[123] Israelson A., Arbel N., Da Cruz S., Ilieva H., Yamanaka K., Shoshan-Barmatz V., Cleveland D.W. *Misfolded Mutant SOD1 Directly Inhibits VDAC1 Conductance in a MouseModel of Inherited ALS*. Neuron (2010), 67, 575–587.

[124] Le Verche V., Przedborski S. *Is Amyotrophic Lateral Sclerosis a Mitochondrial Channelopathy?* Neuron (2010), 67, 523-524.

[125] Ho S.N., Hunt H.D., Horton R.M., Pullen J.K., Pease L.P. *Site-directed mutagenesis by overlap extension using the polymerase chain reaction*. Gene (1989), 77, 51-59.

[126] Horton R.M., Hunt H.D., Ho S.N., Pullen J.K., Pease L.P. *Engineering hybrid genes without the use of restriction enzymes: gene splicing by overlap extension*, Gene (1989), 77, 61-68.

[127] Shi Y., Jiang C., Chen Q., Tang H. *One-step on-column affinity refolding purification and functional analysis of recombinant human VDAC1*. Biochem Biophys Res Comm (2003), 303, 475-482.

[128] Gregg C., Kyryakov P., Titorenko V.I. *Purification of Mitochondria from Yeast Cells*. J Vis Exp (2009), 30, e1417.

[129] De Pinto V., Benz R., Palmieri F. *Interaction of non-classical detergents with the mitochondrial porin: a new purification procedure and characterization of the pore-forming unit*. Eur J Biochem (1989), 183, 179-187.

[130] Benz R., Janko K., Boos W., Läuger P. *Formation of large, ion-permeable membrane channels by the matrix protein (porin) of Escherichia coli*. Biochim Biophys Acta (1979), 511, 305-319.

[131] Benz R., Schmid A., Hancock R.E. *Ion selectivity of gram-negative bacterial porins*. J Bacteriol (1985), 162, 722-727.

[132] Beauchamp C., Fridovich I. *Superoxide dismutase: improved assays and an assay applicable to acrylamide gels*. Anal Biochem (1971), 44 (1), 276-87.

[133] Wienken C. J., Baaske P., Rothbauer U., Braun D., and Duhr S. *Protein binding assays in biological liquids using microscale thermophoresis*. Nat Commun (2010), 1, 100.

[134] Zillner K., Jerabek-Willemsen M., Duhr S., Braun D., Längst G. and Baaske P.*Microscale thermophoresis as a sensitive method to quantify protein: nucleic acid interactions in solution*. Methods Mol Biol (2012), 815, 241–252.

[135] Livak K.J., Schmittgen T.D. *Analysis of relative gene expression data using real-time quantitative PCR and the* $2^{-\Delta\Delta Ct}$ *method*. Methods (2001), 25 (4), 402-408.

[136] Amodeo G.F., Scorciapino M.A., Messina A., De Pinto V., Ceccarelli M. *Charged residues distribution modulates selectivity of the open state of human isoforms of the voltage dependent anion-selective channel* PLoS One (2014) 9 (8), e103879.

[137] Sampson M.J., Decker W.K., Beaudet A.L., Ruitenbeek W., Armstrong D., Hicks M.J., Craigen W.J. *Immotile sperm and infertility in mice lacking mitochondrial voltage-dependent anion channel type 3*. J Biol Chem (2001), 276, 39206-39212.

[138] Hinsch K.D., De Pinto V., Aires V.A., Schneider X., Messina A., Hinsch E. *Voltage-dependent anion-selective channels VDAC2 and VDAC3 are abundant proteins in bovine outer dense fibers, a cytoskeletal component of the sperm flagellum*. J Biol Chem (2004), 279, 15281-15288.

[139] Zachariae U., Schneider R., Briones R., Gattin Z., Demers J.P., Giller K., Maier E., Zweckstetter M., Griesinger C., Becker S., Benz R., de Groot A. *Lange, β-Barrel mobility underlies closure of the voltage-dependent anion channel*. Structure (2012), 20, 1540–1549.

[140] Benz R., Wojtczak L., Bosch W., Brdiczka D. *Inhibition of adenine nucleotide transport through the mitochondrial porin by a synthetic polyanion*. FEBS Lett (1988), 231, 75–80.

[141] Sprague G.F., Cronan J.E. *Isolation and characterization of Saccharomyces cerevisiae mutants defective in glycerol catabolism*. J Bacteriol (1977) 129 (3), 1335-1342.

[142] Colombini M. *Purification of VDAC (voltage-dependent anion-selective channel) from rat liver mitochondria.* J Membr Biol (1983), 74(2), 115-21.

[143] Bendotti C., Calvaresi N., Chiveri L., Prelle A., Moggio M., Braga M., Silani V., De Biasi S. *Early vacuolization and mitochondrial damage in motor neurons of FALS mice are not associated with apoptosis or with changes in cytochrome oxidase histochemical reactivity*. J Neurol Sci (2001), 191, 25-33.

[144] Lemasters J.J., Nieminen A.L., Qian T., Trost L.C., Elmore S.P., Nishimura Y., Crowe R.A., Cascio W.E., Bradham C.A., Brenner D.A., Herman B. *The mitochondrial permeability transition in cell death: A common mechanism in necrosis, apoptosis and autophagy*. Biochim Biophys Acta (1998), 1366, 177–196.

[145] Baines C.P., Kaiser R.A., Sheiko T., Craigen W.J., Molkentin J.D. *Voltage-dependent anion channels are dispensable for mitochondrial-dependent cell death*. Nature Cell Biology (2007), 9 (5), 550-555.

Acknowledgments

I would like to thank all people that have supported me in the last four years in research stuff but not only. First of all, thank to my tutor, Prof. Vito De Pinto, for for believing in me since the beginning. Thanks to all wonderful lab team: Prof. Angela Messina, Dr. Simona Reina, Dr. Francesca Guarino, Dr. Flora Tomasello, Dr. Loredana Leggio, Dr. Maria Carmela Di Rosa.

I would like to thank Prof. Varda Shoshan-Barmatz and all the guys of her lab from Ben-Gurion University of the Negeve, Beer Sheva, Israel, where I spent 6 wonderful months with a EMBO short term fellowship. Thanks to Dr. Adrian Israelson for some materials and advices.